CHEMICAL REVIEWS

Review

Cite This: *Chem. Rev.* 2019, 119, 231−292

pubs.acs.org/CR

The Optoelectronic Nose: Colorimetric and Fluorometric Sensor Arrays

Zheng Li,[†] Jon R. Askim,[‡] and Kenneth S. Suslick*[,†]

[†]Department of Chemistry, University of Illinois at Urbana−Champaign, Urbana, Illinois 61801, United States

[‡]National Institute of Standards and Technology, Gaithersburg, Maryland 20899, United States

ABSTRACT: A comprehensive review on the development and state of the art of colorimetric and fluorometric sensor arrays is presented. Chemical sensing aims to detect subtle changes in the chemical environment by transforming relevant chemical or physical properties of molecular or ionic species (i.e., analytes) into an analytically useful output. Optical arrays based on chemoresponsive colorants (dyes and nanoporous pigments) probe the chemical reactivity of analytes, rather than their physical properties (e.g., mass). The chemical specificity of the olfactory system does not come from specific receptors for specific analytes (e.g., the traditional lock-and-key model of substrate−enzyme interactions), but rather olfaction makes use of pattern recognition of the combined response of several hundred olfactory receptors. In a similar fashion, arrays of chemoresponsive colorants provide high-dimensional data from the color or fluorescence changes of the dyes in these arrays as they are exposed to analytes. This provides chemical sensing with high sensitivity (often down to parts per billion levels), impressive discrimination among very similar analytes, and exquisite fingerprinting of extremely similar mixtures over a wide range of analyte types, in both the gas and liquid phases. Design of both sensor arrays and instrumentation for their analysis are discussed. In addition, the various chemometric and statistical analyses of high-dimensional data (including hierarchical cluster analysis (HCA), principal component analysis (PCA), linear discriminant analysis (LDA), support vector machines (SVMs), and artificial neural networks (ANNs)) are presented and critiqued in reference to their use in chemical sensing. A variety of applications are also discussed, including personal dosimetry of toxic industrial chemical, detection of explosives or accelerants, quality control of foods and beverages, biosensing intracellularly, identification of bacteria and fungi, and detection of cancer and disease biomarkers.

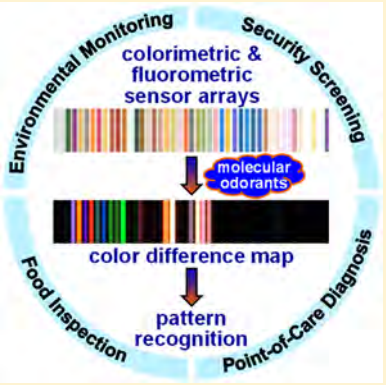

CONTENTS

Special Issue: Chemical Sensors

Received: April 6, 2018
Published: September 12, 2018

DOI: 10.1021/acs.chemrev.8b00226
Chem. Rev. 2019, 119, 231−292

1. INTRODUCTION TO CHEMICAL SENSING AND OPTICAL SENSORS

Chemical sensing aims to detect subtle changes in the chemical environment by transforming relevant chemical or physical properties of molecular or ionic species (i.e., analytes) into an analytically useful output.[1−3] The prototypical example of chemical sensing is the olfactory system of animals. Even for humans beings, who are generally more visual than olfactory creatures, the sense of smell is one of our most basic capabilities, and we are able to recognize and discriminate over 10 000 individual scents, and possibly even billions.[4,5] The chemical specificity of the olfactory system does not come from specific receptors for specific analytes (e.g., the traditional lock-and-key model of substrate−enzyme interactions), but rather olfaction makes use of pattern recognition of the combined response of several hundred olfactory receptors. For typical terrestrial mammals, there are ∼1000 semispecific olfactory receptor genes, which accounts for ∼3% of the entire genome;[6−8] even humans have some 400 active olfactory receptors.[9] Despite the complicated and speculative structures of the transmembrane olfactory receptors (the largest class of G-protein-coupled receptors[4,7]), a large fraction of them are believed to be metalloproteins that are highly reactive to numerous odorant molecules through coordination of the analyte to the metal-binding site.[10−13]

There is a pressing demand to develop effective methodologies that enable rapid, sensitive, portable, and inexpensive detection of toxic analytes in gases or aqueous solutions. Array-based sensor technologies, or "electronic noses",[14−23] use several to many different cross-reactive sensors that interact with analytes, most commonly through physical adsorption, and generate an electrical response (e.g., changes in resistance or capacitance). The pattern of the sensor array, due to the cross-reactivity of the individual sensors, enables molecular recognition by comparison to a predetermined library of responses. The first example of an artificial nose was reported by Persaud et al. in 1982, who tried to mimic the biological olfactory system using semiconductor transducers that were semispecific to analytes:[24] three different metal oxides were employed to sense similar mixtures and discriminate among them. In recent years, an increasing number of cross-reactive analytical devices have emerged and have been applied to environmental monitoring,[25−29] security screening,[30−33] biomedical diagnosis,[34−39] and food inspection.[40−43]

The vigorous development of novel techniques in chemical sensing has resulted in the availability of many useful sensors not based on electrical responses as alternatives to electronic noses. Among these, optical sensors are especially noteworthy.[44−49] The most common optical sensors are based on colorimetric or fluorescent changes originating from intermolecular interactions between the chromophore or fluorophore with the analytes.[44] Combining array-based techniques that employ a chemically diverse set of cross-reactive sensor elements with novel digital imaging methods,[50−58] one can produce a composite pattern of response as a unique optical "fingerprint" for any given analyte.[27,59,60] By analogy, such optical sensor arrays are often referred to as optoelectronic noses or tongues.[61]

Optical arrays based on chemoresponsive colorants (dyes and nanoporous pigments) probe the chemical reactivity of analytes, rather than their physical properties. This provides a high dimensionality to chemical sensing that permits high sensitivity (often down to parts per billion (ppb) or even parts per trillion (ppt) levels), impressive discrimination among very similar analytes, and fingerprinting of extremely similar mixtures over a wide range of analyte categories, in both gaseous and liquid phases. Colorimetric and fluorometric sensor arrays therefore effectively overcome the limitations of traditional array-based sensors that solely depend on physisorption or nonspecific chemical interactions. Such optical array sensing has shown excellent performance in the detection and identification of diverse analytes, ranging from chemical hazards to energetic explosives, to medical biomarkers, and to food additives.

To this end, a comprehensive review will be presented on the development and state of the art of optical array sensing technologies, mainly focused on colorimetric and fluorometric sensor arrays. We will cover recent advances and progress with such sensor arrays and their applications in the detection of volatile organic chemicals (VOCs), explosive screening, food and beverage inspection, as well as disease diagnosis; several commonly used methods for multivariate analyses of the high-dimensional data will also be briefly introduced. Finally, some perspectives regarding the development of the next generation of optical sensors and other chemical sensing techniques will be presented.

New sensor technologies must inevitably face the dilemma of attempting to create sensors that are both increasingly sensitive and increasingly robust; beyond a certain point, the more sensitive a sensor is, the less robust it inherently becomes due to poisoning during usage in real-world situations. Aging of sensors is a particularly acute problem for any sensor array that is intended to be reusable, regardless of the class of sensors. For pattern recognition to work (inherent in the concept of any kind of "nose" technology), the library of patterns must be representative of the sensors' responses in immediate time of application; if sensor response drifts, then libraries can become obsolete very quickly. One path around this dilemma is to develop disposable sensors, thus unlinking the opposing demands that challenge the development of chemical sensing.[61,62]

Present array-based detectors have employed a variety of analytical strategies to trace even subtle changes in either physical properties (e.g., molecular weight, conductivity, surface tension) or chemical reactivity (e.g., Lewis acidity/basicity, hydrogen bonding, redox potential), including the use of conductive polymers and polymer composites, metal oxide semiconductors, quartz crystal microbalances, polymer coated surface acoustic wave devices, and fluorescent molecular frameworks. The chemical sensors that have been reported so far for odorant analysis, generally, can be categorized by their

DOI: 10.1021/acs.chemrev.8b00226
Chem. Rev. 2019, 119, 231−292

signal transduction approaches into optical and nonoptical types.[63] The classification of these sensors is based primarily upon their use of either the physical properties of the analytes or the chemical interactions of the analytes. Electrochemical sensors detect signal changes in resistance, for example, induced by an electrical current passing through the electrodes which contact and interact with chemical analytes. Mass sensors measure differences in the mass of the sensor surface upon exposure to analytes. Optical sensors convert changes in electromagnetic waves (e.g., UV−vis light) into electronic signals. This review will begin with a brief introduction of these classes of sensors, followed by detailed discussions of the concepts, fabrication methods, and applications of optical array sensing technology.

1.1. Nonoptical Sensors

The mammalian olfactory system is, in a way, a large array of bioelectrical receptors. Similarly, electrochemical sensors are made of resistors or capacitors as electronic units that keep track of changes in conductivity or capacitance during interactions between analyte molecules and the electrically active surface.[64−67] Other grouping criteria include the detection basis (i.e., material vs geometry change), the arrangement (i.e., single versus differential), the size of the sensor, the reachable resolution, and the type of readout circuit.[68] Chemiresistive or chemicapacitive sensors are straightforward to fabricate: a pair of parallel electrodes placed on a substrate and separated by a dielectric material, where the sensing component is coated or drop-cast to tune the electrochemical reactivity. An interdigitated electrode array is often used to adjust overall resistance or capacitance.

In attempts to mimic the olfactory receptors, a broad range of electrochemical sensors made of different materials have been explored and designed. The most widely used electrochemical sensors include metal oxide chemiresistive semiconductors (e.g., SnO_2),[69,70] organic field-effect transistors (OFETs),[71−74] conductive polymers of both inherently conductive (e.g., polythiophenes)[75] and those integrated with conductive particles (e.g., graphene− or carbon nanotube−polymer composite).[76−79]

There are several diverse types of electrochemical sensors that have been successfully used in a broad class of real-world applications; this, however, goes beyond the scope of this review. For more details of electrochemical sensors, the readers can refer to recent publications on environmental,[80] biosensing and immunosensing,[81−84] food and beverage,[85−87] clinical,[88,89] and security screening[90,91] applications.

The most common class of electrochemical sensors are metal oxide sensors (MOSs), a type of chemiresistors,[1,3,92] which are usually heated and react with volatile organic analytes to produce changes in electrical properties (e.g., resistivity or capacitance). The primary drawback of the use of traditional electrochemical sensors (e.g., unmodified metal oxide sensors or conductive polymers) for chemical sensing lies in the nearly indistinguishable sensor responses among similar analytes. This is due to the nature of those specific types of sensors in that they rely fundamentally on physical adsorption or nonspecific chemical interactions between the chemical analytes and the sensor receptors. The reliance on physical adsorption, in most cases, leads to poor selectivity of electrochemical sensors toward targeted analytes as well as interference from ambient humidity, which greatly restricts particularly the field usage of this type of sensor. In addition, baseline drift of sensor response resulting from aging also poses a major challenge to the development of electrochemical sensors.[93]

Surface modification of electrochemical sensor surfaces can provide for improved selectivity, especially for bioanalytical applications, for example with molecular imprinted membranes[94−97] or aptamers,[98−101] but at the expense of added complexity and susceptibility to drift from irreversible chemical reactions. Surface modification of electrochemical sensors has also had success using various nanostructures; the enhanced sensitivity is largely due to the extremely high surface area to volume ratio inherent to nanoparticles.[81,88] Nanowires, nanotubes, nanofibers, nanospheres, graphene, and other two-dimensional layered materials have thus far shown great promise, although selectivity among similar analytes can be problematic.[65,81] Hybrid structures of these nanomaterials are likewise excellent candidates for chemical sensors and have drawn significant attention in the past decade. Owing to the low dimensionality of the data resulting from most present incarnations of these sensors, engineering chemical selectivity into these systems remains the key to the future success for applications in chemical sensing or biosensing.

Another class of nonoptical sensors is based on the detection of small changes in the sensor's mass upon exposure to chemical analytes through physisorption of analytes onto the sensor or from specific chemical reactions of the analytes with the sensor. Mass sensors are generally microelectromechanical systems (MEMS).[102] A typical mass sensor is a piezoelectric resonator with an absorbing polymer or molecular receptor coating. Molecular analytes are adsorbed on or absorbed in the film of the sensor, increasing the mass of the sensor and thus decreasing in the resonant frequency. A typical example of mass sensors is the quartz crystal microbalance (QCM, also known as bulk acoustic wave sensors);[103−106] surface acoustic wave (SAW) sensors[107−109] are a related class of sensors based on two or more interdigitated transducers placed on the surface of a piezoelectric substrate that measure delay in surface waves from one transducer to a second through the piezoelectric. For a QCM, a quartz resonator is made by cutting along a particular crystal direction to endow the device with a thickness shear mode, which makes use of a shear wave that has extremely low velocity in the fluid.[105,110,111] Due to their effectiveness in the liquid phase, quartz crystal microbalances have been used for aqueous biosensing[104,112] and immunosensing.[106,113]

Arrays of QCM or SAW sensors have been used to detect and distinguish a wide range of chemical analytes, including industrial toxins, chemical hazards, and biomolecules such as organophosphates,[114] aromatic and halogenated hydrocarbons,[115−117] chemical warfare agents,[118] small molecular biotoxins,[113] and HCN.[119] QCMs have also shown promising results in the in situ analysis of solution supersaturation during cooling crystallization,[120] and the characterization of metallic or polymeric nanoparticle size achieves results comparable to those determined by transmission electron microscopy (TEM) or dynamic light scattering (DLS).[121]

1.2. Optical Sensors

Optical chemical sensors use infrared, visible, or ultraviolet light to probe chemical interactions at liquid or solid interfaces.[122] The classification of optical sensors is associated with the nature of the transduction mechanisms on which they are based, such as absorbance, scattering, diffraction, reflectance, refraction, and luminescence (including photo-, chemi-, electrochemi-, or bioluminescence). Different regions of the electromagnetic

DOI: 10.1021/acs.chemrev.8b00226
Chem. Rev. 2019, 119, 231−292

spectrum are employed with the use of different optical transduction methods, and a diverse set of parameters can be measured for each; these include intensity, lifetime, polarization, quantum yield, and quenching efficiency.[2,49]

In general, colorimetric and fluorometric sensors consist of four key elements: a light source, a wavelength selection device (e.g., filters or monochromator), a substrate or sample cell where changes in absorbed or emitted light occur in the presence of analytes, and a detector which is sensitive at the wavelength of interest (Figure 1). Most recently, rapid growth of the number of

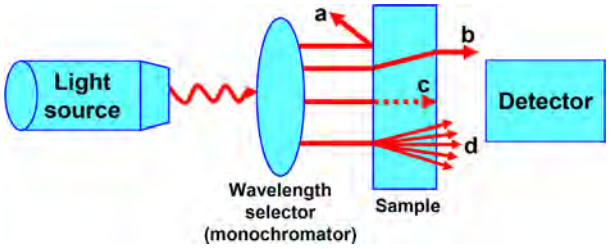

Figure 1. Scheme of a general spectroscopic setup: (a) reflection, (b) refraction, (c) absorption, and (d) fluorescence emission. Reproduced with permission from ref 62. Copyright 2013 Royal Society of Chemistry.

efficient and integrated optical sensors has greatly facilitated the development of new sensing platforms, including fiber optic sensors,[123−125] planar waveguide devices,[126] and sensors based on surface enhanced Raman spectroscopy (SERS).[127−129] This section will focus on the basis and classifications of colorimetric and fluorometric sensor arrays as well as their optical transduction methods involving UV−vis absorbance, reflectance, fluorescence, and nanoparticle-based surface plasmon resonance, along with the introduction of several new types of imaging platforms. There are other classes of optical sensors, based on chemiluminescent or bioluminescent systems, and these are discussed elsewhere in the literature.[130−132]

Fluorescence is the most commonly used spectroscopic method due to its higher sensitivity compared to most other optical sensors. Fluorescence occurs when an electron from a molecule is excited and then relaxes to the ground state by emitting a photon from an excited singlet state (Figure 2a); phosphorescence results instead when the excited singlet state first undergoes a forbidden transition to an excited triplet state, which then subsequently relaxes to the ground state (Figure 2b).[133,134] Fluorescence measurements take advantage of a variety of parameters (e.g., fluorescence intensity, anisotropy, lifetime, emission and excitation spectra, fluorescence decay, and quantum yield) for data analysis, thus conferring substantial flexibility to these approaches.[135,136] Generally, fluorescence techniques can be divided into three major classes: intrinsic fluorescence,[137−140] extrinsic fluorescence,[141,142] and differential fluorescent probes.[46,143,144]

Colorimetry, i.e., quantitative measurement of UV−vis absorbance or reflectance, is one of the oldest analytical methods,[145] dating back to even long before the beginning of chemistry with simple "naked-eye" observations: there are ancient Chinese medicine books, for example, that mention color changes of silver needles or spoons to detect poisons (e.g., arsenic sulfides) in food.[146] Colorimetric sensing is a fairly straightforward technique, and the advent of universal digital color imaging[32,50,58,147] has diversified portable and effective detection methods. While many colorimetric sensors make use of the traditional three-channel visible range (i.e., partially overlapping wavelength ranges corresponding to red, green, and blue, RGB), sensors can also use a larger number of channels with a narrower spectral range for each (i.e., hyperspectral imaging), incorporate nonvisible wavelengths from near IR to UV, or span this full wavelength range using hundreds of color channels (i.e., full spectrophotometry). To simplify data analysis and instrumentation, colorimetric methods often analyze spectra only at a few discrete wavelengths (e.g., by using RGB color imaging) or by selecting the highest peaks in UV−vis spectra.

There are two fundamental requirements for the design of optical sensors: they must be able to interact at least somewhat selectively with analytes, and they must report or provide feedback on such interactions through chromophores or fluorophores, preferably with very high extinction coefficients or high quantum yields, respectively. Such optical sensors may be semiselective (i.e., cross-reactive with multiple analytes) or

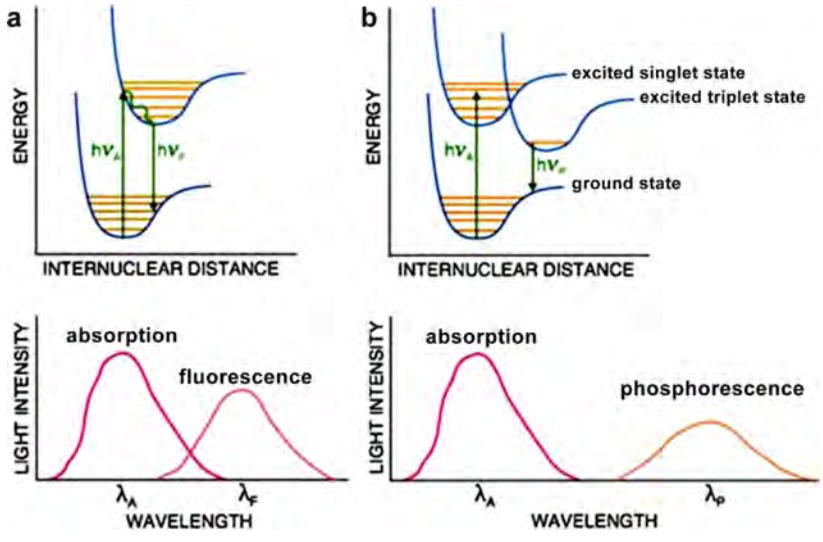

Figure 2. Electronic transition leading to (a) fluorescence emission at λ_F and (b) phosphorescence emission at λ_P. Adapted with permission from ref 1. Copyright 2009 Springer.

DOI: 10.1021/acs.chemrev.8b00226
Chem. Rev. 2019, 119, 231−292

highly selective (i.e., specific for only a single analyte or class of analytes). Structurally, optical sensors must thus contain a probe moiety to provide some degree of molecular recognition through interactions with the analytes and a reporter moiety for optical transduction; a single molecule may (and often does) serve both purposes. Dyes (i.e., molecular chromophores) and nanoporous pigments (i.e., insoluble colorants) are often chemoresponsive; that is, their colors (or fluorescent properties) are dependent upon their chemical environment. pH indicators are an obvious early example.[148−150] In general, pigments, even as micrometer sized solid particles, do not act well as sensors because the very large majority of chromophores are not accessible to analytes; a notable exception is the class of nanoporous pigments, where the colorant centers are exposed to analytes.[151−154]

While many chemical dyes and fluorophores satisfy the requirements of semiselective sensors, there are also a considerable number of sensors (especially supramolecular receptors) that interact very selectively with specific analytes but do not respond via changes in their optical spectra. Macrocyclic structures including cyclodextrins, calixarenes, cyclophanes, crown ethers, cryptands, and cucurbiturils are generally spectroscopically inactive but often display excellent molecular recognition of guest species (e.g., ions and neutral ligands).[155−157] In order to convert these supramolecular receptors into sensors, suitable chromophores or fluorophores need to be attached to the macrocycle in a fashion that leads to changes in optical signals upon analyte binding.

For example, a Li^+-specific sensor based on a novel lithium fluoroionophore and its polymer derivative has been successfully applied to the clinical monitoring of cation concentrations in blood (Figure 3).[158] The fluoroionophore is built on a

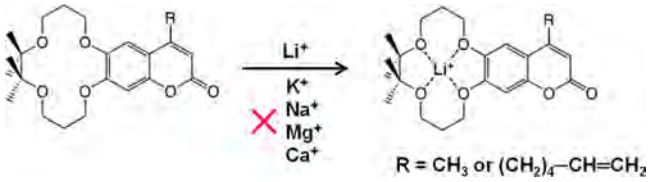

Figure 3. Structure of fluoroionophore that shows selective binding to Li^+. Reproduced from ref 158. Copyright 2007 American Chemical Society.

tetramethyl "blocking subunit" of a 14-crown-4 as a selective binding site of Li^+, and 4-methylcoumarin is employed in this case as a fluorophore. The sensor permits ratiometric detection via the characteristic blue shift and quenching of the fluorescence emission toward Li^+. The sensor also exhibits good reversibility and is free from the interference of pH change and the other major biological cations (e.g., K^+, Ca^{2+}, and Mg^{2+}).

2. OPTICAL ARRAY SENSING: CONCEPTS AND SENSORS

The mammalian olfactory system allows for the discrimination among a huge number of chemical compounds or composite mixtures over an enormous range of concentrations. Such high specificity and efficiency derive from the pattern recognition by the forebrain's olfactory bulb of the responses from hundreds of different types of olfactory receptor epithelial cells.[159] This type of molecular recognition is exactly an opposite case to the traditional prototype of biospecificity, i.e., the lock-and-key model of enzyme−substrate interaction. Optical array sensing, in a similar manner, can incorporate a wide range of cross-reactive sensor elements for pattern-based interactions with any given set of analytes.

2.1. Basis of Intermolecular Interactions

In applying the concept of pattern recognition to sensor arrays, the selection of intermolecular interactions is critical to the construction of effective colorimetric or fluorometric arrays. Fundamentally, chemical sensing is molecular recognition, and molecular recognition is the consequence of interactions between molecules.[160−162] As shown in Figure 4, there is a

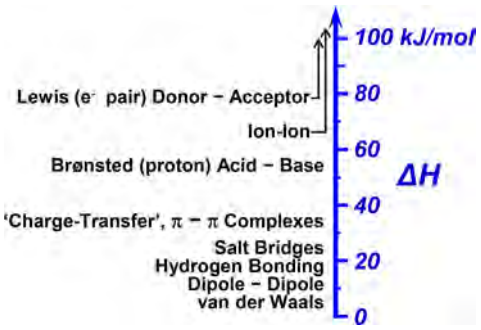

Figure 4. Strength of physical or chemical intermolecular interactions on a semiquantitative scale of enthalpy change. Such interactions are on a continuum from the very weakest van der Waals to the very strongest covalent or ionic bonds. Reproduced with permission from ref 62. Copyright 2013 Royal Society of Chemistry.

wide range of different types of intermolecular interactions that generate a continuum in strength of interaction (i.e., change in enthalpy), from the weakest of interactions such as van der Waals force to the strongest of covalent or ionic bonds. There is a seamless transition from electrostatic ionic bonding, covalent or coordination bond formation, Brønsted or Lewis acid−base interactions, hydrogen or halogen bonding, charge-transfer and $\pi-\pi$ stacking complexation, dipolar or multipolar interactions, and van der Waals and other nonspecific interactions (e.g., quadrupole−dipole).

The advantage of incorporating stronger interactions for sensor arrays is to achieve both greater intrinsic sensitivity and greater chemical selectivity. Coordination of some Lewis base analytes (e.g., amines, thiols) gives a relatively high enthalpy change ranging from ∼40 to ∼300 kJ/mol. In contrast, the enthalpy change of physical absorption of analytes (e.g., into conductive polymers) or adsorption (e.g., onto the surface of metal oxide semiconductors) is only ∼5 to 10 kJ/mol. The equilibrium constant of a typical coordination effect to metal ions is $\sim 10^4$ times higher than that of a typical physisorption process. More importantly, stronger interactions bring a much wider range of chemical interactions than simple physical absorption, and therefore one may probe a much higher dimensionality and greatly improve the capability of distinguishing highly similar compounds or complex mixtures.

Remarkably, almost all prior electronic noses (i.e., metal oxide or conductive polymer sensors) relied exclusively on van der Waals or physical adsorption as the primary interaction of analytes with the sensor: these are the weakest and least specific of sensor−analyte interactions. Disposable colorimetric sensor arrays, however, provide a successful approach to overcome the limitations of nonspecific interactions and to negotiate the opposite trend in sensor sensitivity vs robustness, as discussed in section 1. Colorimetric sensor arrays revisit an earlier, pre-

DOI: 10.1021/acs.chemrev.8b00226
Chem. Rev. 2019, 119, 231−292

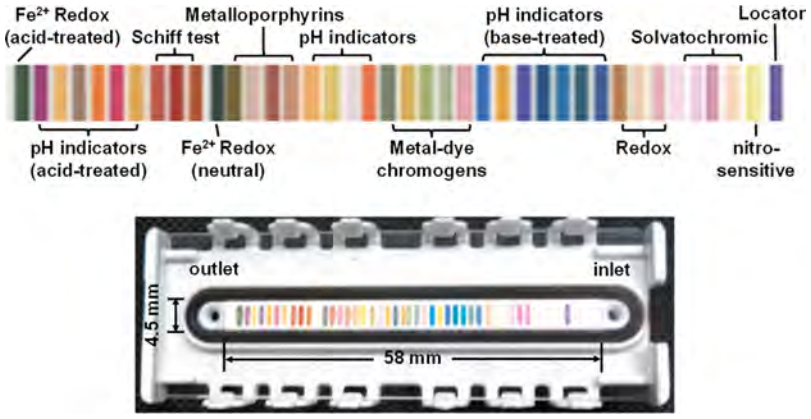

Figure 5. Example of a 1 × 40 linearized colorimetric sensor array using a wide range of chemical dyes, and cartridge packing of the array for gas sensing. Reproduced with permission from ref 32. Copyright 2016 Royal Society of Chemistry.

electronic era of analytical chemistry in many aspects,[148,163−165] but with the addition of modern digital imaging imaging platforms for accurate, prompt, and reproducible data quantification.[50,58,166−168]

Based on the chemical properties of sensor elements, an array can probe a range of analyte−sensor interactions to generate a wide span of molecular specificity.[27,169] At one end, there are individual sensors that are fairly "promiscuous", i.e., highly cross-reactive but less specific; these include polymers and polymer blends with optical receptors that adsorb analytes primarily based on hydrophobicity.[170,171] Promiscuous sensors can contribute to the overall response of the sensor array but are insufficient to provide deep differentiation among similar analytes. At the other end, there are highly selective, or "monogamous" sensors that respond exclusively to one analyte or perhaps one closely related class of analytes. While monogamous receptors can produce high specificity for specific analytes, alone they will not form a sensor array that enables the recognition of other groups of analytes and mixtures;[172] in addition, the design and synthesis of such specific, "monogamous" sensors can be time-consuming and complicated. The optimum optical sensor array will therefore incorporate a range of colorimetric or fluorometric sensor elements with a diversity of specificities and a wide range of chemical interactions.

2.2. Classification of Colorimetric and Fluorometric Sensor Elements

As mentioned, two structural features are essential to the design of colorimetric or fluorometric sensors: functionality sites to interact with analytes, and a chromophore or fluorophore to couple with the active site. The first factor implies that it would be highly advantageous to have multiple classes of strong chemical interactions involved, other than simply van der Waals or physisorption.

Based on the types of intermolecular interactions that can induce significant colorimetric or fluorometric changes, one may divide cross-reactive, chemoresponsive dyes into five classes (albeit with some overlap): (i) Brønsted acidic or basic dyes (e.g., various pH indicators), (ii) Lewis acid/base dyes (e.g., metal complexes with open coordination sites or metal-ion-containing chromogens), (iii) redox dyes, (iv) colorants with large permanent dipoles (i.e., zwitterionic vapochromic or solvatochromic dyes) for detection of local polarity or hydrogen bonding, and (v) chromogenic aggregative materials (e.g., plasmonic nanoparticles and nanoscale transition metal sulfides). In addition, the matrix holding those dyes also can play a role in the improvement of their chemical selectivity, either by modifying the local environment of the dye or by immobilizing the dye molecules in a sterically confining surrounding (e.g., molecularly imprinted polymers). The early versions of colorimetric sensor arrays[50,173] were made of porphyrins and metalloporphyrins as sensor components and utilized mainly Lewis interactions with the metal and Brønsted interactions with the free base porphyrins. With the addition of a wider range of chemical dyes, the diversity of sensors has been impressively broadened over the past decade.[27,169] For example, a recently developed 40-element sensor array comprising a wide range of chemoresponsive dyes has shown promising applications in the detection of toxic or explosive vapors (Figure 5).[27,32,174,175]

The choice of individual sensor elements in an colorimetric or fluorometric sensor array is fundamentally determined by its intended use: for example, is the array meant for a broad range of analyte detection or will it be used for a specialized class of analytes only? If one uses probes that only measure local polarity (e.g., solvatochromic or vapochromic fluorescent probes doped into various polymers[176]), then one may lose the opportunity for effective detection of different, but somewhat similar polar compounds. Keep in mind that potential analytes vary in many aspects of their chemical properties: solubility, hydrophilicity, redox, hydrogen bonding, Lewis donor/acceptor, and proton acidity and basicity of targets need to be taken into account. In general, a comprehensive optical sensor array for general sensing purposes should integrate as much chemical diversity among the individual sensor components as possible. Given the presence of metal ion binding sites in the olfactory receptors themselves,[10−12] inclusion of metal-ion-containing dyes plays an important role in the construction of a chemoresponsive sensor array. One must also consider the presence of possible interferents by ambient, complex environments that may cause false positive responses. Finally, the dye properties themselves must be considered: stability of the printed dyes, printability of the dye formulation, and quantitative contribution of the dye to both the responsiveness and the dimensionality of the array. While these criteria can be applied quantitatively in evaluating the importance of the addition of a new dye to the array, fundamentally the tests are empirical and screening of dyes and dye formulations is inescapable.

2.2.1. Lewis Acid/Base Dyes. *2.2.1.1. Lewis Acidic Dyes.* Most of the strongly odiferous compounds are Lewis bases: amines, carboxylic acids, sulfides, and phosphines. Not

DOI: 10.1021/acs.chemrev.8b00226
Chem. Rev. 2019, 119, 231−292

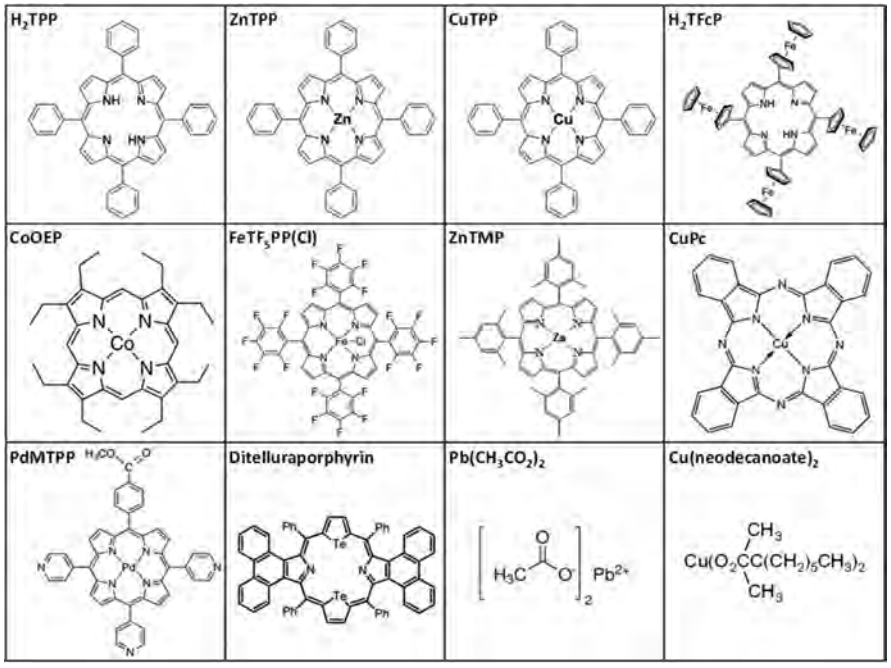

Figure 6. Structures of representative chemoresponsive dyes, including porphyrins or porphyrinoids, and others containing Lewis acid metal ions.

coincidentally, these are also among the most common volatile metabolites of microbes; arguably, the primary function of the olfactory system is to keep our body away from high concentrations of bacteria or other microorganisms, and hence the location of our nostrils immediately above the mouth! Inspired by the important role that metal-binding sites of olfactory receptors play in sensing such Lewis bases,[10−12] Lewis acid dyes are an obvious sensor choice.

Among Lewis acidic dyes, metalloporphyrins[50,61,177−180] are a popular choice for the detection of metal-ligating volatiles due to the open axial coordination sites and the large color changes from both wavelength and intensity shifts of strong $\pi-\pi^*$ absorbances upon ligand binding. Metalloporphyrins can be readily modified to adjust their chemical reactivity by changing metal centers or peripheral substituents to provide shaped pockets that restrict the access to the metal binding sites. This steric effect was first explored by the Collman group[181,182] using picket-fence Fe(II) porphyrins for reversible binding of O_2, and later expanded by other groups. Of special interest was Suslick's development of a series of shape-selective, bis-pocket metalloporphyrins[183−189] that display distinctive steric hindrance toward bonding sites, thus demonstrating potential uses as colorimetric sensors in the discrimination of linear vs branched amines.[173] A wide range of both ligating volatile organic compounds (VOCs) (e.g., amines, carboxylic acids, phosphines and phosphites, thiols) will generate large color changes with metalloporphyrin sensors.[50,61,177−180]

Indeed, examples of metalloporphyrins as strong Lewis acid indicators can be found in daily life. The difference in color of scarlet red arterial blood versus the purple of venous blood is a natural example of the colorimetric detection of O_2 using porphyrins. In addition to the intrinsic binding, porphyrins also possess excellent solvatochromic properties that lead to distinguishable colorimetric changes before and after interactions even with analytes that lack strong ligating functionalities (e.g., arenes, halocarbons, or ketones).[50] Therefore, metalloporphyrins and their derivatives are an ideal group of dyes for colorimetric[50,61,177,180,190] or fluorometric[167,191] (for d^{10} transition metals primarily) detection of metal-ligating volatiles. Representative examples of porphyrins, porphyrinoids, and other types of Lewis acid/base dyes that have been used as optical sensors are shown in Figure 6.

2.2.1.2. Lewis Acidic Dyes for Anion Detection. The coordination of anions was a long-overlooked area of inorganic chemistry. The biological and medical significance of many anions, from the simple (Cl^-, F^-, NO_3^-, PO_4^{3-}, $H_2PO_4^{2-}$, etc.) to the complex (e.g., ATP, lipid anions, nucleic acids, and other phosphorylated biomolecular ions), has demanded and received much greater attention in recent years.[192] Anion recognition chemistry also plays an essential role in catalysis and environmental sciences.

Recently, substantial efforts have been made in the design of anion receptors for sensing by colorimetric or fluorometric means. The use of Lewis acidic dyes for the detection of anions has been extensively reviewed recently.[193−208] Unique challenges still remain in anion complexation. Anion receptors can be neutral or positively charged and anion−receptor interactions are often dominated by electrostatic forces or hydrogen bonding. To build an anion sensor, one can use a Lewis acid that is inherently fluorescent or combine a chromogenic or fluorescent reporter moiety with a specific chelating receptor.

Dye displacement assays, indicators with urea, thiourea, or naphthalimide, and metal ion containing chromogens (especially lanthanide and labile d^8 and d^{10} transition metal ions), have been extensively explored in the past few years for the colorimetric or fluorescent detection of anions.[209−212] As an example, Kakuchi and co-workers have developed a novel poly(phenylenebutadiynylene) fluorescent probe that contains urea functionalities for anion detection (Figure 7).[213] A fluorescence turn-on response is ascribed to an anion-triggered disassembly process of the initially formed polymeric aggregates. The sensor allows for accurate discrimination of eight different anions at ∼1 mM with distinct fluorescent intensities. Using aggregated polymers with rationally designed functionalities as

DOI: 10.1021/acs.chemrev.8b00226
Chem. Rev. 2019, 119, 231−292

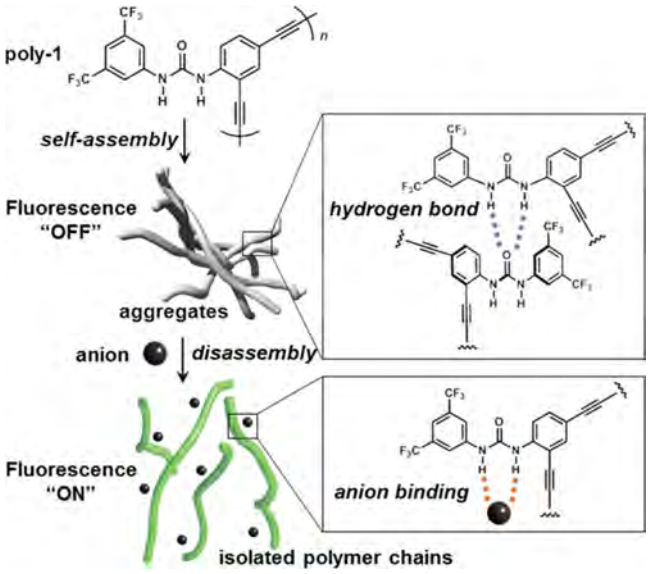

Figure 7. Schematic illustration of fluorescence turn-on sensing of anions based on disassembly of initially nonfluorescent (self-quenched) polymer aggregates upon anion binding. Reproduced from ref 213. Copyright 2012 American Chemical Society.

novel sensor elements has proven to be a promising strategy for anion sensing and contributes greatly to the understanding of supramolecular chemistry of anions.

2.2.1.3. Lewis Basic Dyes for Cation Detection. Lewis bases include mostly chelating and macrocyclic ligands that can have extremely high affinities for Lewis acids. Modern supramolecular chemistry finds its origins in the design of crown ethers, cryptands, cyclodextrins, and calixarenes, whose sizes govern their specific binding of metal ions.[155−157] Indeed, the beginning of the use of semispecific chelating Lewis acidic dyes as colorimetric sensors for metal cation detection,[158,214−217] or so-called complexometric indicators (Figure 8),[218] dates back over 150 years. Many of the traditional complexometric indicators were discovered in the early 19th century from nature products and are widely manufactured and used as histological stains nowadays.

Complexometric indicators[219,220] have chelating sites that enable strong coordination with metal ions and induce a rapid color change, often with significant selectivity among possible metal ions. These ionochromic dyes, or p*M* indicators (as a class of analogues to pH indicators) are designed to bring about a color change during the interaction any given metal ion.[216,221] Complexometric indicators, depending on their chemical structure, may have greater or lesser degrees of specificity: as examples, Eriochrome Black T is used to detect Ca^{2+}, Mg^{2+}, and Al^{3+}; calcein is used for Ca^{2+}; hematoxylin is used for Cu^{2+}; murexide is used for Ca^{2+}, Ni^{2+}, and rare earth ions; and xylenol orange is used for Ga^{3+}, In^{3+}, and Sc^{3+}. The classical complexometric titrations are on the basis of displacement reactions, which start with the metal ions bound to the indicator and then replaced by the addition of EDTA, so the free dye molecule (rather than the metal ion complex) acts as the end point indicator. The limited selectivity of indicators and the presence of multiple pK_a values of the chelators, however, usually require the addition of masking agents and a careful control of pH during the titration. Those strict requirements call

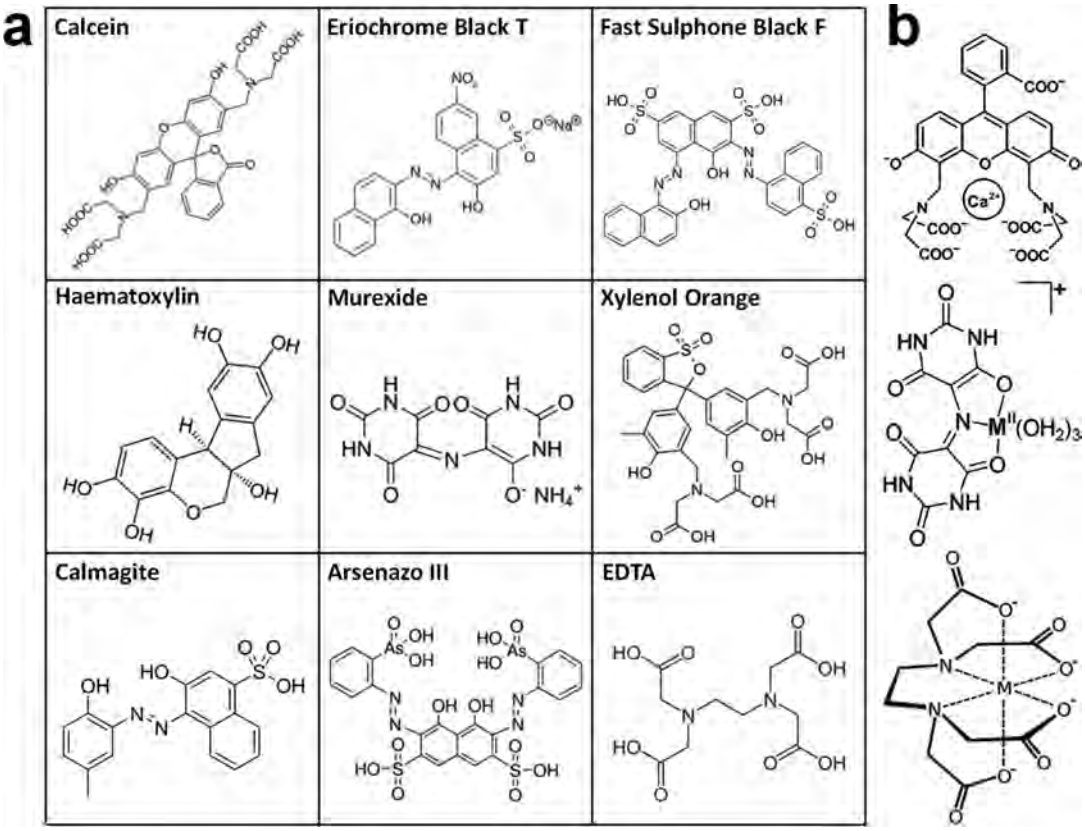

Figure 8. Complexometric indicators. (a) Several traditional indicators used for complexometric titrations. (b) Representative metal complexes of calcein, murexide, and EDTA, from top to bottom.

DOI: 10.1021/acs.chemrev.8b00226
Chem. Rev. 2019, 119, 231−292

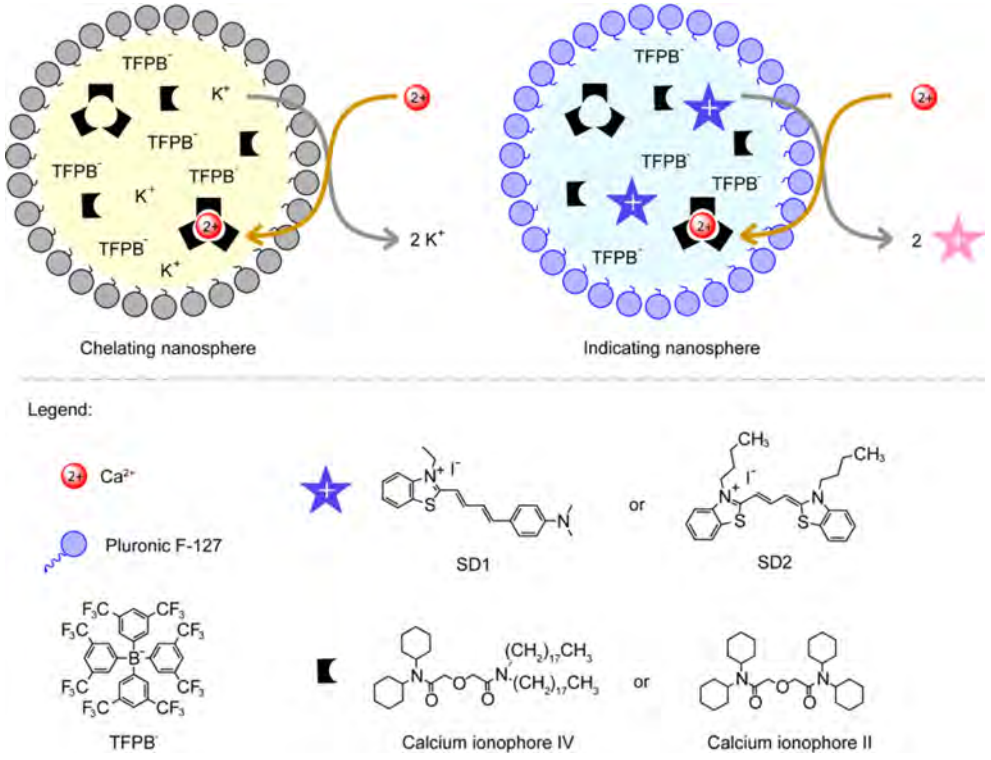

Figure 9. Schematic illustration of ion-selective nanospheres for complexometric titration of Ca^{2+}. Solvatochromic dye resides in the nanospheres when no Ca^{2+} is present, while it is exchanged by Ca^{2+} into the aqueous solution at the end point, with a color transition from blue to pink. Reproduced from ref 224. Copyright 2015 American Chemical Society.

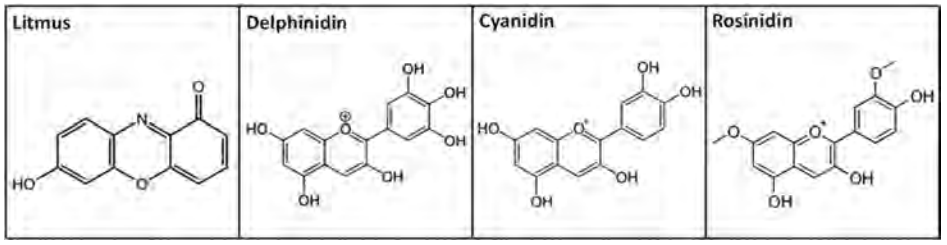

Figure 10. Some naturally occurring pH indicators. Litmus is from a lichen, delphinidin from cabernet sauvignon, cyanidin from blueberries, and rosinidin from rose periwinkle.

for a new design of complexometric indicators that are pH independent, sensitive, and selective. Recent advances in this area have taken advantage of either cross-reactivity of solution-based arrays of complexometric indicators, or pH-independent titration in a heterogeneous phase rather than a homogeneous aqueous phase. Successful examples include the use of a microtiter plate,[222] an immersed membrane,[223] and, very recently, an emulsified nanosphere[224,225] for selective recognition of individual metal ions in water.

As a recent example using a nanosphere emulsion, Bakker and co-workers developed pH-independent "optode" nanospheres as indicators for complexometric titrations (Figure 9), which can accurately quantify Ca^{2+} concentration in mineral water without interference from other metal ions.[224] The nanospheres contain an ionic solvatochromic dye, ion exchanger, and ionophore: only the solvatochromic dye will be expelled into the aqueous solution at the end point, resulting in a significant colorimetric change. The titration curves are independent of pH change and have sharper end points than with previously reported complexometric sensors or any similar indicators.

2.2.2. Brønsted Acid/Base Dyes. The origins of chemistry as a discipline are closely related to our obsession with "pretty colors", and the contribution of the dye industry to the early development of chemistry cannot be understated.[226−228] The colors of Brønsted acids or bases are pH-dependent; i.e., their UV−vis absorption spectra change through protonation or deprotonation as the pH changes. Litmus, or 7-hydroxyphenoxazone, is a representative pH indicator that was available to alchemists even in medieval times; litmus literally means "colored moss" in Old Norse, which is extracted from a mixture of lichens, particularly *Roccella tinctoria* in South America. There are dozens of pH indicators that can be obtained naturally from many plants, especially the anthocyanin dyes that are abundant in blueberry, raspberry, black rice, red cabbage, and black soybean (Figure 10).

Synthetic pH indicators received tremendous attention during the first half of the 20th century,[148] but even now there is substantial exploration of new pH indicator formulations.[149] For example, there are recent developments of indicator nanoprobes using indicators immobilized in polymer hydrogels for intracellular sensing,[229] and a wide range of organic

DOI: 10.1021/acs.chemrev.8b00226
Chem. Rev. 2019, 119, 231−292

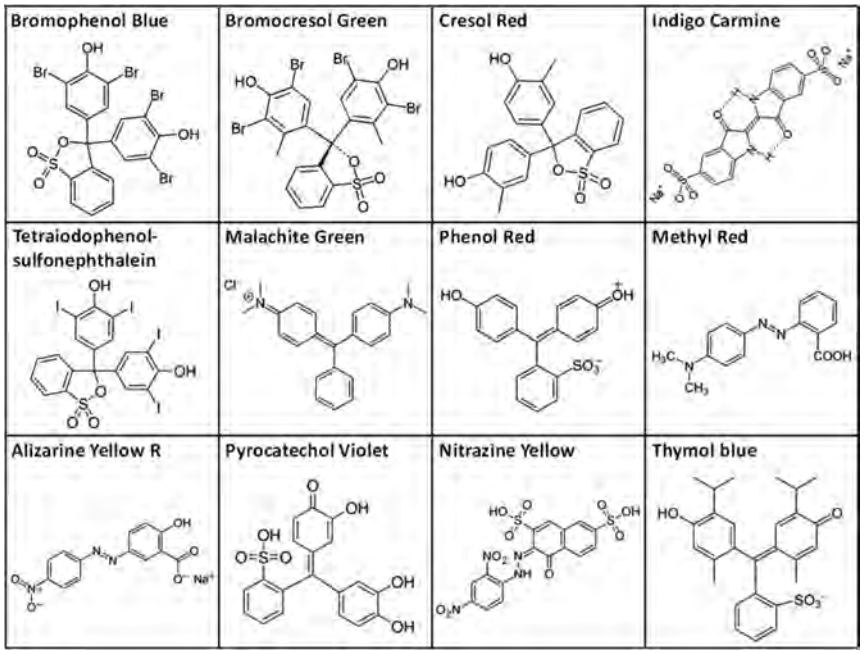

Figure 11. Several some typical pH indicator dyes.

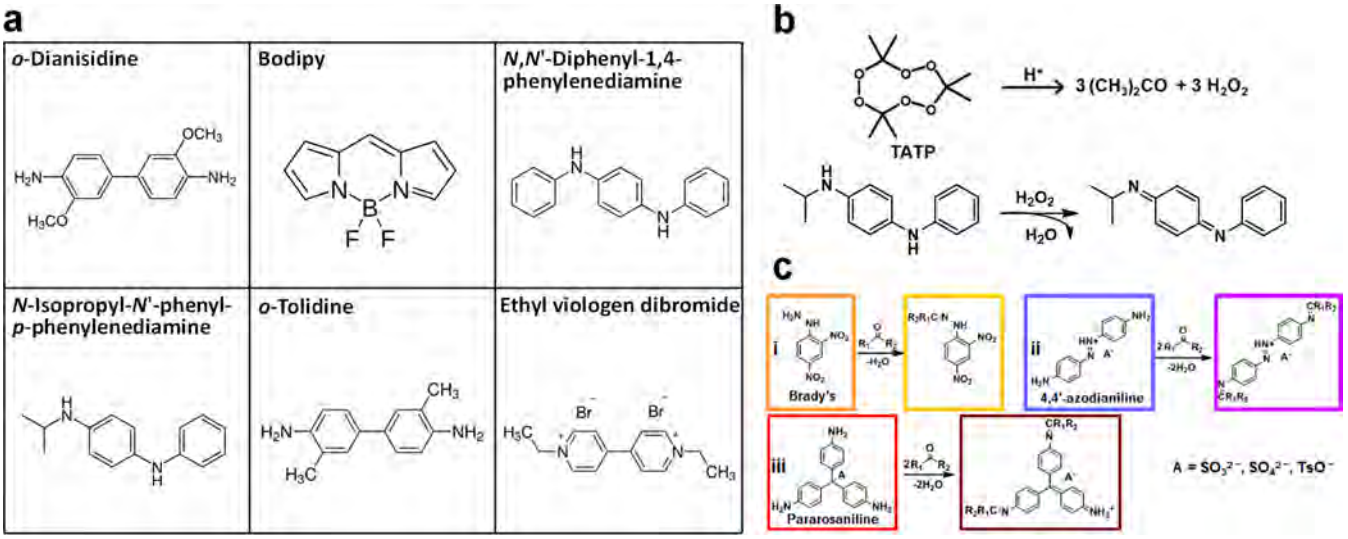

Figure 12. Structures of some common pH-independent redox dyes. (a) Six representative redox dyes. (b) Detection mechanism of triacetone triperoxide (TATP) using *N*-isopropyl-*N*′-phenyl-*p*-phenylenediamine. (c) Colorimetric recognition of general aldehydes and ketones using 2,4-dinitrophenylhydrazine, 4,4′-azodianiline, and pararosaniline. Reproduced from ref 242. Copyright 2010 American Chemical Society. Reproduced with permission from ref 243. Copyright 2017 Wiley.

chromophores (e.g., azo dyes, triphenylmethane dyes, nitrophenols, phthaleins, sulfophthaleins, aniline-sulfophthaleins) have been prepared to determine the pH of aqueous solutions or as histological stains for biological uses.[230,231] The pK_a values among various pH indicators in aqueous solutions range, of course, from below 0 to above 14, depending on the ease of protonation or deprotonation. The examples of some pH indicators that have been incorporated in colorimetric sensor arrays are shown in Figure 11.

2.2.3. Redox Indicator Dyes. Reduction/oxidation (redox) indicators are colorimetric reagents which provide a characteristic color change at a specific electrode potential.[232−236] There are a large number of organic dyes exhibiting reversible redox reactions, including bodipy, *o*-dianisidine, diphenylamine, eriogreen, fenamic acid, methylene blue, Nile blue, and 2,2′-bipyridine.[237−240]

Due to the participation of protons in the electron transfer process in most media, redox indicators are sometimes classified into two groups by whether they are pH dependent or not. For example, to build an optical sensor for sensitive and accurate determination of glucose (i.e., in the concentration range 10^{-6}–10^{-2} mol/L, with high reproducibility), a thionine-based reversible redox sensor was immobilized on gel beads to monitor the level of byproducts (e.g., a coenzyme, NADH) involving enzymatic redox reactions of glucose.[241] A linear calibration range of 5.7×10^{-4}–2.0×10^{-3} mol L^{-1} was achieved for glucose, with a relative standard deviation of <5%. As another example, to detect triacetone triperoxide (TATP) vapor at sub

DOI: 10.1021/acs.chemrev.8b00226
Chem. Rev. 2019, 119, 231−292

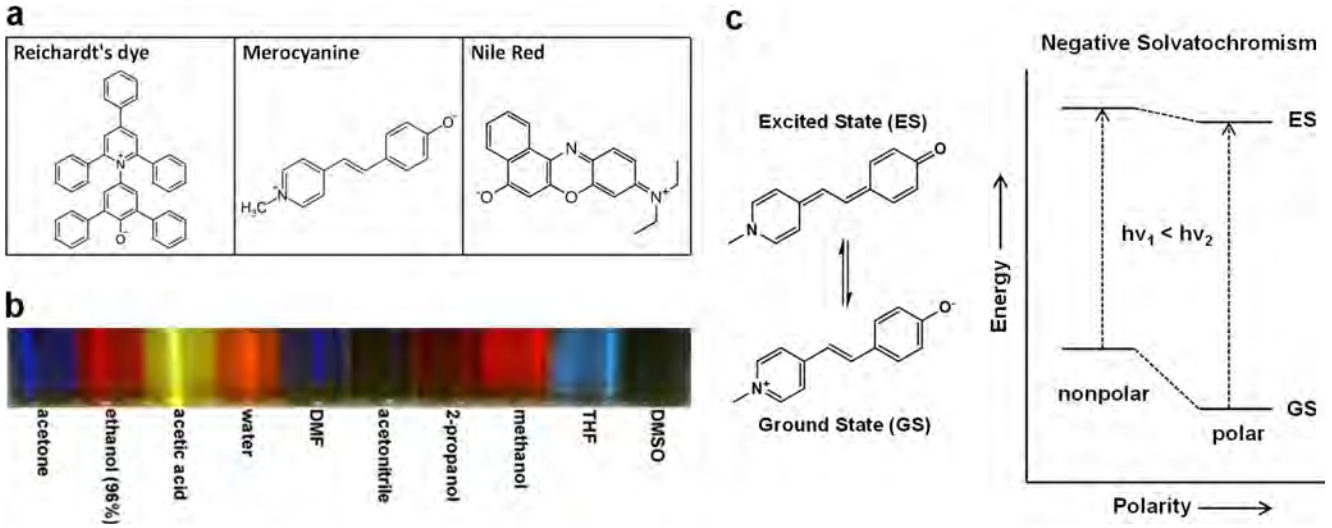

Figure 13. Structure of some representative solvatochromic dyes. (a) Three typical solvatochromic dyes. (b) solvatochromic shifts of a merocyanine dye, 1-methyl-4-[(oxocyclohexadienylidene)ethylidene]-1,4-dihydropyridine, in various solvents with different polarities. (c) Frontier orbital energy changes for negative solvatochromism (e.g., as in merocyanine dyes).

parts per million levels (i.e., in the range from 50 ppb up to several parts per million), a colorimetric sensor array comprising *o*-dianisidine, diphenyl amine, *N*-phenyl-1,4-phenylenediamine, *N*,*N*′-diphenyl-1,4-diphenyldiamine, and Lissamine Green B (Figure 12) was constructed by Lin and Suslick.[242] Using a solid-state acidic catalyst that enables the decomposition of TATP to more detectable species (i.e., hydrogen peroxide and acetone), the array was capable of detecting vapor concentrations of TATP below 2 ppb and distinguishing TATP from other chemical oxidants.

2.2.4. Solvatochromic or Vapochromic Dyes. Solvatochromic or vapochromic dyes[244−247] undergo color changes in response to changes in the polarity of the local environment; the mechanism comes from differential stabilization of the more polar of the ground or excited states of the chromophores. If the excited state has a larger dipole moment than the ground state, it will be more stabilized relative to the ground state in a more polar environment—positive solvatochromism—and vice versa. Nearly all dyes intrinsically show more or less solvatochromic properties. Optimal solvatochromic dyes have the largest changes in dipole moments. The spectral changes can be so large that dramatic color or fluorescence changes will be observed, depending on the polarity of the solvent where the dye is dissolved (Figure 13).

Common classes of solvatochromic dyes include the merocyanines, azobenzenes, thiazines, oxazones, nitro-amino-substituted polythiophenes, and pyridinium *N*-phenolate betaine dyes (Figure 13). A common structural feature of most solvatochromic dyes is that they have "push−pull" structures with a strong zwitterionic component to their electronic structure, i.e., a large conjugated π system with strong electron donor groups at one end and strong electron withdrawing groups at the other.

A series of solvent polarity scales[244] have been proposed to quantify the interactions between solvatochromic dyes and solvent molecules. Different physicochemical properties can be used to define such scales, including both single-parameter approaches that solely depend on equilibrium constant, reaction rate constant, or wavelength shift, and multiparameter approaches that combine several properties. Some important polarity scales include Reichardt's $E_T(30)$, Brooker's χ_R scale, and Taft's π^* scale.[244−247] A cross-reactive colorimetric sensor array comprising solvatochromic dyes in semiliquid matrices was reported by Suslick and co-workers that enables successful identification of 11 common organic solvents, with polarities evenly distributed over a broad range of $E_T(30)$ values.[176] Solvent polarity is a multiparameter property that is determined by dipolar, quadrupolar, and multipolar interactions, hydrogen bonding donor and acceptor properties, Lewis acid−base interactions, etc. Studies on the thermodynamic and theoretical analysis of the origin and mechanism of solvation, solvent polarity, and solvatochromism are carried out actively;[246−248] especially useful are interrelations and comparisons between different solvent scales and new methodologies to relate scales to theoretical descriptors.[249,250] Of particular interest for optical sensors, innovations in the structures of solvatochromic dyes, such as the design of phenol-linked imidazole derivatives that exhibit remarkable color change via proton tautomerism, have shown potential uses as the next generation of solvatochromic dyes in the construction of environmental stimuli-responsive materials.[251] In addition, sensor arrays using primarily solvatochromic dyes have been examined for identification and purity of organic solvents from a head-gas analysis.[176] Solvatochromic probes in combination with bioimaging technologies have also been extensively explored for the detection of a wide range of biomolecules involving nucleic acids, proteins, and biomembranes.[252]

A separate class of solid-state materials that can change color in response to solvent vapors are referred to as vapochromic or vapoluminescent solids. A number of organometallic or coordination complexes have been identified as vapochromic pigments, the majority of them coming from square planar Pt(II) and Au(I) compounds.[253,254] The vapochromism is induced by intercalation of solvent molecules into the crystals, and the color or luminescence changes stem from relatively weak interactions within the solids including coordination of solvent molecules to the metal binding sites, $\pi-\pi$ stacking, hydrogen bonding, and general nonspecific host−guest interactions; these interactions can lead to changes in the ordering of excited states and therefore cause significant luminescent differences. Chiral

DOI: 10.1021/acs.chemrev.8b00226
Chem. Rev. 2019, 119, 231−292

vapochromic complexes have been used for enantiomerically selective detection of chiral solvent vapors.[255] A particularly remarkable example has been recently reported using a chiral C_3-symmetric Cu(I) cubane cluster, $[Cu_4I_4(TMP)_4]$ (TMP = tris(3-methylphenyl)phosphine), which possesses excellent properties in luminescent thermochromism, solvatochromism, and vapochromism.[256] The limitations of vapochromic materials, however, remain in the very slow response time due to the slow diffusion of vapor molecules into the solid materials, and the weak interactions involved that restrict their selectivity and sensitivity as sensors. One potential solution is possibly to develop nanoscale and porous coordination complexes that may efficiently reduce diffusion time and expand surface area for analyte exposure, thus enhancing interactions occurred at the solid−gas interface.

2.2.5. Chromogenic Aggregative Indicators. The synthesis of chromogenic indicators whose color is induced by particle aggregation has become a hot area of research and has achieved massive progress in recent years. The early version of aggregative indicators, e.g., simple precipitation of metal salts or formation of metal nanoclusters upon reactions with sulfides, indeed derives from classical qualitative spot tests.[163−165] In recent developments, nanomaterials of all sorts,[257−263] including metallic and metal oxides, carbon-based nanotubes, graphene variants, carbon dots, or quantum dots, have been employed as chromogenic aggregative probes and widely applied to biosensing or immunosensing.[264−267] Processes that cause aggregation, dispersion, or formation of colloidal materials generate changes in color or fluorescence through multiple optical mechanisms, including the simple absorption or scattering of colloidal particles, plasmonic absorbance, aggregation-caused quenching (ACQ), or aggregation-induced emission (AIE) of luminescence.[257]

Critical to the use of chromogenic aggregative sensors is control over the nanostructure of the sensing nanomaterials. For example, a fluorescent "off−on" type probe can be built on gold, silver, or copper nanoparticle agglomerates[263] that effectively quench attached or adsorbed fluorophores, while fluorescence will be recovered with the release of fluorophores or dispersion of agglomerates induced by analyte binding.[268−271] Prudent choice of particle functionalization and of fluorophore provides a versatile platform for solution phase sensing.

2.2.6. Displacement Strategies for Fluorescent Sensors. In general, there are three classes of fluorescent probes for chemical sensing in solution: (i) intrinsic probes (where the sensor is itself fluorescent); (ii) conjugated or extrinsic probes (where a fluorophore is attached or conjugated to the sensor binding site and its fluorescent property is modulated by analyte binding); (iii) displacement or differential probes (where the analyte species competitively binds to an artificial or natural receptor that has already bound a fluorophore, and the release of the fluorophore causes a change in the fluorescent signal).[46,143,144,272−275] Displacement probe strategies require a reversible interaction between a receptor and a reporting fluorophore/chromophore; the binding of the receptor molecule must trigger differences in fluorescence or UV−vis absorbance of the reporter; the receptor can be designed to be either highly specific for a certain class of analytes or more promiscuous if used as part of an array.

Indicator displacement assays that use a parallel set of multiple not-too-selective displacement probes are often referred to as of differential selectivity and generate a pattern of responses somewhat similar to the aforementioned, cross-reactive colorimetric sensor arrays. This strategy has been well-established by the Anslyn group in the recent decade.[143,144,272,273,276] A potential disadvantage of displacement methods is diminished sensitivity due both to the requirement of reversibility of the fluorophore binding and to the necessary binding competition between the incoming analyte and the already bound fluorescent or colorimetric reporter.

Sensor arrays are normally thought of as single physical solid devices, e.g., a printed solid-state sensor array on substrates such as a polymer membrane or a set of fiber optic probes. Displacement strategies, however, are generally limited to solution phase sensing and do not lend themselves easily to a printable sensor array that could be immersed in a solution of analytes. Instead, solution phase array sensing has to be carried out by parallel analyses of multiple aliquots of the analyte solution, each with an added, distinct homogeneous probe, e.g., using microwell plates with a microwell fluorescent scanner.

As an example, Anslyn and co-workers have cleverly employed different commonly available serum albumins with a set of fluorophores as nonspecific probes for hydrophobic molecules.[48,172,277,278] In this case, nonspecific hydrophobic binding interactions were combined with an indicator displacement strategy to provide multiple sites for AIE-active (aggregation-induced emission) probes within a single albumin framework, as shown in Figure 14. This led to the sensor's capability of classifying hydrophobic, structurally similar species, i.e., edible oils.[172,279]

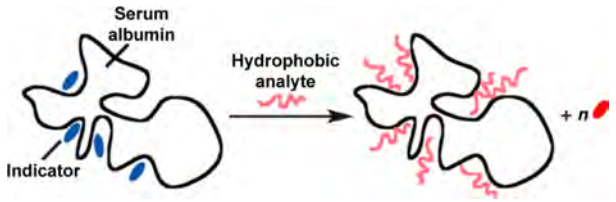

Figure 14. Schematic representation of a displacement strategy using serum albumin proteins as a nonspecific receptor to detect hydrophobic analytes. Indicators are initially bound in disparate binding sites of albumin proteins, and significantly increased fluorescent signals are induced upon their displacement. Reproduced from ref 46. Copyright 2015 American Chemical Society.

2.2.7. Molecularly Imprinted Sensors. One way to improve the selectivity of optical sensors against potential interferents is the use of molecular imprinting approaches.[280,281] Molecularly imprinted polymers (MIPs) are created by the polymerization of monomers (and cross-linking agents) with potential receptor site functional groups in the presence of a target molecule (i.e., the template). The template is then exhaustively removed after the polymer is formed, thus leaving complementary cavities with tailor-made binding sites for specific analyte recognition. Generally, the monomers used for synthesis are required to possess or combine with functionalities for target applications. Common analytes for molecularly imprinted polymer sensors include molecular, ionic, nanocomposite species, and enantiomers.[282−285] MIPs have to be sufficiently cross-linked to retain internal structural integrity, but not too rigid to prevent template removal. Similar to displacement assays, MIP sensors are also generally limited to detections in solution phase and have potential problems of limited sensitivity and remnant trace analyte.

MIP sensors have been broadly applied to the screening of explosives. For instance, Xu and co-workers designed a

DOI: 10.1021/acs.chemrev.8b00226
Chem. Rev. 2019, 119, 231−292

molecularly imprinted sensor for 2,4,6-trinitrotoluene (TNT) detection (Figure 15).[286] The sensor was constructed through a

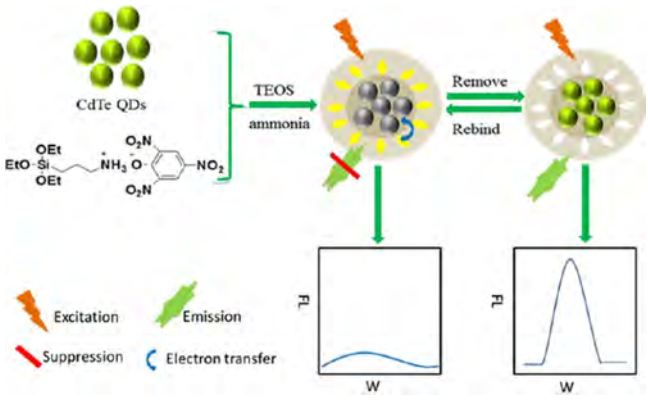

Figure 15. Schematic representation of a quantum-dot-encapsulated molecularly imprinting sensor based on a sol–gel seed-growth method that gives an easily distinguishable fluorescence response to TNT. Reproduced from ref 286. Copyright 2013 American Chemical Society.

sol–gel seed-growth approach, using functionalized siloxanes as monomers and trinitrophenol as a dummy template, and then capped with CdTe quantum dots as fluorophores. The sensor shows selective binding affinity to TNT against other possibly competing explosive molecules with distinct fluorescence quenching.

It is also possible to use discrete soluble macromolecules as molecularly imprinted macromolecules. Zimmerman, Suslick, and co-workers, for example, created cross-linked dendrimer substituted porphyrins based on octa-substituted bis-pocket porphyrins and then hydrolyzed away the central porphyrin. The resulting hollow dendrimer showed excellent selectivity for binding specific substituted porphyrins that fit the hollow left in the dendrimer.[287,288]

3. SENSOR FABRICATION AND INSTRUMENTATION

3.1. Array Fabrication: Substrate Considerations

3.1.1. Printed Arrays. While the choice of chromophores or fluorophores will dominate the optical response, there are other factors that are important to the efficacy of the sensor array: most notably, the formulation of the dye (included added acids or bases and the plasticizer or matrix in which the dyes are immobilized) and the substrate upon which the dye formulations are printed. Sensitivity, response time, reproducibility, selectivity, susceptibility to interferents, and shelf life of the sensor array will be heavily influenced by the choice of substrates and matrices of the colorants.

A common weakness in many electronic gas sensors is their sensitivity to changes in ambient humidity.[44,93,180] For any real-world applications, humidity changes from day to day or from indoors to outdoors are often tens of thousands parts per million in water vapor concentration. Any significant response to humidity proves fatal to the detection of parts per million levels of VOCs. One solution to the reduction of array response to humidity over a wide range (10 to ~100% relative humidity) is to use hydrophobic materials as both matrices and substrates of sensor inks.[50,61,169,175,180] Sufficiently humidity-unresponsive arrays sometimes can even be applied to aqueous phase sensing.[32,40,43,289]

A large number of solid supports have been used for the construction of colorimetric and fluorometric arrays. The desired properties of such substrates include good chemical resistance (e.g., stability toward acids or bases, gases, or solvents), high surface area (for sufficient contact with analytes), suitable permeability, optical transparency or high reflectivity, ease of handling, etc.[290−292] A simple method for production of colorimetric sensor arrays was developed by the Suslick group, involving robotic dip-pen printing dye formulations on the surface of reverse phase silica gel plates, acid-free paper, or porous membranes made of polymeric materials including polyethylene terephthalate (PET), polyvinylidene difluoride (PVDF), and polypropylene (PP).[27,32,169,293] Various methods have been used to print colorimetric sensor arrays, including spin-coating[294] (which cannot adequately print arrays using multiple spots), ink- or aerosol-jet printing,[295,296] and a modified robotic microarray pin printer (Figure 16) used to print spots with controllable shapes.[32]

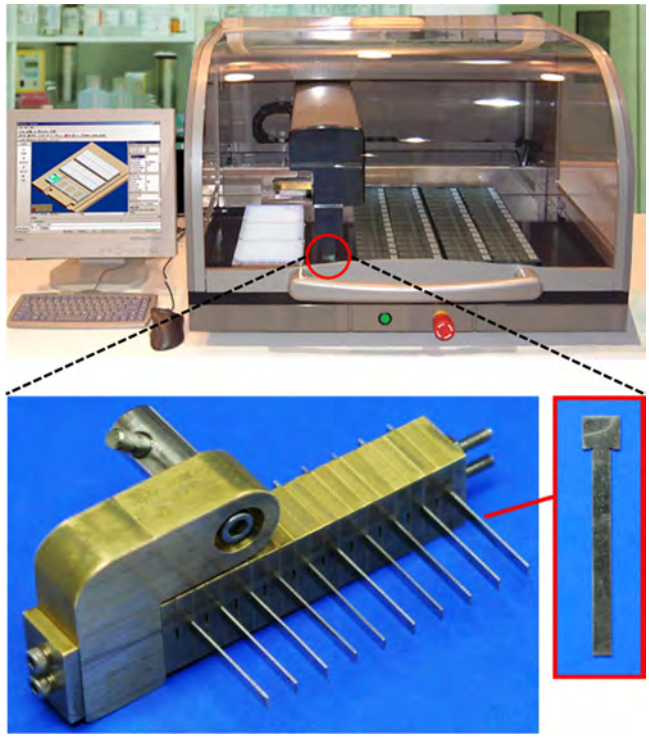

Figure 16. Robotic pin printer (upper) with a printhead holding an array of rectangular pins (lower) that enables the mass production of colorimetric sensor arrays (~200 arrays/h). Adapted with permission from ref 32. Copyright 2016 Royal Society of Chemistry.

For chemical sensing applications, one class of formulations uses soluble molecularly based dyes with an added plasticizer deposited as viscous films on polymeric membranes with high surface area (which allows analyte molecules to access the dissolved colorants within an acceptable response time). In contrast, pigments (which by definition are insoluble colorants) are generally impermeable to analytes and therefore reactive only on the periphery of the colorant, which dramatically reduces any colorimetric or fluorometric response to the presence of analytes. Molecular-based dyes, however, can have a limited shelf life as sensors, particularly when incorporated into viscous polymer films due to the crystallization of dyes that diminishes analyte accessibility to the colorant centers.[152]

DOI: 10.1021/acs.chemrev.8b00226
Chem. Rev. 2019, 119, 231−292

An alternative formulation makes use of nanoporous pigments made from dyes embedded in hydrophobic porous sol−gel glasses to generate chemically responsive colorants.[152,290,297] A useful nanoporous pigment sensor array can be made by immobilizing chemoresponsive dyes in organically modified silicate (i.e., "ormosil") prepared from the hydrolysis of suitable silane monomers in high-boiling-point solvents.[27,153,175,298] In addition, the physical and chemical properties of the matrix (e.g., hydrophobicity, porosity) can be readily adjusted using different ormosil formulations, and different solubilities of dye molecules may require the addition of silane precursors with different functional groups.[134] The use of nanoporous pigments significantly improves the stability and shelf life of the colorimetric sensor arrays and allows for the direct dye printing onto nonpermeable polymer surfaces. Furthermore, we have indeed observed that the silicate sol−gel matrix may serve as a preconcentrator for analyte molecules, hence improving the overall responsiveness of the array.

Regardless of the formulation, the open question remains as to how many different printed sensors is optimal for a sensor array. In principle, it is always advantageous to have a greater number of sensors with more chemically diverse dyes. In practice, however, the quality of the printing, the reproducibility of each sensor spot's response, and the inconvenience of preparation of formulations impose significant limitations on the practical limits of the sensor array size. Although arrays have been prepared with as many as 144 individual colorimetric sensors, in general 20 to 40 sensors present a "sweet spot" in terms of the compromise between convenience and data quality.

RGB color analysis of the sensor spot image shows that printing of these nanoporous pigments can give a uniform color distribution across the center of the spot (Figure 17).[152]

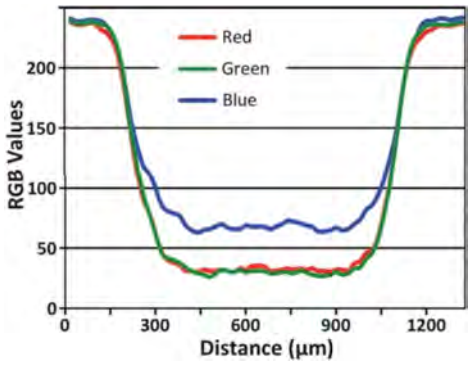

Figure 17. RGB values of a line scan across the diameter of a typical sensor spot, which is made of an ormosil colorant and printed on PET membrane. Reproduced with permission from ref 152. Copyright 2011 Royal Society of Chemistry.

Reproducibility of the optical densities of printed spots can be excellent, and colorimetric sensing experiments generally compare before- and after-exposure images of the sensor array, which further reduces errors in the pattern analysis. Note that it is important in the image analyses of the printed spots to utilize the average RGB values of the central portion of each printed spot to eliminate artifacts from the spot edges.[169]

The development of optically based chemical sensing platforms has increasingly employed substrates fabricated with advanced processing techniques, and their overall morphologies, especially some microstructures or nanostructures, must be fully characterized in order to gain a comprehensive insight into optimization of their function. Scanning electron microscopy (SEM) has shown that the printed nanoporous pigment films are typically ∼3−4 μm thick with uniform silicon distribution throughout the spot (Figure 18); transmission electron

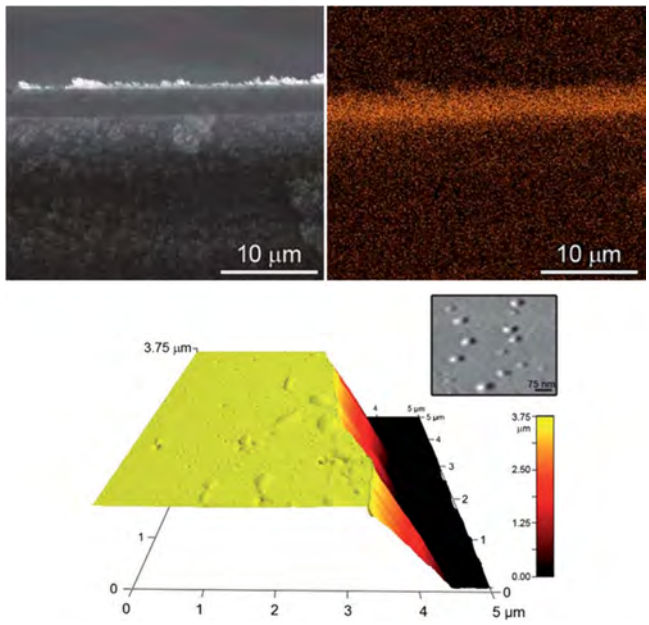

Figure 18. SEM micrograph of the cross section (top left), EDS elemental mapping (on Si) of a typical sensor spot (top right), and AFM micrograph (bottom) showing the height of the nanoporous pigment at the spot center compared to the base height of the polymer membrane. Inset displays the structure of surface pores (<100 nm). The spot is made of an ormosil colorant and printed on PET membrane. Reproduced with permission from ref 152. Copyright 2011 Royal Society of Chemistry.

microscopy (TEM) along with atomic force microscopy (AFM) micrographs reveal the presence of nanopores (<100 nm in diameter) in these ormosil films, which assist in mass-transport process, and are responsible for the fast response times observed during gas sensing experiments (∼90% response generally occurs in <2 min for most VOCs).[152]

Another means of producing nanoporous dyes has been reported by Bang et al.[154] using an ultrasonic-spray aerosol−gel pyrolysis method to synthesize silica microspheres from tetramethoxysilane (TMOS) and methyltrimethoxysilane (MTMS) precursors. The as-synthesized materials have a well-defined porous microstructure that permits the sufficient encapsulation of pH indicators and solvatochromic dyes for effective identification of amines.

3.1.2. Fiber Optic Arrays. A powerful array-based tool for the construction of cross-reactive fluorescent sensors is the fiber optic array. Over the past 20 years, Walt and co-workers have pioneered a fluorescence-based platform combining multifiber optical bundles with microwell arrays for measuring analytes of interest, particularly for biomolecules.[299,300] The platform is a chemically etched, two-dimensional array of microwells (total size ∼1 mm) comprising ∼50 000 individual micrometer-size (2 to 10 μm) fibers in which beads (i.e., synthesized microspheres) functionalized with one or a few fluorescent probes embedded in different polymers are randomly deposited. In order to identify themselves during the measurement due to random positioning, these beads are encoded with different types or concentrations of dyes so as to determine the locations of each bead type. The

DOI: 10.1021/acs.chemrev.8b00226
Chem. Rev. 2019, 119, 231−292

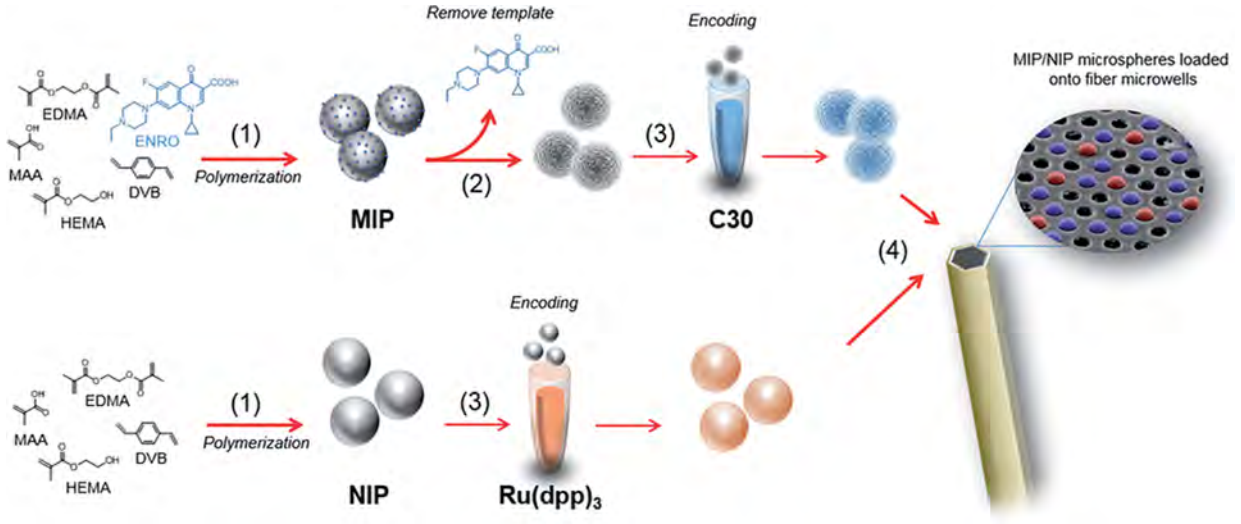

Figure 19. General workflow of fabrication of MIP-based bead microarrays for selective recognition of an antibiotic, enrofloxacin (ENRO), and NIP (i.e., polymers without template) microarray as a negative control. MIP and NIP beads are encoded with coumarin-30 (C30) and tris(4,7-diphenyl-1,10-phenanthroline)ruthenium(II) dichloride respectively and incorporated in etched fiber optic bundles. Reproduced with permission from ref 301. Copyright 2015 Royal Society of Chemistry.

physical properties and chemical compositions of the beads must be carefully considered for effective analyte recognition. The encoding schemes used, however, should not interfere with analyte binding. A graphical representation that shows the fabrication of an MIP-based fiber optic array is given in Figure 19;[301] SEM micrographs of the fiber optic bundles are shown in Figure 20.

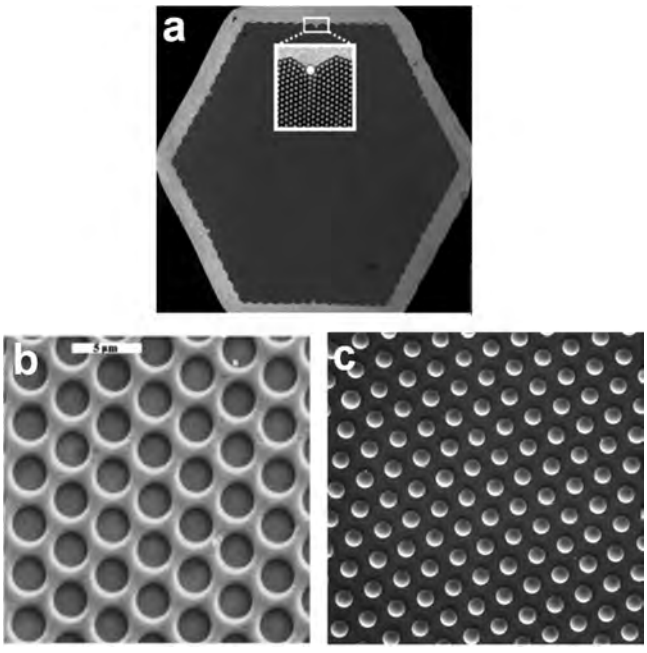

Figure 20. SEM micrographs of fiber optic bundles. (a) Optical-fiber-based array (total size ~1 mm) with hexagonal pits contains ~50 000 optical fibers; inset shows magnified views of the individual fibers (bright dots). (b) Structure of microwells with etched fibers. The bottom face of each microwell is the optical fiber core, which has etched into the surrounding clad. (c) Beads loaded into the microwells. Reproduced with permission from ref 125. Copyright 2010 Royal Society of Chemistry. Reproduced from ref 299. Copyright 2008 American Chemical Society.

In an attempt to accomplish simultaneous, multianalyte, high-throughput, and high-sensitivity analysis, the fiber optic arrays are normally composed of thousands of individual single-core fibers using a random assembly approach. The engineered structure allows for each individual well to be recognized by the optical fiber defining its base, providing a high-density array of miniaturized sensors that can be simultaneously and independently interrogated by light. Excitation light is introduced into the unfunctionalized end of the fiber, while emission signals from individual sensor elements return through the fiber and are magnified and projected onto a charge-coupled-device (CCD) camera, thus generating a pattern of fluorescence response for all sensors.[302]

These fiber-based optic sensor arrays have shown remarkable applications in biological sensing through the immobilization of desired biomolecular probes[303−305] and even whole cells[306,307] in the fibers. Of special interest is the use of digital enzyme-linked immunosorbent assay (ELISA) on a single-molecule array ("simoa")[308−310] for the sensitive protein quantification at or around picomolar concentrations. The single-molecule array is indeed a femtoliter-sized reaction well, which provides an ultrasensitive method for counting single protein molecules, thus permitting the detection of low numbers of protein molecules with a wide dynamic range.

3.2. Instrumentation: Digital Imaging of Colorimetric and Fluorometric Sensors

3.2.1. Digital Imaging of Colorimetric Sensor Arrays. A miniaturized system that is of low power and low cost but of high stability and high sensitivity is always welcomed in the design of novel sensing devices. For devices capable of reading colorimetric sensor arrays (or with proper illumination fluorometric arrays), one may take advantage of the rapid recent advances in digital imaging technology: flatbed scanners, digital cameras, contact image sensors (CISs, used in business card scanners), and cell phones.

From digital analysis of colorimetric dye arrays, one can obtain the characteristic sensor array response of individual compounds or complex mixtures. Using red, green, and blue (RGB) wavelength regions in lieu of full spectrophotometric

DOI: 10.1021/acs.chemrev.8b00226
Chem. Rev. 2019, 119, 231−292

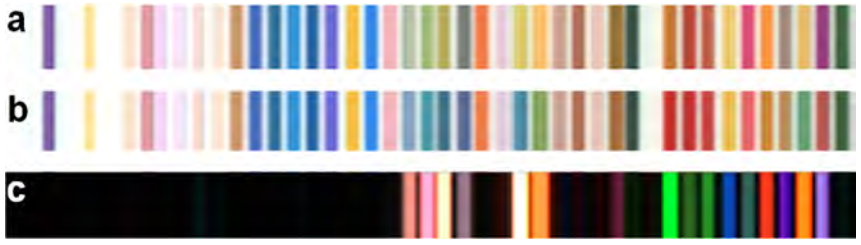

Figure 21. Digital images of the 1 × 40 colorimetric sensor array (a) before and (b) after exposure to headspace gas of ammonium nitrate, and (c) a scaled color difference map generated from the subtraction of the before and after exposure images. The color difference map represents the difference vector in 120 dimensions. For purposes of display, the color range of difference maps is usually expanded from the effective dynamic range to the full RGB display range (i.e., 4 bit color expanded to 8 bit color scale in this case, or 0−15 expanded to 0−255 in RGB values). Reproduced with permission from ref 32. Copyright 2016 Royal Society of Chemistry.

analysis, the resulting data is represented as a vector of 3*N* dimensions, where *N* = total number of sensor spots. Given minor variations in printing, it is best to image the array before exposure to analytes and subtract the resulting vector from that obtained during or after exposure. Based on those color difference vectors, statistical and quantitative analyses can be performed in the multidimensional space. Maps of these color difference values may be used for visualization of color changes of the sensor array: displayed color values are generally the absolute values of the differences, and color ranges are expanded for effective visualization (Figure 21).

For colorimetric array sensing, images of sensor arrays are commonly achieved on an ordinary flatbed scanner in a laboratory environment, which can provide high resolution, accurate positioning, and constant illumination for imaging. For environments outside the laboratory (e.g., in the field), development of a portable, low-noise, and inexpensive optical instrument with the capability of onboard analysis is necessary. Several imaging devices have been developed for digital data collection, including a customized handheld reader imbedded with a color contact image scanner,[31,32,58] a commercial CCD digital camera,[293] and even a cell phone camera.[311] Based on the array images collected during analyte exposure, a color difference map (Figure 21) can be easily generated by digital subtraction: red value of after-exposure image minus red value of before-exposure one, green minus green, and blue minus blue. Averaging of the centers of sensor spots effectively avoids edge artifacts caused by the nonuniformity of the printed spots. The other purpose of using color differences in RGB values is to cancel out discrepancies in color of either before- or after-exposure images resulting from variability in printing or small changes in lighting (e.g., due to temperature fluctuations), as the color differences are only a weak function of variations in the concentration of molecular dyes from array to array.[169]

The recently developed handheld optoelectronic reader[58] is a truly portable, self-contained and inexpensive analytical device for on-site collection and analysis of colorimetric data on a broad range of gaseous or liquid analytes, including biomarkers,[311] explosives,[31,32] food, and beverages.[243,312] The handheld device employs a color contact image sensor (CIS) that is commonly used in business card scanners, which contains a linear array of complementary metal oxide semiconductors (CMOS) for optical transduction (Figure 22).[313,314] CISs are much smaller than charge coupled devices (CCDs), use typically a tenth as much power, and are well-suited for low power and portable applications. A CIS consists of a linear array of detectors that receive light reflected off the object to be imaged through self-focusing lens arrays (i.e., refractive gradient cylinders); the

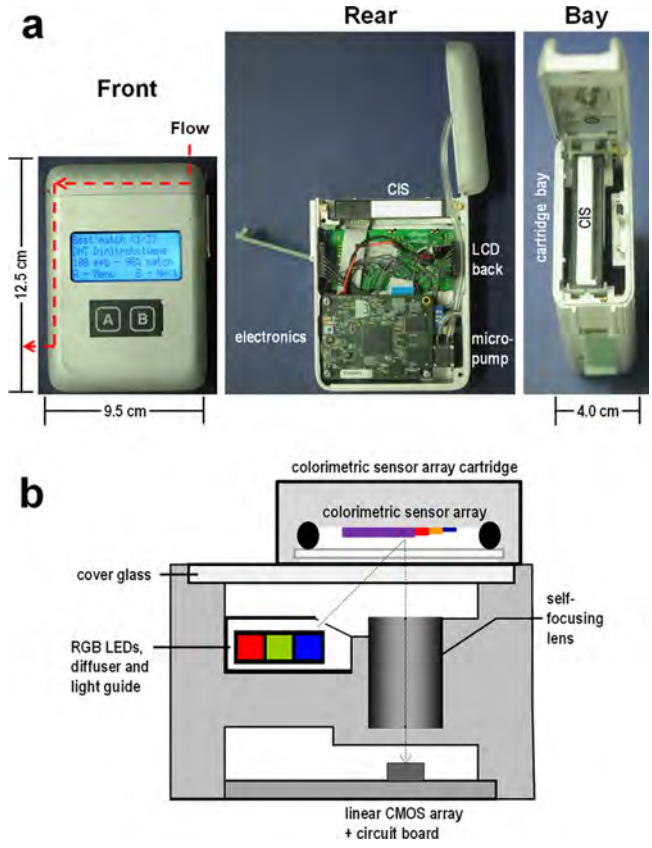

Figure 22. Handheld reader of colorimetric sensor arrays. (a) Labeled photographs showing the design of the handheld reader (12.5 × 9.5 × 4.0 cm) including front, interior, and cartridge bay views. (b) Cross-sectional schematic of a color contact image sensor (CIS), showing the components positioned to read a linear colorimetric sensor array; the red, green, and blue LEDs used for illumination are flashed sequentially for color analysis, typically with >5 MHz temporal resolution and >300 dpi. Reproduced from ref 58. Copyright 2015 American Chemical Society.

illumination is provided in timed pulses of red, green, and blue light-emitting diodes (LEDs). A sealed cartridge loaded with a disposable, linear colorimetric array is tightly stacked on the CIS for effective imaging during exposure of gaseous analytes. The handheld reader also contains a diaphragm micropump for control over gaseous analyte flow and onboard electronics to provide instant and real-time measurements of red, green, and blue reflectivity of the linearly arranged colorimetric sensor array; programming modules are incorporated to perform statistical evaluation of collected data.

DOI: 10.1021/acs.chemrev.8b00226
Chem. Rev. 2019, 119, 231−292

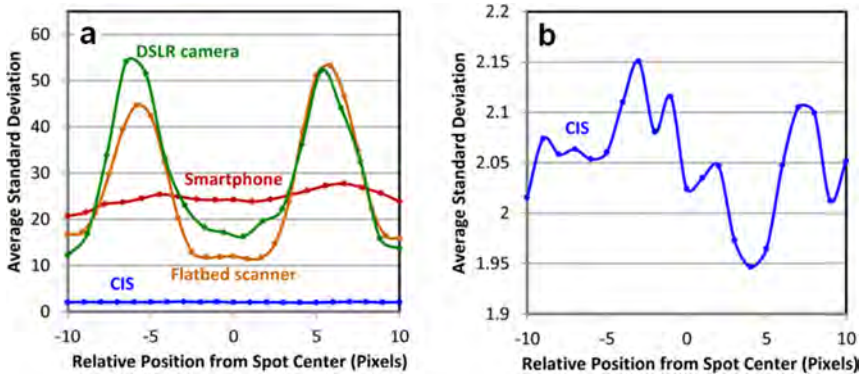

Figure 23. Reproducibility of sensor spot imaging as a function of position across the spot, showing the appearance of edge effects. (a) Comparison of the observed noise from four imaging devices (i.e., digital single-lens reflex (DSLR) camera, smartphone, flatbed scanner, and color contact image scanner (CIS)) vs distance from the physical center of the dye spot, averaged out of all sensor spots. (b) Expanded scale for the standard deviation of the noise measured using CIS imaging; no significant edge artifact is observed for the CIS. A linearized, 29-element sensor array was used for all scans, and observed noise for each spot was calculated and averaged for each pixel over 10 scans. Reproduced from ref 58. Copyright 2015 American Chemical Society.

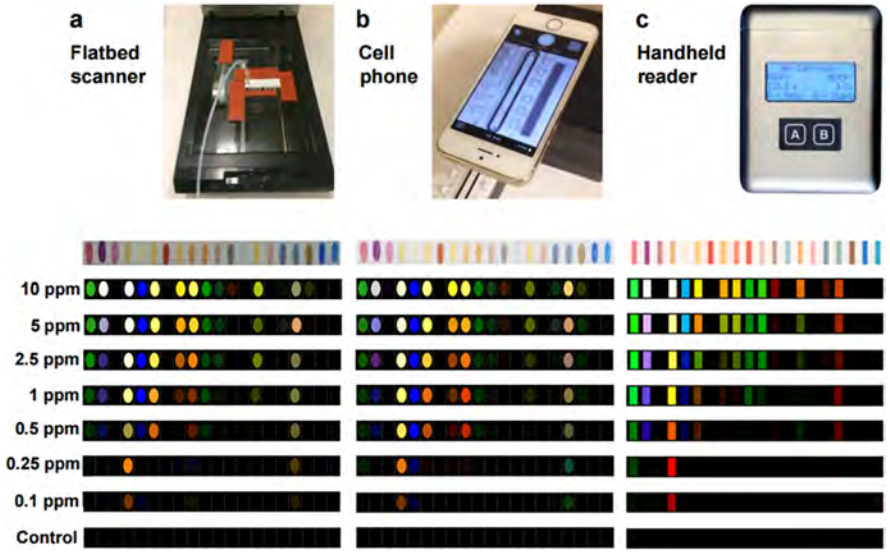

Figure 24. Comparison of sensor array responses on three devices.[32] Color difference maps were averaged out of septuplicate trials after 2 min exposure of a series of TMA concentrations collected by (a) flatbed scanner, (b) iPhone 5s camera, or (c) handheld reader. The color range is expanded from 4 to 8 bits per RGB color (i.e., RGB color range of 4−19 expanded to 0−255). Reproduced from ref 311. Copyright 2016 American Chemical Society.

The customized line scanner handheld reader provides 3−10 times higher signal-to-noise ratios than other scanning devices, with the substantially decreased noise level across the center of any spot (Figure 23).[58] The reader was also examined to compare to other methods for the acquisition of colorimetric data (e.g., flatbed scanner vs cell phone camera, Figure 24) in the detection of a typical biogenic amine, trimethylamine (TMA), and, after sample preparation, trimethylamine oxide.[311,315] All three sets of data give accurate classification results on different concentrations of TMA vapors; low parts-per-billion-level detection limits were achieved on all three devices: ∼3 ppb for handheld scanner, ∼4 ppb for flatbed, and ∼6 ppb for cell phone.[32]

3.2.2. Cell-Phone-Based Microplate Reader. In the past decade, a large number of handheld optoelectronic devices have been developed for microplate technology[316−319] and have demonstrated promising applications as easy-to-use imaging tools for efficient biomedical sensing of complicated diagnostic systems. These portable scanning instruments often integrate optical, electronic, and mechanical components with mobile devices (e.g., digital camera, GPS, or cell phone) that enable on-site, rapid, reproducible, and sensitive imaging and sensing of biologically relevant analytes of interest. Among various choices for such devices, smartphones with built-in cameras[320−324] have drawn tremendous attention due to their relatively low cost, high portability, and high availability.

Very recently, Ozcan and co-workers developed a portable, automated, and cost-effective cell-phone-based microplate reader with nanometer level resolution for real-time biomedical imaging.[325,326] The device contains a 3D-printed optomechanical attachment to hold and illuminate a 96-well microtiter plate using either a light-emitting-diode array or a laser diode incorporated in an optical or fluorescence microscope for both colorimetric and fluorometric sensing. The light is optically transmitted through each of the 96 optical fiber bundles to each individual well of the microplate; a sample region of interest is imaged by the smartphone's built-in camera module coupled to a focusing lens (Figure 25). Captured images of the 96-well plate

DOI: 10.1021/acs.chemrev.8b00226
Chem. Rev. 2019, 119, 231−292

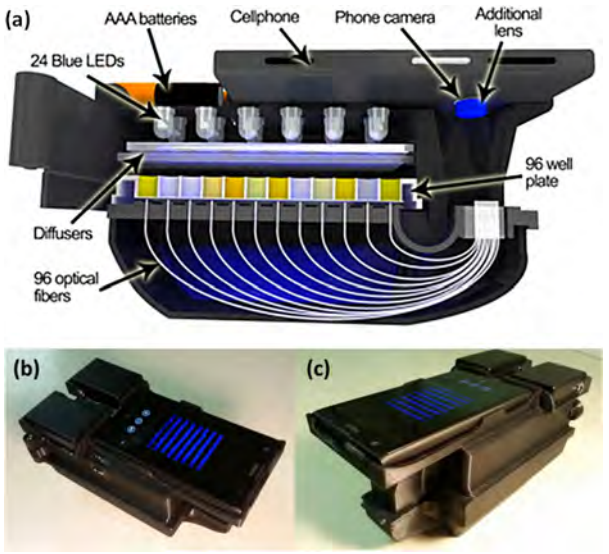

Figure 25. Portable 96-well microplate reader based on a cell phone platform. (a) The portable device consists of a customized hardware attached to the smartphone, which uses an LED array to illuminate 96-well plates through a diffuser and optical fiber bundles. (b) Top view of the device. (c) Side view of the device. Reproduced with permission from ref 334. Copyright 2016 Nature. Reproduced from ref 326. Copyright 2015 American Chemical Society.

are transferred to the servers, and data processing is performed on a custom-designed application using a machine learning algorithm,[327] which provides visualized diagnostic results within 1 min. The system has been successfully used for colorimetric or fluorometric imaging of single DNA molecules, viruses, and nanoparticles[328−330] and has shown a wide range of potential applications particularly in point-of-care medical diagnosis including nucleic acid amplification tests,[331] pathogen quantification,[332] biomarker monitoring,[333] and antimicrobial susceptibility test.[334]

4. STATISTICAL ANALYSIS AND MODELING

The output space of a chemical sensor has a total dimensionality that depends on the number of chemical properties probed by the sensor. A sensor that probes chemical reactivity rather than physical properties (e.g., mass or dipole moment), for example, may probe a very large number of chemical properties which are partially or fully orthogonal to each other; these interactions include Lewis acid/base, Brønsted acid/base, redox, hydrogen bonding, etc. that ultimately affect reactivity. Differentiation among chemical species using these types of sensors likewise involves analysis within this high-dimensional output space, and as such is potentially capable of differentiating among a huge number of disparate targets. The evolved olfactory system takes advantage of this sort of paradigm: the combined responses of multiple cross-reactive sensors provide a high-dimensional sensor space that is used by the olfactory bulb to recognize patterns corresponding to particular odorants or families of odorants.

In contrast, a sensor that takes advantage of weak physical interactions (e.g., van der Waals interactions that are largely responsible for physisorption) will have an output space that is largely dominated by only one dimension; physisorption will dominate any interactions involving samples with simple surfaces (e.g., metal oxide electrical sensors) or polymer coatings (e.g., coated quartz crystal microbalances, conductive polymer fibers). The physical interactions responsible for adsorption onto surfaces or absorption into polymers are roughly equivalent to what is commonly referred to as "hydrophobicity".

Consequently, physisorption-based sensors, the basis of traditional electronic nose technology, are almost always dominated by a single dimension in a statistical sense.[14,59,335] The sensor may indeed be constructed as an array—that is, they can be constructed from many rows and columns containing different metal oxides or polymer composites—but the resulting output space is highly covariant, and that results in a low overall dimensionality. In general, in such arrays, there is a single dominant dimension that describes the vast majority (>90%) of both the raw output space and discriminatory ability: most often this dimension is essentially hydrophobicity. As a consequence of this low dimensionality, most electronic nose technology is not able to distinguish among libraries of similar complex mixtures: targets with similar hydrophobic characteristics appear similar to each other. In addition, for any technology that relies on physisorption, interference from variation in humidity is inevitable, given the very strong tendency of water vapor to adsorb on surfaces.

At a first naïve glance, these low-dimensional sensors do have some advantages in analysis. Because of the high amount of covariance between sensors, analysis can be significantly simplified and some techniques become significantly more accurate (e.g., linear discriminant analysis, vide infra). Additionally, because of the low changes in enthalpy involved in physisorption/desorption, these sensors show improved reversibility over the higher-dimensional sensors mentioned, especially over short periods of time; this is a double-edged sword, however, as this enhanced reversibility leads to a commensurately decreased sensitivity simply by virtue of the equilibrium behavior of weaker interactions.

Sensors based on chemical reactivity, as mentioned, have an intrinsically high-dimensional output space. This higher dimensionality implies a greater ability to differentiate among similar targets: i.e., an enhanced discriminatory power. Similarly, the compatible analyte scope is larger as the likelihood of overlapping sensor responses in multiple dimensions is decreased (i.e., the multidimensional hypervolume over which analytes are distributed is much larger) relative to a physisorption-based sensor. As the enthalpic changes in chemical interactions are higher, sensors based on chemical reactivity are likewise less reversible than physisorption-based sensors; this can be overcome by making the sensor arrays disposable, which then provides general improvements in sensitivity, discriminatory power, and analyte scope.

A high-dimensional output space demands a more complex approach to analysis than that which chemists are typically accustomed to.[336] One problem inherent with high-dimensional sensors is that the potential output volume increases *much* more rapidly than the available data; these data sets are usually formally "sparse" (compared to the traditionally understood "dense" data sets) and must be treated as such in order to obtain meaningful information. Traditional analysis methods that are effective for analyzing highly covariant, dense data sets tend to fail (often spectacularly) when one attempts to apply them to sparse data sets; these sparse data sets run headlong into the so-called "curse of dimensionality" which can create significant difficulties in all aspects of analysis, including function approximation (i.e., regression), model fitting, parameter extraction, and numerical computation.[337]

DOI: 10.1021/acs.chemrev.8b00226
Chem. Rev. 2019, 119, 231−292

Analysis techniques for sensors all share the same common goals: evaluation of the quality or character of the data set, predicting information about unknown samples based on a known library, and displaying output data effectively in order to communicate with users. Methods that emphasize one of these goals tend to have a trade-off with regard to the others: a sensor array with 50 useful output dimensions that is optimized for multiclass identification, for example, will be exceedingly difficult to present in a traditional two- or three-dimensional plot, even after dimensional reduction techniques; on the other hand, a sensor with only two useful output dimensions is straightforward to explain or present, but has commensurately less discriminatory power. Keeping this in mind, we will discuss several of the most common approaches to high-dimensional data: hierarchical cluster analysis (HCA), principal component analysis (PCA), linear discriminant analysis (LDA), support vector machines (SVMs), and artificial neural networks (ANNs).

In general, traditional analysis for high-dimensional chemometric data can be divided into two distinct families: clustering and classification.[338−340] *Clustering* methods seek to describe a data set into groups of related targets (i.e., clusters); clusters are defined by determining how the individual measurements are related to one another by use of some sort of optimized distance metric (e.g., nearest neighbor, within-cluster variance minimization). *Classification* methods, on the other hand, attempt to predict information about an unknown sample based on previously acquired data. Each method is generally optimized for a specific task and is not well-suited for other tasks; a typical clustering technique, for example, may provide useful information about the relationships among samples, but would not be at all useful for classification. Techniques can usually be shoehorned into providing additional utility (for example, adding predictive algorithms to said clustering technique), but one must be mindful that these approaches are not fully optimized for the new task.

Analytical methods can be either *supervised*, in which case the evaluation algorithm incorporates information regarding known individual samples and is forced (i.e., biased) to treat them accordingly, or *unsupervised* (also called "model-free"), where all cases are evaluated identically without external information.[338−340] Since unsupervised models are ignorant of any prior information, they generally follow simple, straightforward algorithms and are used primarily for descriptive analysis; these methods are used to provide quantitative information about the data set which may not otherwise be readily apparent (e.g., similarity between samples, sample clustering/grouping). Unsupervised methods are also commonly used to discover features (e.g., class labels) that are later used in supervised methods. Supervised models, on the other hand, incorporate known external information (typically sample labels and concentrations) and can be used to predict extremely useful information related to these extra parameters (e.g., classification and regression). This potential increase in utility comes at a significant cost, however: models can be very complex, and data sets require larger numbers of samples in order to adequately incorporate the known external parameters. Supervised methods are almost always augmented with unsupervised methods in order to improve or evaluate the accuracy and generalizability of predictive results (e.g., as in bootstrap resampling, cross-validation, etc.).

4.1. Descriptive Methods

4.1.1. Hierarchical Cluster Analysis (HCA). HCA is a clustering technique in which groups of points (clusters) in a multidimensional space are created in a discrete number of steps and connected using some sort of distance metric (Euclidean distance, Mahalanobis distance, etc.). HCA can be treated using either a divisive "top-down" approach (i.e., successively dividing larger clusters) or an agglomerative "bottom-up" approach (successively merging smaller clusters); the agglomerative approach is significantly more common. At each step in the agglomerative process, typically two existing clusters (for the first step, data points) are merged to form a new cluster by using a linkage criterion (e.g., mean, centroid, minimum variance); this is repeated until only a single cluster remains. The most common linkage criterion is Ward's minimum variance method, in which the total within-cluster variance is minimized at each step. An example is shown in Figure 26.[339,340]

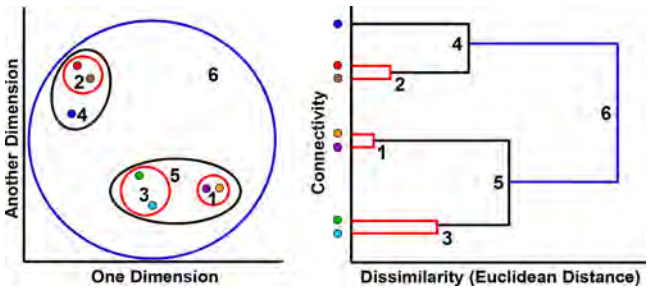

Figure 26. Schematic representation of a hierarchical cluster analysis (HCA) of multidimensional data (left) that forms a dendrogram based on clustering of experimental measurements (right). Reproduced with permission from ref 62. Copyright 2013 Royal Society of Chemistry.

The resulting tree-like dendrogram displays connectivity between parent and child clusters and has one quantitatively important axis that shows the cumulative error score—effectively the quantification of dissimilarity—based on the chosen distance metric. In the context of chemical analysis, connectivity displays relative similarity (i.e., which samples are similar to each other) and distance displays the magnitude of this similarity.

HCA dendrograms provide a straightforward method of displaying cluster similarity semiquantitatively and can effectively communicate the relationships between similar chemical species. A representative example containing 100 VOCs is shown as Figure 27: similar chemical classes tend to cluster together (i.e., have low dissimilarity distances) owing to the nature of the chemical reactivity of the particular chemical sensor array.

There are three primary limitations in using HCA. First, as with all unsupervised methods, HCA is not easily capable of predictive analysis—it is a descriptive technique. Second, HCA dendrograms must be completely recreated whenever a new data point is added to a data set. This not only increases computational burden for assessment of data sets that are in the process of being collected, but also limits the ability to compare between dendrograms (even those with similar data sets); comparisons are typically limited to qualitative statements (e.g., "which cluster does this new sample appear to fit into?") and not a quantitative evaluation (e.g., "what is the probability that this new sample is that known analyte?"). Third, HCA dendrograms can be easily misinterpreted due to the nature of

DOI: 10.1021/acs.chemrev.8b00226
Chem. Rev. 2019, 119, 231−292

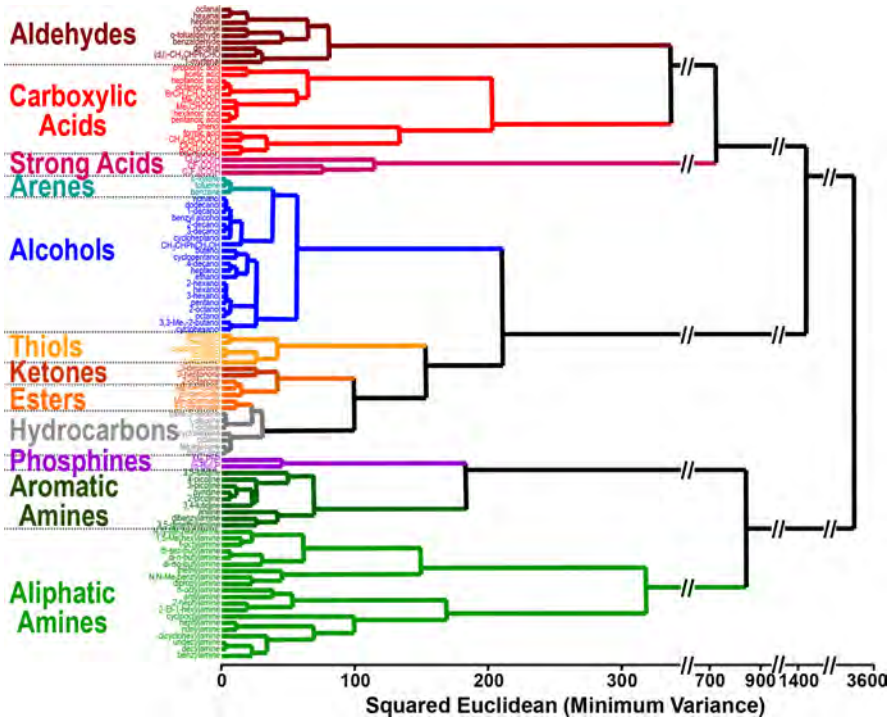

Figure 27. Dendrogram from HCA of the colorimetric array responses to 100 common organic compounds at full vapor pressure at 300 K. Reproduced from ref 169. Copyright 2006 American Chemical Society.

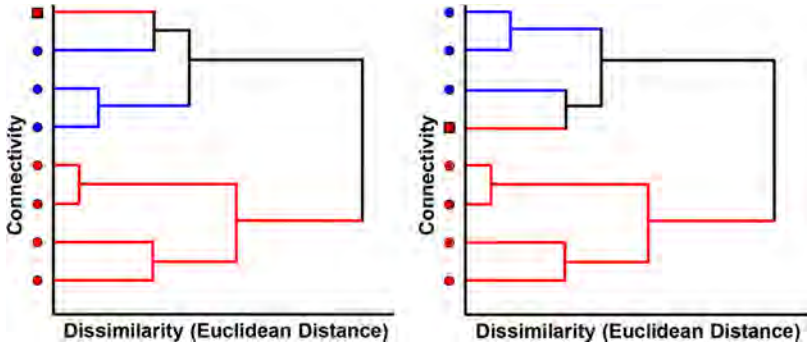

Figure 28. Effect of cluster orientation in dendrograms showing two classes of data, red and blue with one mis-clustering shown as a red square. These two dendrograms are mathematically identical and represent exactly the same data: the *y*-axis is not quantitative. At first glance, however, the data point represented by the red square appears much further out of place in the dendrogram on the left compared to the dendrogram on the right. Reproduced with permission from ref 62. Copyright 2013 Royal Society of Chemistry.

having only a single quantitatively meaningful display axis (distance). For a given cluster created from parent clusters A and B, the exact orientation between A and B (i.e., whether A is situated above B) does not matter: HCA dendrogram connectivity is invariant toward rotation about the cluster. The human eye, however, may be misled due to an apparent proximity along the connectivity axis: noisy data can be easily misinterpreted as appearing too similar or too dissimilar, depending on the arbitrary orientation of the dendrogram. An example is shown in Figure 28.

4.1.2. Principal Component Analysis (PCA). PCA is an unsupervised descriptive technique that creates a new orthogonal set of dimensions using linear combinations of the initial dimensions. The first dimension (also known as a direction, component, coordinate, etc.) is determined by finding the vector that gives the maximum variance when the (centered) data set is projected onto that vector; each subsequent dimension is orthogonal to all previous dimensions and maintains this same condition of maximum variance.[1,338,339,341] This procedure is straightforward and readily available in commercial software packages (which greatly contributes to its popularity): one simply needs to perform an eigenvalue decomposition on the covariance matrix of the data set, for which there are several methods that are outside the scope of this review (worth noting, however, is that it is rarely necessary or desirable to calculate the actual covariance matrix, which is prohibitive for high-dimensional data).

PCA thus describes a data set by showing how the data in the set varies: a dimension associated with a large variance means that samples vary significantly across this dimension, while a dimension associated with a small variance means that samples are mostly near the mean value. The magnitude of the variance is also relevant, as typically a number of dimensions are kept that add up to a proportion of the total variance across all dimensions (usually 95%).

DOI: 10.1021/acs.chemrev.8b00226
Chem. Rev. 2019, 119, 231−292

Since PCA functions as a descriptive dimensional reduction technique, plots of PCA scores (i.e., projection of the data onto the new PCA dimensional space) are often easier to visualize than raw data. This is only strictly true, however, when the resulting PCA space has a low dimensionality (i.e., the dimensions in the sensor data are highly correlated with each other). PCA is widely used in visualizing electronic nose data, and it is easy to see why—as mentioned above, electronic noses often require only two or three principal components to fully describe the variance even when they use a much larger number of physical sensors. For low-dimensional data, PCA provides a straightforward method of describing the variability in a sample set, i.e., how similar samples are to each other.

When dealing with a wide range of analyte classes, a sensor array with a large total chemical reactivity space (i.e., an array that could potentially output high-dimensionality data) is generally desirable in order to take advantage of the array's specificity and decrease the likelihood of overlap due, for example, to changes in concentration or addition of new analytes. As such, PCA is substantially less useful for visualizing high-dimensional data compared to low-dimensional data: humans are limited to visualization in only two or three dimensions, and the first few PCA dimensions from high-dimensional sensors will not be fully descriptive.

In the absence of noise, the theoretical maximum dimensionality of the generated PCA space is the lesser of either the number of sample classes or the size of the chemical reactivity space. When using a narrow class of analytes or using a sensor array with a small total chemical reactivity space, then apparent high dimensionality of a sensor's output is indicative of a large contribution of noise—essentially, a low signal-to-noise ratio (S/N).

As a consequence of the correlation between sensors and the influence of noise, the dimensionality of output data—the size of the PCA dimensional space—is not determined directly by the number of sensors in an array. As an example, Lin and Suslick[242] designed a colorimetric sensor array containing 16 redox-sensitive sensors to target a specific class of reactivity, focused on discrimination between several peroxide-based oxidants and peroxy-based explosives of varying concentrations. The array probes only a small chemical reactivity space, and the PCA score plot reveals that only two dimensions (*not* 16) were required to describe 95% of the total variance, as shown in Figure 29.

Since principal components are combinations of responses of array components, the magnitude of the variance described by each principal component gives some information about the contribution of each chemical property toward the overall sensor response. In an array that probes only pH, for example, a single dimension may describe more than 95% of the total variance. Similarly, an array that probes pH, hydrophobicity, dipole moments, film permeability, and nucleophilicity would be expected to have a significant variance contribution from at least five dimensions when using a diverse sample set. This variance-per-dimension breakdown is often described using a scree plot showing cumulative variance, as in Figure 30.

As with HCA, PCA is an unsupervised descriptive technique: it is best suited for evaluation of data sets rather than prediction. Unlike HCA, however, PCA generates its own dimensional space that can be used to make rudimentary predictions: one simply needs to project the unknown sensor response onto the PCA dimensional space and determine whether or not the new data point lies in close proximity to data from the training set. Successfully classifying data using this method, however, relies

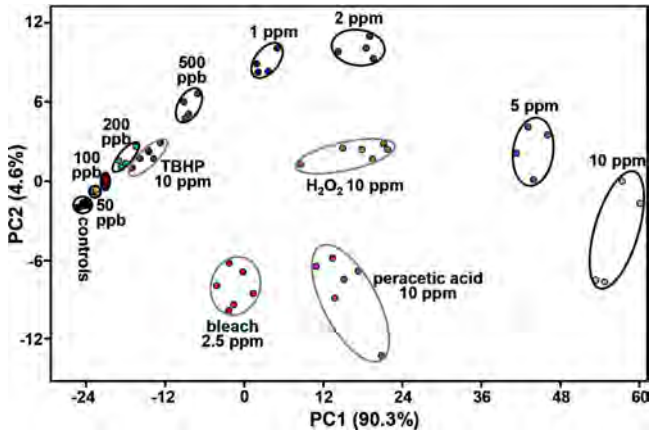

Figure 29. PCA score plot showing two-dimensional separation of multiple classes of redox-active analytes generated from triacetone triperoxide vapor (TATP, concentration-only labels) and other redox-active analytes. Circled areas represent 95% confidence intervals. Note that only two dimensions were required to reach 94.9% total variance, implying a small chemical reactivity space probing only two chemical properties within the sample set. This particular sensor array used several one- and two-electron redox-sensitive dyes encapsulated in a xerogel matrix, and was designed with no other reactivity in mind. Reproduced from ref 242. Copyright 2010 American Chemical Society.

on one major (and usually invalid) assumption: that the variation within a sample class is significantly lower than the variation between sample classes in the PCA dimensional space.

PCA dimensions are generated by total variance among all samples (and completely unrelated to sample class labels), and *the magnitude of variance is completely unrelated to discrimination ability*; further, PCA usually discards dimensions corresponding to low explained variance (and even if one keeps them, they are often mathematically unstable). This lack of optimization for the purposes of discrimination means that one may qualitatively use PCA plots to explain when sample classes are "obviously separable"; when sample classes are obviously separable on a PCA plot, then better-optimized classification techniques (vide infra) are likely to have high classification accuracy. *The inverse is not true*: samples may appear inseparable on a PCA plot but still have high classification accuracy using a technique that is better optimized for discrimination. A descriptive example of this is shown in Figure 31.

4.2. Classification Methods

Classification methods involve development of algorithms that can identify (i.e., classify) an unknown sample using some mathematical construct created using established data (known as a library or training set). Classifiers are typically of the form of "one vs one" or "one vs the rest" and used in some sort of voting paradigm for the ultimate decision. In chemical sensors, linear classifiers are by far the most common; these classifiers determine planar decision boundaries (i.e., hyperplanes) to effectively divide the aforementioned pairs. Mathematically, this is equivalent to projecting the data point onto the normal vector for the hyperplane and determining whether or not the magnitude exceeds a particular threshold. Classifiers are necessarily supervised methods, as the identities of the training data must be known.

Linear classifiers are especially suitable for chemical sensors, as chemical sensor output is generally normally distributed about a multivariate sample mean. As such, linear decision boundaries are actually the theoretically optimal solution for

DOI: 10.1021/acs.chemrev.8b00226
Chem. Rev. 2019, 119, 231−292

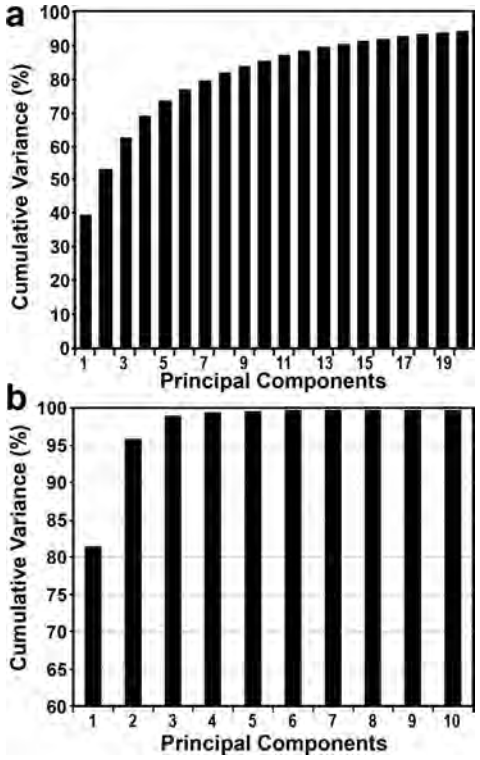

Figure 30. (a) Scree plot of data from a 36-element colorimetric sensor array tested with 100 VOCs, showing relatively high dimensionality: 20 dimensions were required to describe 95% of the total variance. (b) Scree plot from a 16-element colorimetric sensor array tested with 14 natural and artificial sweeteners, showing low dimensionality: two dimensions were required to describe 95% of the total variance. It can be inferred that the chemical reactivity space being probed by the sensor array used in (a) is large and includes many classes of reactivity, while that of the sensor array used in (b) is small where pH is the primary component. Reproduced from ref 169. Copyright 2006 American Chemical Society. Reproduced with permission from ref 342. Copyright 2009 American Chemical Society.

discriminating among any particular pair of analytes. Further, forcing this a priori known linear separability on any sort of classification model reduces the potential of overfitting that could occur using a nonlinear decision surface and allows for linear methods that can only generate linear decision boundaries (such as LDA, vide infra).

HCA and PCA, mentioned above, are unsupervised descriptive methods that can be used to obtain useful information about a data set. Because they are unsupervised, they provide no direct method for classification and require some sort of additional processing methodology in order to obtain a classifier; one may develop rudimentary decision boundaries on a particularly well-separated set of PCA outputs, for example. As described, however, descriptive methods are not optimized for discrimination ability: HCA clusters based on some sort of method designed to fit a specific mathematical form (nearest neighbor, centroid, variance minimization, etc.) and PCA dimensions are based on total variance along a particular vector. Rather than use these nonoptimized methods to develop classifiers using their respective outputs, there are several common methods that have been specifically developed to maximize discrimination ability either using a hypothesis and analytical methods (e.g., linear discriminant analysis) or empirically (e.g., support vector machines or artificial neural networks).

4.2.1. Linear Discriminant Analysis (LDA). LDA shares some similarities with PCA: both construct a set of orthogonal dimensions consisting of linear combinations of the original dimensional space, and both methods reduce dimensionality by keeping a number of dimensions meeting a threshold criterion. LDA uses a different method for determining these linear combinations, however: dimensions are selected so as to maximize the ratio of between-class variance to within-class variance, roughly analogous to maximizing their signal-to-noise ratio for discrimination ability.

The methodology for classification using LDA is essentially the same as for PCA: construction of a decision threshold that best separates the two classes along some particular vector. Unlike for PCA, however, the LDA output space is optimized such that the vector connecting two class-means provides the highest possible separability (i.e., the ratio of between-class to within-class variance) between those two classes and determines the normal vector for the decision boundary plane; the threshold

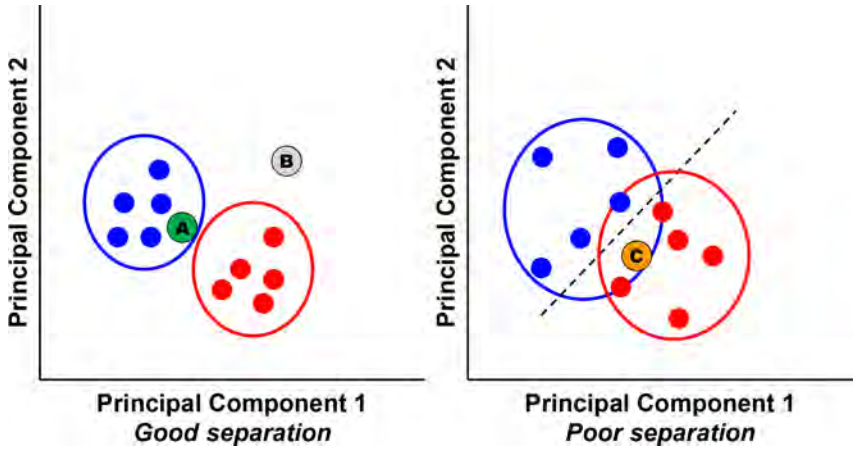

Figure 31. PCA score plot showing red and blue classes and three unknown experimental points A, B, and C. Circled areas represent confidence intervals. By using a data set with large separation (left), it can be inferred that green circle A belongs to the blue class and gray circle B does not belong to either blue or red classes. Using a data set with poor separation (right), orange circle C cannot be unambiguously identified despite appearing to be closer to the other members of the red class, with the dashed line representing an obvious (by eye) separation between the two classes. Reproduced with permission from ref 62. Copyright 2013 Royal Society of Chemistry.

DOI: 10.1021/acs.chemrev.8b00226
Chem. Rev. 2019, 119, 231−292

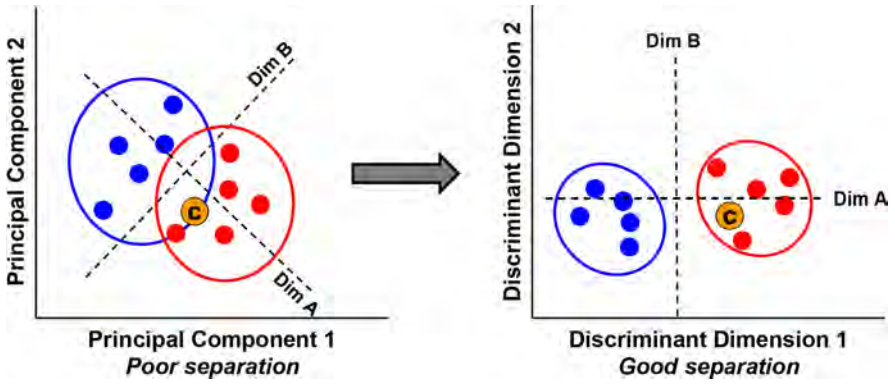

Figure 32. Score plots comparing data analyzed with PCA (left) and LDA (right). Circled areas represent confidence intervals. The most obvious separation by eye in the PCA plot is along dimension A, which is orthogonal to dimension B; these dimensions correspond to the discriminant dimensions in the LDA plot. Orange circle C is clearly identified as belonging to the red class using LDA, while identification is ambiguous using PCA. In order to create a classification method, a decision threshold would need to be constructed using the two sample means. Reproduced with permission from ref 62. Copyright 2013 Royal Society of Chemistry.

value is typically chosen to be halfway between the projections of the two class means. Due to this optimization, compared to PCA, LDA will show better ability to differentiate among sample classes; a general example of this improvement is shown as Figure 32.

The primary weakness of LDA is a requirement for a large number of samples in order to construct the classifier. All discriminant methods (including LDA) require a large sample size, and in fact LDA was deliberately created in order to reduce the number of requisite sample replicates compared to other discriminant methods. Of the methods presented in this review, discriminant methods are unique in that they require the calculation of class covariances; accurate prediction requires that the prediction matrix—the inverse of the empirically determined sample covariance matrix—is both accurate and solvable. To avoid division by zero, solving the prediction matrix requires, at a bare minimum, M independent measurements for an M-dimensional sensor response (i.e., the covariance matrix must be full rank); obtaining an *accurate* prediction matrix, on the other hand, may require a sample size 100 times larger (or more). Because of this inversion, the prediction matrix is unstable when the number of samples acquired is not substantially larger than the dimensionality of the sensor; this is obviously a major problem for high-dimensional sensors which require a proportionally higher sample size.[337]

To address this problem, LDA uses a prediction matrix that is defined by the average of all the class covariances, commonly referred to as a "pooled covariance"; thus, instead of requiring M replicates for each class, an M-dimensional sensor only requires M replicates in total. Even using this rather clever trick, LDA still suffers from instability and can suffer from drastically fluctuating results with low sample populations; this phenomenon is better known as overfitting, and results from the prediction method being overly influenced by the presence of noise in the sample set instead of a predictive property. In order to be accurate, the true covariance matrix for each sample class must also be identical—this is referred to as the homoscedasticity (also spelled homoskedasticity) assumption. Since the noise in a chemical sensor response is typically proportional to the response, the homoscedasticity assumption becomes increasingly less accurate as the number of independent dimensions in the sample set and sensor array increases; this subsequently results in increasingly poorer prediction accuracy as the total dimensionality increases.

There are two primary advantages to LDA. First, as with PCA, LDA is extremely well-suited for analysis of low-dimensional data (i.e., only probing one to three physical parameters, usually dominated by a parameter such as hydrophobicity): in these data sets, the homoscedasticity assumption is mostly accurate and the number of sample replicates easily exceeds the number of selected independent dimensions (i.e., usually two or three). Second—and most importantly—usage of LDA is easily defensible: the maximization criteria used to select the construct the discriminant dimensions, as well as the mathematical methodology used to implement those criteria, are well-known and analytically solvable. LDA uses no optimized parameters and has no model choices to justify; the only arbitrary choice in the methodology involves selection of the decision threshold, as mentioned above. A representative example of a two-component LDA plot is shown as Figure 33, showing obvious separation among a low-dimensional sample set (i.e., 98.3% total variance is described by two dimensions).

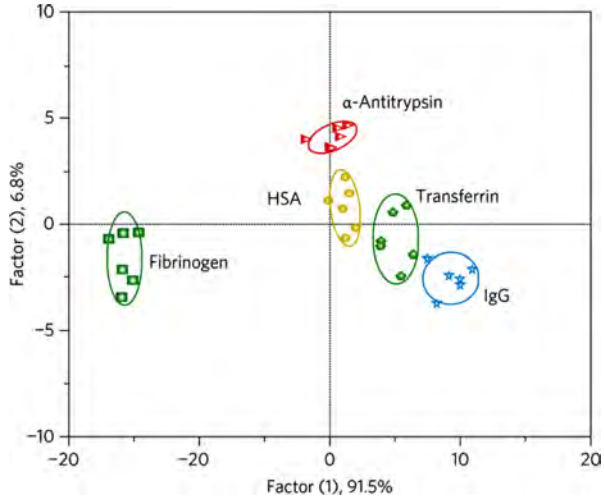

Figure 33. LDA score plot showing separation among five serum proteins at 25 nM concentration. Fluorescent displacement sensing was used with multiple solutions doped with five GFP−NP sensors for the five proteins at pH 7.4. Circled areas represent 95% confidence intervals. Reproduced with permission from ref 343. Copyright 2009 Nature.

DOI: 10.1021/acs.chemrev.8b00226
Chem. Rev. 2019, 119, 231−292

Tensor discriminant analysis (TDA)[344−347] is a technique related to LDA for improved dimensional reduction with high-dimensional data sets using tensors to better describe the known physicality of the sensors (as examples: the independence of temporal behavior from sensor response or the tendency of RGB values for a single colorimetric sensor to correlate). TDA is used to classify multiway array measurements (i.e., tensor measurements) rather than traditional vector measurements. For the sake of further discussion, it should be clarified that the term "way" is, in common mathematical and computer science terminology, referred to as a "dimension" but obviously cannot be used in that sense here. A vector is a one-way tensor (with size referred to here as its dimensionality); a matrix is a two-way tensor (i.e., a vector of vectors), and so on.

Data collected using sensor arrays is, when taken in total, approximated well by a three-way tensor: the first way corresponds to the choice of the probe, the second way corresponds to any multidimensional responses for a particular probe (e.g., for an optical sensor array, changes in red, green or blue values, i.e., ΔR, ΔG, ΔB, or some other spectral decomposition), and the third way corresponds to the time-course progression of that sensor (i.e., kinetic responses). The general strategy for tensor discriminant analysis is to expand the LDA methodology using expanded tensors rather than vectors, which notably allows for the inclusion of temporal data. This methodology can improve the sensitivity and specificity of these methods, but most importantly allows for the reduction in the computational (and statistical) burden for high-dimensional and temporally resolved sensors. For example, a 36-element colorimetric sensor array with 100 time-resolved points would be treated as an essentially unresolvable $36 \times 3 \times 100 = 10\,800$-dimensional sensor array using LDA, while TDA treats this as a sensor array with $36 + 3 + 100 = 139$ dimensions; the removed dimensions would mostly account for noise or nonlinearities that are inadequately handled by the model (e.g., nonlinear saturation kinetics).

4.2.2. Support Vector Machines (SVMs). SVM is an optimization-based discrimination technique that seeks to find a decision boundary that best separates two classes in a linear fashion. This is similar to LDA classification in some respects, though the two methods differ greatly in approach. The fundamental premise of SVM is based upon the idea that points far from the decision boundary are easily classified; when a point is far from the decision boundary, small variations in the position of that boundary will not affect the identification. As such, the decision boundary is constructed by analyzing the points most likely to be misclassified: points near a candidate decision boundary are weighted more when considering the position of the boundary. These potentially contentious points (whose position is defined by a multidimensional vector) are called "support vectors".

Optimization of the decision boundary is based on iterative minimization of a structural risk function (i.e., defined by a set of structural equations rather than similarity to an empirical target). The core goal is to maximize the "margin", i.e., the distance between the support vectors and the decision boundary, with additional penalties for offside/misclassification errors. A general explanation of the process is shown in Figure 34.

SVM optimization is well-developed for discrimination within multidimensional data sets, and has been widely applied in computer vision applications, notably in rapid face and eye detection. User-defined parameters can be adjusted in order to best suit the form of the input data; these include, e.g., factors affecting the convergence of the gradient descent algorithm and relative weighting for offside/misclassification errors (especially important if one expects class data to partially overlap). The SVM optimization algorithm with generally accepted default parameters has been built into many modern statistical packages including LIBSVM, an open-source SVM library.[348]

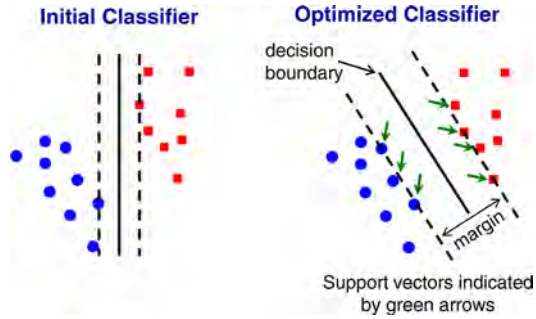

Figure 34. Graphical illustration of SVM classifier optimization. A simplified initial guess is performed (left) and then algorithmically optimized through multiple iterations to maximize discrimination by attempting to maximize the size of the margin and minimize the magnitude of offside errors (right). The margin is defined as the sum distance from weighted contentious points (i.e., the support vectors, indicated by green errors) to the decision boundary. Reproduced from ref 32. Copyright 2016 Royal Society of Chemistry.

While sometimes associated with artificial neural networks (ANNs, see section 4.2.3), SVM is distinct for several reasons and is not properly categorized as an ANN: (1) it uses structural risk minimization instead of empirical risk minimization, which defines a global minimum rather than potentially converging into one of many local minima; (2) because the output is rigidly defined as a linear decision hyperplane, SVM is highly resistant to overfitting (a problem which plagues ANNs); and (3) computational complexity for SVM scales linearly with dimensionality (in contrast, ANN complexity scales quadratically or exponentially with dimensionality).

Because SVM is an optimization-based method rather than an analytical method (e.g., it does not attempt to invert a covariance matrix or perform eigendecomposition), it is compatible with arbitrary nonlinear algorithms (i.e., kernels) that transform the input into a linear form. These kernels are ubiquitous, and this "kernel trick" is generally considered to be a core part of SVM. The most common kernel used in sensors (other than application of no transformation at all, i.e., a linear kernel) is the radial bias function, which is essentially a form of a Gaussian confidence test in which the decision boundary simply represents the Euclidean distance from the mean of the class; this would be used, for example, if one were trying to classify unknown data using a "one against the rest" strategy in which the class data is normally distributed, but the collection of "the rest" is not. On the other hand, if data is expected to be pairwise linearly separable (i.e., data lies on one side of a linear surface or the other, but not both), then it is more common to use a "one against one" strategy with a linear kernel (i.e., no transformation); this is the case in most chemical sensors, as data points for a class are usually normally distributed about a mean sensor response.

The "one against one" strategy applied to N classes in a total set generates $N^*[N - 1]$ total classifiers, and provides unambiguous discrimination between any two well-defined classes within the set (i.e., analyte A vs analyte B). The "one

DOI: 10.1021/acs.chemrev.8b00226
Chem. Rev. 2019, 119, 231−292

against the rest" strategy, on the other hand, generates N total classifiers and provides discrimination between any chosen class (say analyte A) and "the rest" (i.e., the difference set of the total minus class A); as such, a kernel such as the radial bias function must be applied to account for the multimodal distribution of the set difference. Both paradigms are commonly used: the "one against one" paradigm is faster in high-dimensional sensors with small numbers of classes (due to the lack of a nonlinear kernel) and is significantly more accurate when discriminating between two closely related species, while the "one against the rest" paradigm is more amenable to large numbers of classes and can more easily be adapted to account for poorly defined interfering species that do not necessarily have a defined class-mean.

The classifier for each pair of classes is given by a vector and a decision threshold scalar, exactly analogous to the classifiers in LDA or PCA. Evaluation of a classifier simply involves projecting the unknown sensor response onto the classifier vector (i.e., the inner or dot product) and comparing to the threshold value.

SVM has several major advantages over LDA and other discriminant methods, and in fact addresses the two most crippling challenges: SVM is both highly stable and does not require large sample populations. SVM does not use covariance information, which means that the "curse of dimensionality" largely does not apply—there is no expectation regarding response similarities (e.g., homoscedasticity, as in LDA) and sparse data sets (i.e., where many of the dimensions are completely uncorrelated) have no effect on the prediction accuracy whatsoever. Because it is an iterative optimization, SVM can function with extremely small sample populations—in fact, only one point per class is strictly required (though obviously not likely to be accurate). The high stability of SVM derives from the nature of the margin optimization: because only the contentious points (i.e., the points near the decision boundary) are important, variability in the vast majority of points is largely ignored.

For all these advantages, SVM suffers from one major weakness: it is an optimization method, not an analytical solution. It is not possible to apply a mathematical formula and obtain a "best" set of classifiers—though carefully chosen, kernel choice and optimization parameters are arbitrary and must be justified appropriately, similarly to the choice of a linear classifier above. SVM optimization is a mature, highly active research area and has reached an impressive level of sophistication; techniques are incorporated into many statistics and statistical programming packages and implementation is typically straightforward.[32,58,348]

4.2.3. Artificial Neural Networks (ANNs). Artificial neural networks (ANNs) are a special class of general-usage algorithms that can be developed and used for nearly any data-driven application, including descriptive analysis and feature discovery; ANNs are included here under classification techniques due to their ability to address unique nonlinear classification challenges in chemical sensing.[349] A particularly well-explained example can be found in the application of convolutional neural networks toward gaseous analytes by Peng et al.[350] There is a wealth of ongoing research addressing the intricacies of building and training ANNs; more thorough discussions are available on the fundamental theory and exploration of architecture in ANNs.[351−355]

Most analytical methods for sensor data (e.g., PCA, LDA, SVM) are inherently linear methods: PCA and LDA, for example, rely on linear correlations between dimensions, while LDA and SVM rely on linear separability (i.e., the notion that sample classes can be effectively divided by a carefully chosen hyperplane). When data has a nonlinear correlation between dimensions, the standard approach is to use what is known as the "kernel trick"—a known nonlinear function that transforms the data into a linearly separable form. As mentioned in section 4.2.2, by far the most frequent kernel in use is the radial bias function (i.e., distance from center or Euclidean distance) which is commonly used in classifiers taking advantage of "one vs the rest" voting paradigms; when used in this way, the radial bias function is roughly equivalent to a probability estimate using a Gaussian distribution. In general cases, however, the kernel is usually unknown or is poorly chosen, leaving residual nonlinear behavior in the data that can degrade the performance of a classification method or make a regression method unreliable, which can generate spurious dimensionality derived from linear approximations of nonlinear data. When nonlinear behavior is expected, ANNs can be a particularly powerful tool for analysis.

ANNs can be thought of as an extension to numerical multivariate regression techniques, and they use many of the same mathematical principles. In general, networks are built from multiple layers, with each layer mapping data from its input space to its output space (i.e., the input space for the next layer) using linear combinations of its input data (i.e., multiplying by its weight tensor) and application of a kernel transformation known as an activation function. A general schematic is shown in Figure 35.

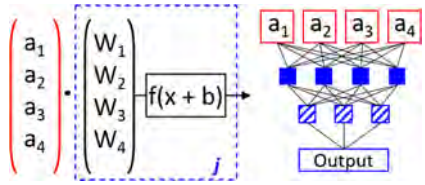

Figure 35. General schematic of ANN architecture. (left) A single neuron j is denoted within the dashed blue lines. Output is determined by computing the dot product of the input tensor ($\mathbf{a}_1 \cdot \mathbf{a}_n$) with the neuron's weight tensor ($\mathbf{W}_1 \cdot \mathbf{W}_n$) and passing the resultant value through the activation function $f(x)$; a biasing term independent of inputs (denoted as b) is also often included (this effectively acts as an x-intercept). (right) Example of a simple four-layer, fully connected feed-forward neural network (also known as a multilayer perceptron); layers are shown as rows, neurons are shown horizontally, and connections are denoted by black lines. The raw input data ($\mathbf{a}_1 \cdot \mathbf{a}_n$) is treated as a separate input layer with one neuron per input dimension that does not have weights or activation functions. The inputs for each succeeding neuron layer are from neurons in the previous layer; in this example, the succeeding layer is connected fully to every neuron in the previous layer. The number of neurons and types of activation functions chosen for the output layer determine the dimensionality and format of the output data.

Weight tensors are almost always randomly initialized (note that there are carefully developed methods for directing this randomization), and the network is subsequently trained by providing a training data set consisting of known inputs and target outputs; in this way, the network converges to a set of weights that minimizes some sort of cost function (also known as loss, or occasionally error functions) and best solves the input-to-output transformation. This is known as empirical risk minimization, which is in contrast to structural risk minimization (as in SVMs). Networks are usually trained using a gradient descent algorithm; when combined with randomized weight

DOI: 10.1021/acs.chemrev.8b00226
Chem. Rev. 2019, 119, 231−292

initialization, this methodology is commonly referred to as stochastic gradient descent (SGD). Another common training technique worth mentioning is a "genetic algorithm" that uses methodology similar to biological natural selection. While the discussion of the relative strengths and weaknesses of each training method is outside the scope of this review, it should be noted that SGD is by far the most commonly used.

The primary strength of ANNs lies in their flexibility—networks can be easily designed to output classification results (i.e., discrete-domain label prediction) or regression results (i.e., continuous-domain label prediction) as well as to learn multiclass and nonlinear structures of input data. The type of output, for example, can be altered by changing the activation functions in the final (output) layer; regression usually involves use of a linear activation function (i.e., a simple linear combination), while classification involves use of a probability-related function (such as the sigmoid function). In general, activation functions are picked due to their relative similarity to the desired output: e.g., bounded functions for probability estimates, unbounded functions for regression, discrete functions for binning, etc. Each function also has its own strengths and weaknesses including, e.g., computational complexity, training speed, stability, and saturation behavior. Four of the most common activation functions are shown in Figure 36: Sigmoid, Tanh (hyperbolic tangent), ReLU (rectified linear unit), and Softplus.

An idealized binary classification algorithm would make use of the Heaviside step function (i.e., a simple two-valued on/off function) that would answer the question of "class A vs not class A". This function cannot be used in SGD, however, because its gradient is either zero or undefined over its entire domain (and thus the network would be untrainable). A smooth, differentiable approximation of the Heaviside step function is the sigmoid function, $(1 + \exp(-x))^{-1}$, and is similarly useful in binary classification when combined with a nontrained thresholding method (representing a probability confidence threshold). Integrating the Heaviside step function leads to the ReLU function, while integrating the sigmoid function leads to the Softplus function. These last three functions are suitable for SGD, and are among the most commonly used functions in ANNs. The tanh function is another approximation of the Heaviside step function and is generally considered an improvement over the sigmoid function; it is numerically related and has the same computational complexity, but its gradient has a narrower shape, leading to faster network convergence as neurons approach the local minimum.

Regression and multiclass analysis are of particular interest in sensor development, as the most commonly used methods for analyzing sensor data are specialized for descriptive analysis (e.g., PCA) or are specialized for pairwise classification (e.g., LDA, SVM). While pairwise classifiers can be extended into multiclass classification using a voting paradigm (i.e., "one against one" with N^2 classifiers, or "one against the rest" with N classifiers), ANNs can be designed to handle similar tasks natively without this additional step using specialized methodology (e.g., using dimensional pooling and the softmax activation function) and can also potentially output additional useful information that is not as straightforward to obtain using other techniques (e.g., correlation, confidence).

Regression analysis presents a potential major advantage of ANNs over traditional analysis techniques, as while analyte classes are often linearly separable (owing to Gaussian noise processes inherent in instrument methods), signal responses are almost never linearly related to chemical input (e.g., concentration) over the entire relevant range of the input values. ANNs can learn these nonlinear response behaviors using a combination of activation functions; in contrast, methods such as PCA, LDA, SVM, etc. each treat regression as a linear problem. Even with an appropriate kernel, linear methods which prove highly reliable for classification may be unsuitable for regression due, for example, to the manner in

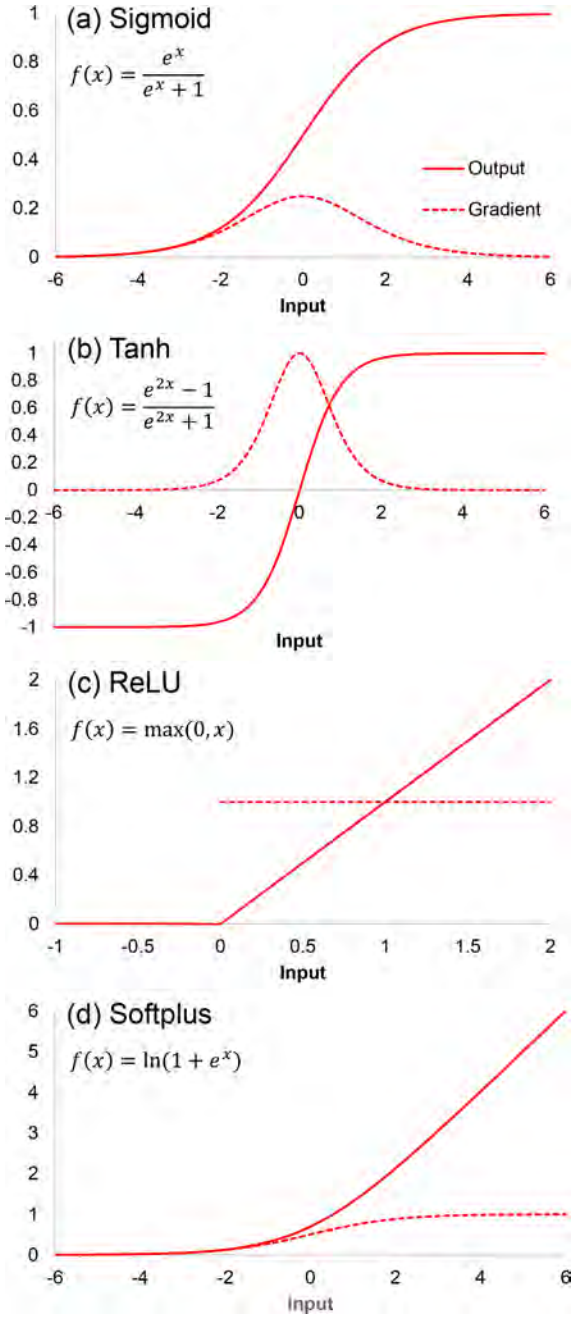

Figure 36. Outputs of common activation functions (blue lines) used in ANNs and their gradients (red dashed lines). The shape of the activation function determines the general shape (e.g., smoothness) of the final combined output. Bounded functions (a) and (b) are related to common probability distributions and are commonly used in classification; unbounded functions (c) and (d) as well as the linear activation function (i.e., $f(x) = x$, not shown) are commonly used for regression. All of these functions are generally used for intermediate (hidden) layers; choice is largely empirical.

DOI: 10.1021/acs.chemrev.8b00226
Chem. Rev. 2019, 119, 231−292

which the methods handle noise coming from the instrument compared to the variability in chemical input.

This flexibility, however, is also the primary weakness of ANNs; a carelessly designed (i.e., "overengineered") or poorly trained network can easily learn and predict undesired or nonexistent nonlinear behaviors. This "overfitting" behavior usually manifests as large fluctuations in output upon small fluctuations in input data, and is even more pronounced than in discriminant methods such as LDA. The most straightforward (i.e., naïve) solution to correcting this behavior is simply to use an extremely large number of training samples to best fit the overall system; this is usually not feasible, however, within the experimental scope of normal research laboratory procedures. Overfitting behavior can often be corrected through clever network design or training paradigms; common methods, for example, involve generating artificial training data or generating additional neural redundancy through addition and selective application of known noise sources. As with all classification methods, segregation of the training and evaluation sets is also vitally important to ensure that one does not underestimate the magnitude of overfitting.

In contrast, all but the simplest ANNs are inherently nonlinear and do not follow a rigid transformation pattern except that defined by the limits within the network. In many ways, ANNs have the opposite problems of the simpler linear methods mentioned above: enforcing approximately linear separability on all but the simplest ANNs can be challenging. As such, ANNs have the biggest advantage over other methods when the relationships between dimensions and samples are known (or strongly suspected) to be nonlinear, and the relationship is unknown or difficult to solve analytically. In all cases, ANNs should be carefully designed and trained to avoid overfitting as well as thoroughly evaluated with an independent evaluation set to provide an accurate estimation of their generalizability.

5. APPLICATIONS OF COLORIMETRIC AND FLUOROMETRIC SENSOR ARRAYS

5.1. Applications to Single Analytes

5.1.1. Volatile Organic Compounds. The colorimetric sensor array, as first developed by Rakow, Suslick, and co-workers, employed an array of different metalloporphyrins exclusively for the visual identification of different families of volatile organic chemicals (VOCs).[50,147] Coordination of analytes to metalloporphyrins induced strong color changes, and the pattern of color changes was used for analyte recognition. The sensor array was able to respond to broad classes of organic compounds such as alcohols, amines, ethers, aldehydes, ketones, thioethers, phosphines, phosphites, thiols, arenes, and halocarbons, often with sensitivities at sub parts per million level and without response to changes in ambient humidity. Using a variety of metalloporphyrins with a wide range of properties including chemical hardness, ligand-binding affinities, and solvatochromic effects allowed for precise discrimination among a wide range of VOCs.

By broadening the types of sensors in the colorimetric array to include shape-selective bis-pocketed porphyrins, pH indicators, and solvatochromic dyes to a total of 24 sensors, Rakow et al.[173] were able to selectively discriminate among structurally related aliphatic or aromatic amines with sub parts per million sensitivities. The sensor array was able to fully discriminate among C3−C8 linear or cyclic alkyl amines, notably including isomeric amines. A similar array was designed by Citterio and co-workers[356] based on a polarity-based method that enabled sensitive detection of seven primary amines with different alkyl chain lengths, with high discrimination ability of the sensor array down to amine concentrations of 50 ppmv.

With further expansion of the array to 6 × 6 colorimetric sensors with several new classes of dye sensors, Suslick and co-workers were able to demonstrate error-free discrimination among 100 different VOCs with common organic functional groups including primary, secondary, tertiary, and aromatic substituents of amines, arenes, alcohols, thiols, aldehydes, ketones, carboxylic acids, esters, hydrocarbons, halocarbons, and phosphines. The array was able to discriminate among VOCs by probing a wide range of intermolecular interactions between analytes and sensor elements, including Lewis acid−base, Brønsted acid−base, metal ion coordination, hydrogen bonding, and dipolar interactions. Figure 37 presents a selection

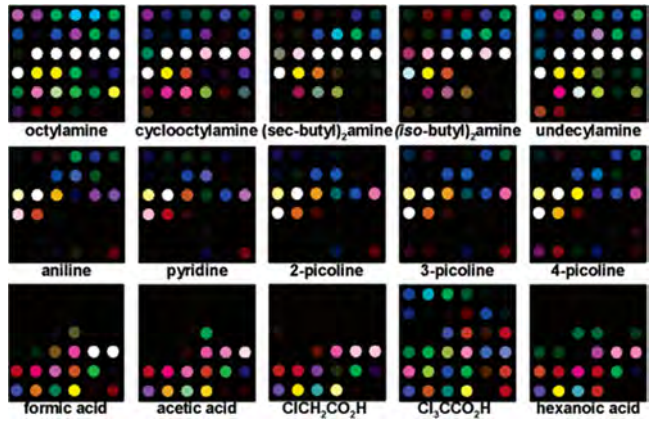

Figure 37. Colorimetric array response to VOCs visualized as color difference maps. Shown are 24 representative VOCs after equilibration at their vapor pressure at 295 K. Reproduced from ref 169. Copyright 2006 American Chemical Society.

of the difference maps of a representative subset of 15 VOCs, including carboxylic acids, aliphatic amines, and aromatic amines. Limits of detection (LODs) are analyte dependent and were not determined in this specific study, but were generally in the low parts per billion volume range for amines, carboxylic acids, thiols, and phosphines. The sensitivity of the array to bases and acids results from the strong metal−analyte or dye−analyte interactions, either by metal ligation (i.e., coordination or dative bonding) or by Brønsted acid−base interactions. Weakly coordinating vapors such as esters, ketones, alcohols, arenes, and hydrocarbons give a lower response, which one also sees with the mammalian olfactory system. It is noteworthy that, with the proper choice of dyes and substrate, the array is essentially insensitive to changes in humidity.

While these colorimetric sensor arrays work exceedingly well for reactive organic volatiles, they do not show particularly strong responses to less reactive vapors. For example, common indoor air pollutants (e.g., alcohols, aromatic hydrocarbons, chlorocarbons, and some organic solvents) are generally not reactive and are not detectable at low vapor levels, which require an effective method for analyte pretreatment to enhance their sensitivity. Lin, Jang, and Suslick[60] invented a dramatic improvement in the sensitivity of colorimetric sensor arrays for the detection and identification of less-reactive VOCs by the use of a disposable preoxidation technique in which the analyte stream was passed through a strong oxidant (e.g., chromic acid

DOI: 10.1021/acs.chemrev.8b00226
Chem. Rev. 2019, 119, 231−292

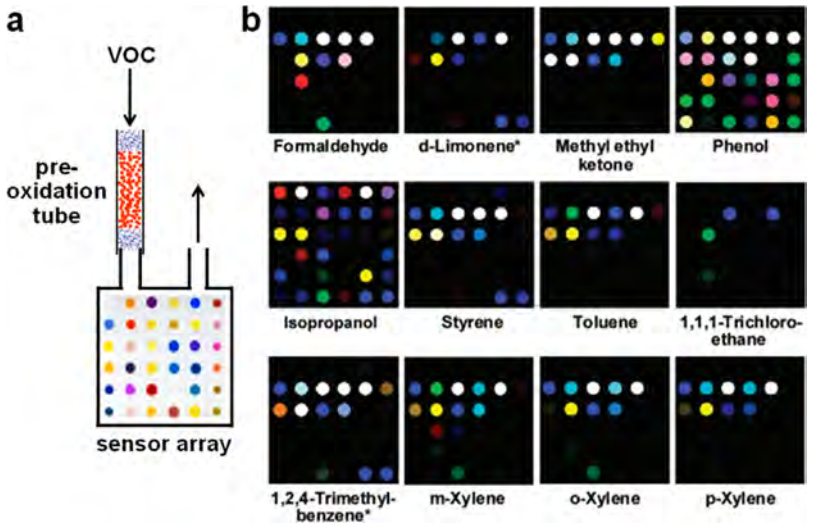

Figure 38. Colorimetric identification of less-reactive VOCs using preoxidation. (a) Schematic illustration of the preoxidation technique. A Teflon tube is packed with chromic acid on silica to pretreat the gas flow before it is passed over the colorimetric sensor array. (b) Color difference maps showing colorimetric array responses to 12 representative VOCs after preoxidation. Reproduced from ref 60. Copyright 2011 American Chemical Society.

Table 1. LODs of 20 VOC Pollutants Commonly Found in Indoor Air with or without Preoxidation (Reproduced from Ref 60. Copyright 2011 American Chemical Society.)

VOC	$LOD_{no\ preox}$ (ppm)	$LOD_{with\ preox}$ (ppm)	$LOD_{no\ preox}/LOD_{with\ preox}$
acetone	1100	16	69
benzene	5000	0.20	10000
camphene	140	1.1	130
chloroform	290	0.60	480
p-dichlorobenzene	100	1.6	63
ethanol	130	0.50	260
ethyl acetate	760	7.4	100
ethylbenzene	350	1.3	270
formaldehyde	50	0.10	500
D-limonene	100	0.90	110
methyl ethyl ketone	1400	2.2	640
phenol	0.50	0.60	0.80
isopropanol	260	18	14
styrene	100	0.50	200
toluene	300	1.3	230
1,1,1-trichloroethane	8000	5.0	1600
1,2,4-trimethylbenzene	300	0.60	500
m-xylene	500	0.50	1000
o-xylene	500	0.60	830
p-xylene	550	0.60	920

loaded on silica) before reaching the array (Figure 38). Preoxidation converts VOCs to chemically reactive species such as aldehydes, ketones, carboxylic acids, and quinones which have a stronger interaction with relevant colorimetric sensor elements. This results in an average of ~300 times enhancement of sensitivity with a concomitant increase in discriminatory capability (Table 1).

Remarkably, since the colorimetric sensor array is based on analyte-array chemical reactivity, chemical class information becomes readily available from the data analysis.[169] Figure 37 shows the familial similarities of the color difference maps of alkyl amines vs aromatic amines vs carboxylic acids, simply by recognizable color patterns. The more detailed analysis afforded by HCA provides quantitative information on how well that chemical class is discriminated against one another (Figure 27). Part of the reason for this successful discrimination among very large numbers of VOCs is the high dimensionality of the data obtained from this colorimetric sensor array. The PCA of the database representing the 100 VOCs shows an extraordinarily high level of dimensional dispersion by the colorimetric sensor array: 14 dimensions are needed to account for 90% of the total variance, 22 dimensions for 95% of the total variance, and 40 dimensions for 99% (Figure 30a).

In an attempt to improve the discriminatory power of the sensor array among volatile carbonyls (e.g., aldehydes, ketones, and esters), Li et al.[243] have recently designed specific amine-containing indicators stabilized by a polymeric plasticizer for selective differentiation of aliphatic or aromatic aldehydes and ketones at parts per million and sub parts per million vapor levels (Figure 39). The newly designed colorimetric sensor array for

DOI: 10.1021/acs.chemrev.8b00226
Chem. Rev. 2019, 119, 231−292

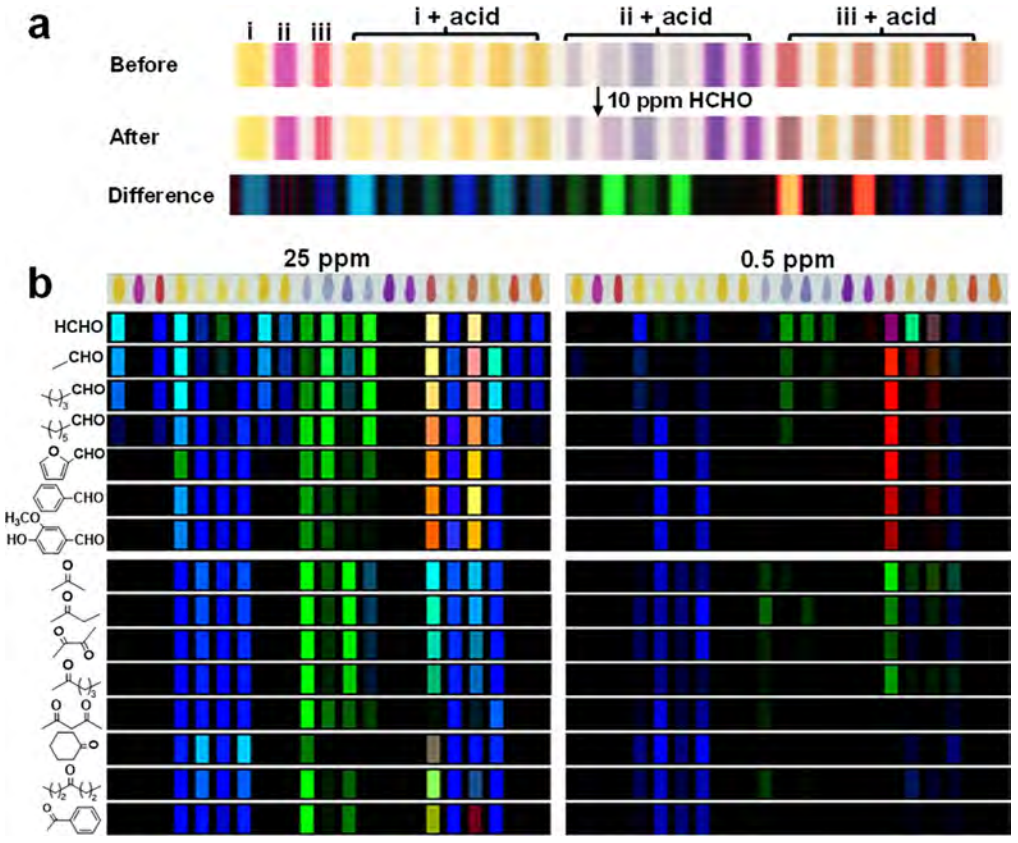

Figure 39. Colorimetric sensor response to aldehydes and ketones. (a) Before exposure, 2 min after exposure, and color difference profile of the array for a typical measurement on 10 ppm formaldehyde. (b) Color difference profiles of seven aldehydes and eight ketones at 25 ppm (left panel) and 0.5 ppm (right panel) after 2 min exposure. Reproduced with permission from ref 243. Copyright 2017 Wiley.

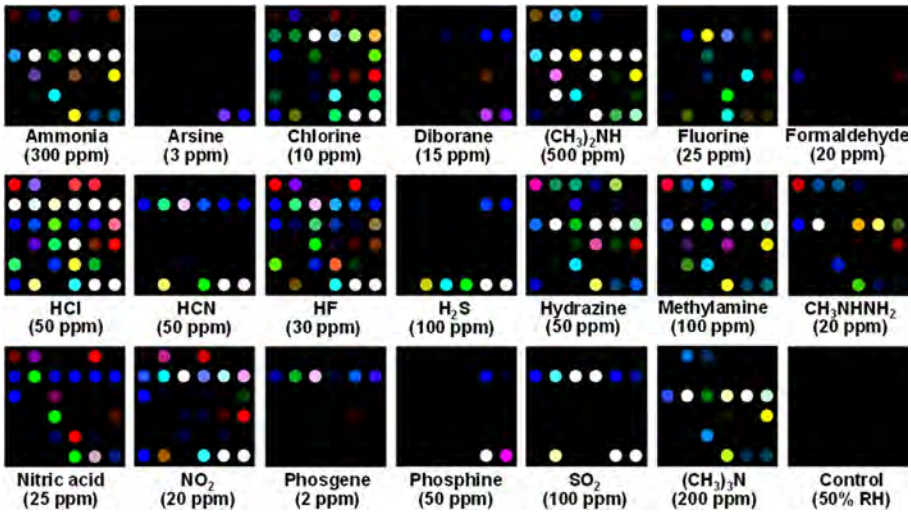

Figure 40. Color difference maps of 20 representative TICs at their IDLH. Reproduced with permission from ref 174. Copyright 2010 Royal Society of Chemistry.

formaldehyde or ketone detection discards commonly used chemoresponsive dyes[357] for a wide variety of VOCs and only retains carbonyl-responsive indicators, and therefore becomes more chemically specific for the recognition of formaldehydes and ketones. This method relies on nucleophilic addition to carbonyl functionalities of analytes by amino indicators in the formation of imines, which gives a substantial change in the visible spectrum and hence a large change in color. Motivated by classic qualitative spot tests including Brady's or Schiff test,[164] aniline and phenylhydrazine compounds were selected as the sensor components and optimized with the addition of different types and amounts of nonvolatile acids. The sensor array allows for the discrimination of aliphatic or aromatic aldehydes and ketones within 2 min, with high accuracy of classification >99% according to HCA, PCA, and SVM analysis. LODs of several representative ketones or aldehydes were calculated to range from 40 to 800 ppb, which are all below 10% of their respective PELs (permissible exposure limits) and substantially better than

DOI: 10.1021/acs.chemrev.8b00226
Chem. Rev. 2019, 119, 231−292

other optical, acoustic, or electrochemical methods in which LODs are generally observed to be at parts per million levels.

5.1.2. Toxic Industrial Chemicals. Toxic industrial chemicals (TICs) are chemically reactive species whose toxicities derive from a wide variety of specific chemical reactions with multiple biochemical systems in cells and organisms. Some acute toxins target specific and critical metabolic enzymes (e.g., HCN inhibits cytochrome *c* oxidase while phosgene inhibits pulmonary function); some cause cell lysis in the lungs creating pulmonary edema (e.g., HCl, HF); other potent oxidants or reductants (e.g., O_3, phosphine) target various relevant biosystems. There remains an urgent need for rapid, sensitive identification and quantification of TICs,[358] yet we have no miniaturized, inexpensive, and effective technology for personal dosimetry of TICs in the chemical workplace or in cases of emergencies such as industrial fires or chemical spills. The chemical workplace has no equivalent to a radiation badge for personal monitoring of exposure to TICs and to provide warning at IDLH (immediately dangerous to life or health) or PEL (permissible exposure limit) concentrations.

There are numerous conventional methods for the detection of gas phase hazardous chemicals, including gas chromatography/mass spectrometry (GC/MS), ion mobility spectrometry (IMS), electronic noses or tongues, and of course colorimetric detectors tailored to specific single analytes. Most such detection techniques, however, suffer from severe limitations: GC/MS is expensive and generally nonportable; IMS has limited chemical selectivity; electronic nose technologies have restricted selectivity and specificity (due to their heavy reliance on weak interactions). Moreover, interference from large environmental changes in humidity or temperature remains highly problematic.

Colorimetric sensor arrays, however, are exceptionally well designed to incorporate a diverse set of chemically responsive indicators for the detection, identification, and quantification of TICs.[27,174,175] Suslick and co-workers developed the use of nanoporous sol–gel or plasticized pigments[27,153,174,175] as the chemoresponsive elements in a series of extremely sensitive colorimetric sensor arrays. They selected high hazard TICs from the reports of the NATO International Task Force 40[359] and examined the ability of their array to discriminate among 20 TICs (Figure 40); LODs for TICs are generally well below the PEL (in most cases below 5% of PEL) and all are below 100 ppb with the exception of formaldehyde, which has been subsequently resolved using a specific aldehyde-sensitive array that can detect as low as 40 ppb formaldehyde (Figure 39).

The sensor array was able to accurately discriminate among those 20 TICs at both their IDLH concentrations within 2 min of exposure and PEL concentrations within 5 min of exposure; HCA showed no errors in misclustering and jackknifed LDA gave an error rate below 0.7% out of 147 trials (Figure 41). The colorimetric sensor array was not sensitive to changes in humidity or temperature over a substantial range. The sensor array has shown excellent stability and reproducibility that the response is independent of the fluctuation in relative humidity and the presence of various common gaseous or liquid interferents.

While LODs are defined absolutely with respect to S/N, that term only defines at which concentration one can determine that a certain analyte is present. Limits of recognition (LORs) are much more useful to define the sensor's discriminatory capability, but they are also library dependent (i.e., relying on the choice of analyte types). Figure 42 demonstrates the limit of recognition for a subset of five TICs (i.e., HCN, NH_3, PH_3, SO_2, and NO_2) is well below 5% of their PEL, which may become of special interest for epidemiological studies. Consistent with the array's capability of discriminating among many possible TICs over a series of parts per million or sub parts per million concentrations below their PELs, PCA and LDA confirmed the high dimensionality of the data achieved by the colorimetric sensor array that requires 17 PCA dimensions to capture 95% of the total variance.[175]

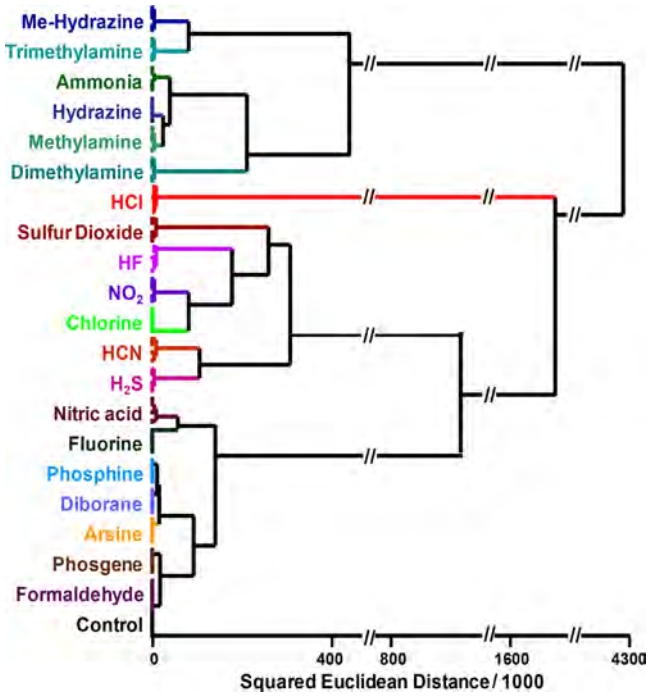

Figure 41. HCA dendrogram for 20 TICs at IDLH concentrations and a control. All experiments were performed in septuplicate; no confusions or errors in clustering were observed in 147 trials. Reproduced from ref 175. Copyright 2010 American Chemical Society.

Other studies of interest in the design of more specialized optical arrays for specific detection of TICs have been actively reported. For example, Hoang et al.[360] developed a dye-impregnated nanofiber sensor array for accurate quantification of gaseous ammonia between 0 and 100 ppm. The sensor's detection sensitivity could be easily regulated using different amounts of acidic additives or types of pH indicators. Bang et al.[154] synthesized organosilica microspheres incorporating pH indicators as nanoporous pigments used in an array to differentiate different aliphatic amines; the array also successfully discriminated a series of vapor concentrations of ammonia, with a reported LOD of 100 ppb (<0.2% of its PEL). Sen et al.[361] developed a disposable colorimetric sensor array which can detect hydrogen sulfide concentrations in the range of 50 ppb–50 ppm at ambient temperature. Sen and co-workers[362] also expanded their work to a more generalized sensor array for ammonia, hydrogen chloride, chlorine, and sulfur dioxide. The array is able to rapidly measure IDLH concentrations of SO_2 (100 ppm) with a response time within half minutes.

As to applications of fluorometric sensor arrays in gaseous TIC detection, a typical example is from Koo et al.,[363] who reported multiple DNA–polyfluorophores as sensor elements for successful identification of eight toxic gases including SO_2, H_2S, MeSH, NH_3, $NHMe_2$, HCl, Cl_2, and BF_3. A set of 15 responding sequences attached with different fluorescent aromatic hydrocarbons or heterocycles was synthesized and

DOI: 10.1021/acs.chemrev.8b00226
Chem. Rev. 2019, 119, 231–292

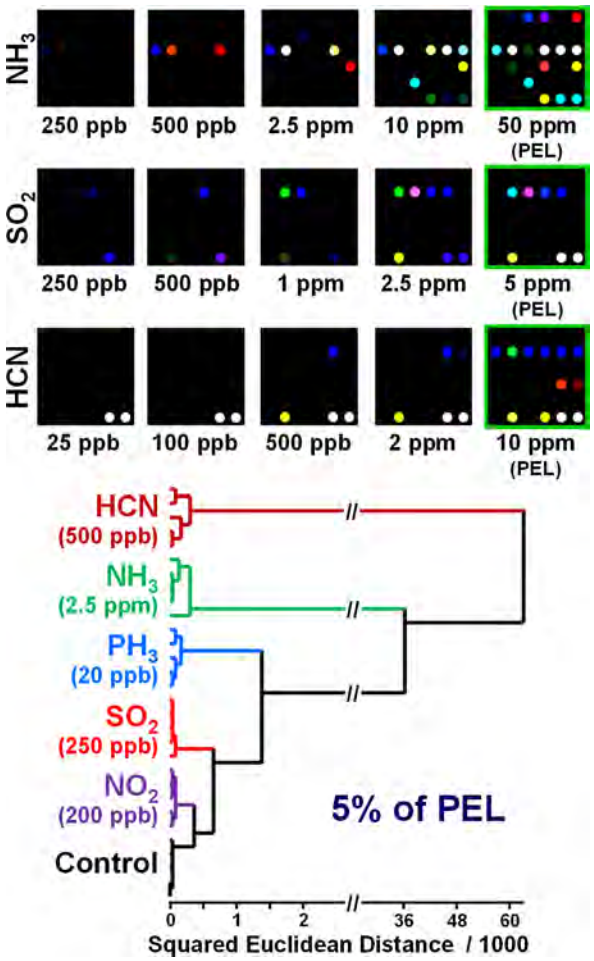

Figure 42. Limits of recognition for the identification of TICs. (left) Effect of concentration on array response to NH_3, SO_2, and HCN. (right) HCA of a subset of five TICs demonstrates a limit of recognition well below 5% of the PEL. Reproduced with permission from ref 174. Copyright 2010 Royal Society of Chemistry.

cross-screened under a microscope against toxic gases. In the imaging analysis, responses were measured according to changes in fluorescence wavelength and intensity, which were quantified as ΔR, ΔG, ΔB, and ΔL (changes in red, green, blue, and overall luminosity) values analyzed from sensor bead images. The polyfluorophore sequences (in Table 2, sequences S3, S7, and S11) were found to give the most quantitative color response plots and were therefore selected for statistical analysis. HCA and PCA based on the subset of those three chemosensors both show clear separation of all gas analytes.

5.1.3. Aqueous Analytes. To make it possible for the sensor array to respond to the volatile vapors of solutes, a colorimetric sensor array (CSA) can be prepared on a hydrophobic membrane with the dye formulations encapsulated in hydrophobic matrices, so as to reduce the blooming of sensor spots and dissolution of dye molecules upon immersion into an aqueous solution. Zhang et al.[289] designed a simple colorimetric sensor array that enables the detection of different organic compounds at very low concentrations (<1 μM) in water. Unique color difference profiles over a wide range of dissolved organic compounds can be readily differentiated by the naked eye.

Monitoring toxic metal ions in water has also been accomplished using a nanoporous pigment array. Feng et al.[364] reported a CSA for identification of trace heavy metal ions (including Hg^{2+}, Pb^{2+}, Cd^{2+}, Zn^{2+}, Ag^{2+}, Cu^{2+}, Ni^{2+}, and Co^{2+}) at wastewater-discharge standard concentrations. Five pyridylazo-based metal chelating probes were immobilized in a phosphate plasticizer and organized into an array via a filtration method. Discrimination of heavy metal ions was performed without interference of Na^+, K^+, Ca^{2+}, and Mg^{2+} ions. The lowest concentration needed for discrimination of eight heavy-metal ions was determined to be 50 μM. Sener et al.[365] demonstrated a facile colorimetric array using 11-mercaptoundecanoic acid capped gold nanoparticles (AuNPs) and amino acids (Lys, Cys, His, Tyr, and Arg) for the simultaneous identification of common heavy metal ions including Hg^{2+}, Cd^{2+}, Fe^{3+}, Pb^{2+}, Al^{3+}, Cu^{2+}, and Cr^{3+} with the LOR as low as 20 μM (Figure 43). The array gave high responsiveness to Pb^{2+} and Fe^{3+} with LODs of 2 and 10 μM, respectively. The AuNP-based colorimetric array showed excellent reproducibility that all tested metal ions in three parallel experiments could be discriminated with no errors.

Recently, Park, Lim, and co-workers have integrated colorimetric sensor arrays with paper-based microfluidics for effective sensing of aqueous anlaytes.[366] This has substantial implication for sensor formulations that are inherently hydrophilic and otherwise prone to blooming if printed on an unconfined substrate (e.g., cellulous paper or polymer membrane). Flower-shaped microfluidic sensor arrays were photolithographically patterned using photocurable monomers, and successfully applied to the aqueous detection and discrimination of eight antioxidants including flavonoids, phenolic acids, and polyphenols in the millimolar range. Four tea products that are abundant in those antioxidants were tested and successfully identified. The microfluidic sensor array can also potentially be applied to the screening of other food and beverages, water pollutants, and biomolecules.

Detection of pesticides in aqueous phase and in real samples has also been accomplished using colorimetric array technologies. A 1 × 5 colorimetric sensor array comprising five probes sensitive to H_2O_2 or thiocholine was reported by Lin et al.;[367] the selectivity of the array is based on the inhibition of different pesticides on acetylcholinesterase (AChE) that produces different amounts of H_2O_2 or thiocholine. Five organophosphates and five carbamates were distinguished at low investigated concentration (10^{-7} g/L) from other classes of pesticides, herbicides, and controls (Figure 44). The sensor array allowed for the prediction of the presence of pesticide residues in apple juice or green tea products, and the test was not influenced by potential interfering agents in the food such as Na^+, K^+, sucrose, glucose, vitamin C, etc.

Fluorescent displacement assays have been extensively employed for identification of amino acids in solution. It was reported that β-cyclodextrin derivatives bearing a metal-binding site and a dansyl fluorophore were combined with pendant L-amino acids and used for selective identification of natural amino acids in aqueous buffer (Figure 45).[368] This method offers effective enantioselective fluorescence probes for the discrimination of enantiomers of the amino acids (e.g., valine and proline). In this work, the authors developed a fast protocol based on fluorescence quenching by using the Cu(II)/amino acid complexes in a fluorescence microplate reader, which allowed for the detection of samples with high enantiomeric excess. Larkey et al.[369] reported a double-strand displacement biosensor for the detection of miRNA. The sensor was able to bind to the target miRNA, while the self-complementary reporter was displaced and folded into a hairpin structure,

DOI: 10.1021/acs.chemrev.8b00226
Chem. Rev. 2019, 119, 231−292

Table 2. Cross-Screening Results of DNA–Polyfluorophore Sequences and Their Blended Difference Images Showing the Responses to 1000 ppm of Each Toxic Gas As Shown by Microscopy (Reproduced with Permission from Ref 363. Copyright 2011 Royal Society of Chemistry.)

	Sequence	SO_2	H_2S	MeSH	HCl	Cl_2	BF_3	NH_3	$NHMe_2$
S1	5'-DYYD-3'								
S2	5'-DDPD-3'								
S3	5'-DDDD-3'								
S4	5'-YYPE-3'								
S5	5'-YEYE-3'								
S6	5'-DPYY-3'								
S7	5'-EDDY-3'								
S8	5'-EYPY-3'								
S9	5'-PPDD-3'								
S10	5'-YEEE-3'								
S11	5'-YYDY-3'								
S12	5'-DEDD-3'								
S13	5'-EDPY-3'								
S14	5'-DEDY-3'								
S15	5'-EDYP-3'								

causing a decrease in fluorescent signal. Recognition of miRNA occurred within 10 min and required no additional hybridization, labeling, or rinsing steps, with LODs at several nanomolar. As a potential application in medical diagnosis, selective detection of a cancer regulating microRNA, Lethal-7, was achieved by this reporter-probe biosensor.

Fluorometric displacement assays based on intramolecular indicators have been used for identification of metal ions. Minami et al.[209] developed an intramolecular indicator displacement assay (IIDA) that utilizes a receptor and a spacer with an attached anionic chromophore in a molecular assembly, for the discrimination of different anions and particularly for phosphates, including phosphate (Pi), pyrophosphate (PPi), AMP, ADP, ATP, and the environmentally important compound glyphosate. Two sensors were designed and introduced into a microtiter array for the detection of phosphate anions: sensor 1 features thiourea and amide groups as anion recognition moieties that induce characteristic blue fluorescence, while two naphthalimide moieties were included to generate bright fluorescence in the case of sensor 2. The assay was used for both anions in the presence of excess NaCl as an interferent. Based on the fluorescence signal obtained after 1 min, excellent qualitative and quantitative recognition results were achieved using only two IIDA sensors. LDA gave accurate classification of all 11 anions and a control (Figure 46); sensitive detection of phosphate with sub parts per million LODs (e.g., 0.2 ppm for glyphosate) was obtained for most of the 11 anions.

Nanoparticles (NPs) present in the environment are a new type of potential aqueous contaminant due to the increasing prevalence of nanomaterials and nanomaterial-enabled technologies. Currently, few studies have been carried out on the detection of trace levels of NPs; there is a pressing need for sensors that can provide rapid, sensitive, and highly portable detection and identification of NPs at nanomolar or even subnanomolar range. Ideally, such sensors should also be able to unambiguously discriminate among NPs with different sizes, shapes, core materials, and surface chemistries, especially since their physicochemical properties (e.g., chemical, optical, electrical, magnetic, and surface corona) have substantial impacts on their potential toxicity. Mahmoudi et al.[370] demonstrated a simple colorimetric array that was able to detect various AuNPs with different shapes (nanospheres or nanorods) and a wide range of sizes (2–40 nm in diameter of nanospheres, 2.4 and 3.5 aspect ratios of nanorods) in aqueous solutions. The sensor array consists of five cross-reactive dye indicators, whose visible absorbances change in response to their interactions with NPs. Although no single dye is specific for any AuNP, the color difference patterns provided by all five dyes display unique molecular fingerprints for each specific NP studied (Figure 47). Based on the digital data obtained from

DOI: 10.1021/acs.chemrev.8b00226
Chem. Rev. 2019, 119, 231–292

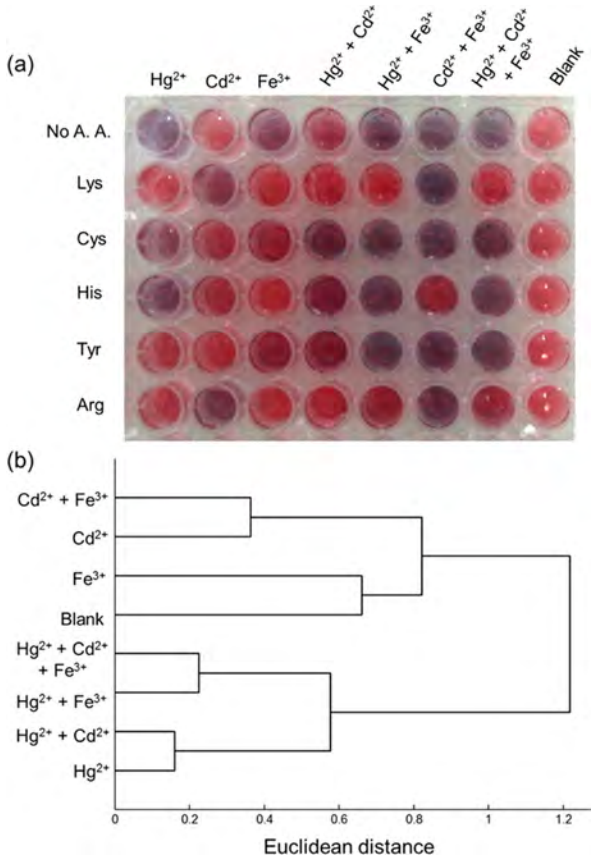

Figure 43. Colorimetric response of the colorimetric array against Hg^{2+}, Cd^{2+}, and Fe^{3+} at 20 μM and their binary and ternary mixtures. (a) Representative photograph. (b) HCA dendrogram. Reproduced from ref 365. Copyright 2014 American Chemical Society.

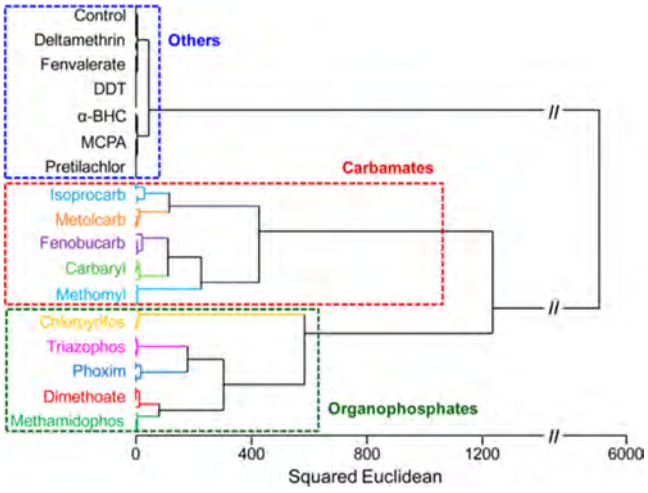

Figure 44. HCA for organophosphates, carbamates, organochlorines, pyrethroids, herbicides, and a control. No confusions or errors in classification for organophosphates and carbamates were observed in 68 trials. The organophosphates and carbamates were tested at 10^{-7} g/L; all other pesticides were at 10^{-4} g/L. Reproduced from ref 367. Copyright 2015 American Chemical Society.

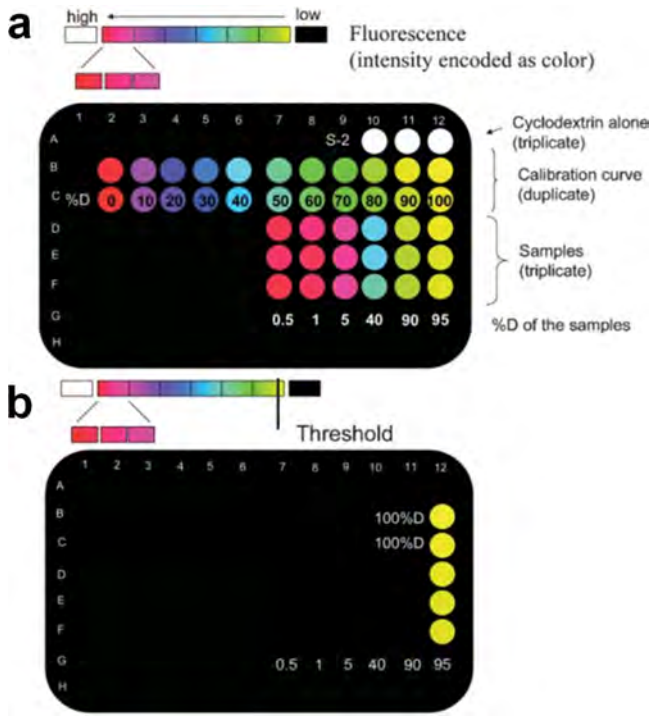

Figure 45. Microplate reader output obtained by a cyclodextrin species (6×10^{-5} M) upon addition of 10-fold excess of $Cu(Val)_2$ complex of different enantiomeric excesses. The fluorescence intensity was encoded as a color. (a) Total output; (b) displayed data below a lower threshold corresponding to 95% D-Val. Reproduced with permission from ref 368. Copyright 2005 Royal Society of Chemistry.

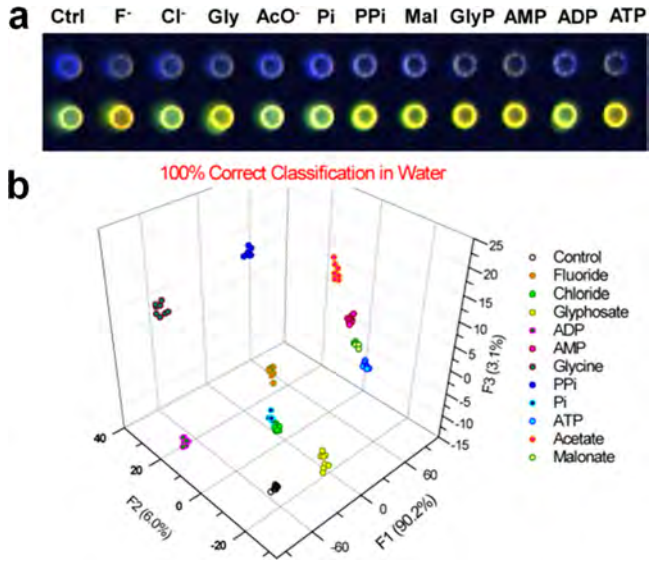

Figure 46. Sensing images of various biological anions and their classification results. (a) Digital images of a microarray chip with the polymer-embedded IID sensors 1 (blue features) and 2 (yellow-green). (b) Graphical output of the linear discriminant analysis showing clusters of 11 anions and a control. Reproduced from ref 209. Copyright 2014 American Chemical Society.

sensor responses of various dyes, a semiquantitative determination of concentration of each type of NP was successfully accomplished, with an excellent detection limit below 100 ng mL^{-1}. Standard chemometric methods were used to precisely discriminate those chemically distinct NPs against each other, and against multifunctional carbon nanospheres without errors in 112 trials. This sensor array therefore may pave the way for a reliable, rapid, and inexpensive approach to detect nanopollution and to characterize the physical or chemical properties of NPs.

DOI: 10.1021/acs.chemrev.8b00226
Chem. Rev. 2019, 119, 231−292

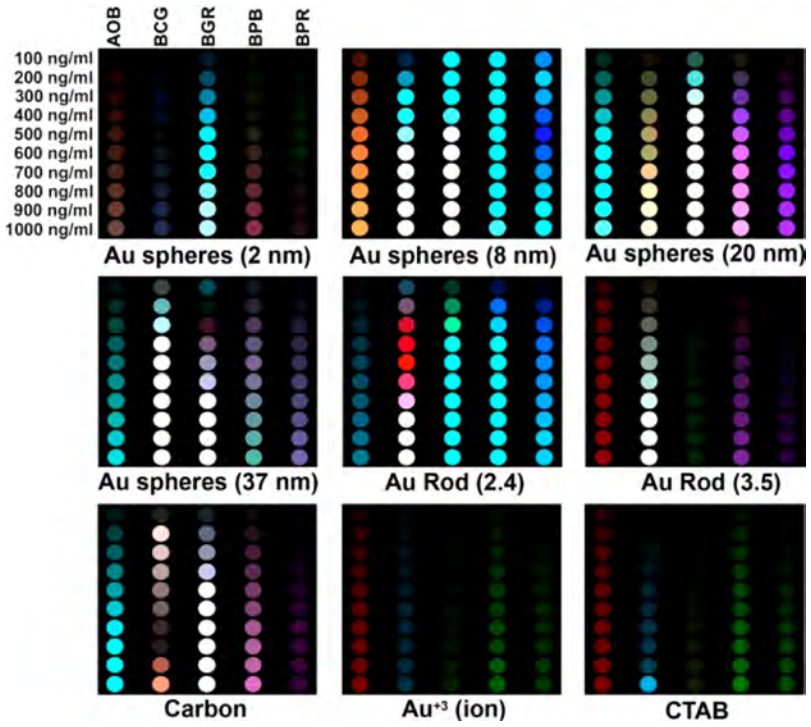

Figure 47. Color difference profiles of five sensor dyes after interaction with various NPs at different concentrations. For display purposes, difference maps were generated by subtraction of the solution absorbance before exposure from that after exposure in response to various NPs, carbon nanospheres, and precursor controls with three selected wavelengths (i.e., 480, 590, and 620 nm) assigned to RGB values; at each of these three wavelengths, absorbances from 0 to 0.484 optical density were mapped linearly to 0−255 in RGB values. Reproduced from ref 370. Copyright 2016 American Chemical Society.

5.1.4. Explosives. As is obvious to anyone who often enters an airport, explosives detection has received great attention over the past decade. While attempts have been made over the years to develop optical sensors that are sensitive enough for practical use, optical methods have yet to measure up to mass spectral approaches, most notably ion mobility spectroscopy; fluorescent detection of nitro-based explosives is an exception, where the electron-deficient nature of nitro groups provides unique fluorescent quenching.[371−373] Nevertheless, examples of optical array sensors for detection and discrimination among relatively volatile peroxide-based explosives and among homemade explosives whose volatiles signature (so-called explosive bouquet[374]) have been reported in recent years. The majority of attempts to optically distinguish nitro explosives (e.g., especially trinitrotoluene, TNT, and cyclotrimethylenetrinitramine, RDX) primarily rely on the unique electronic properties of nitro groups.[375−377] Several of these studies, including approaches to detect other explosives-related compounds and other chemical or biological hazards (e.g., chemical warfare agents, microbes), were discussed in detail by Diehl et al. and Kangas et al. in their recent reviews.[45,378] A more recent array-based approach developed by Parkin and co-workers[379] used multicolor quantum dots featuring several functional surface ligands, which are quenched in the presence of electron-deficient nitro compounds. The multichannel fluorescent array was able to detect and differentiate five nitro explosives, including dinitrotoluene (DNT), TNT, trinitrophenylmethylnitramine (tetryl), RDX, and pentaerythritol tetranitrate (PETN) at their low aqueous concentrations, with LOD < 0.2 μg mL^{-1}.

The peroxides, as one of the most powerful classes of explosives, have emerged as a major explosive of choice used in terrorist activities in recent decades. Peroxide-based explosives, including triacetone triperoxide (TATP) and hexamethylene triperoxide diamine (HMTD), can be readily prepared by an acid catalyzed reaction of acetone with hydrogen peroxide at low temperature.[380] Owing to a lack of UV absorbance, fluorescence, and facile ionization, it is difficult to detect TATP or HMTD from gaseous or liquid samples directly.[381] Techniques that are able to detect peroxide-based explosives generally demand expensive instrumentation, extensive sample preparation, or time-consuming preconcentration of TATP vapor using solid-phase microextraction. To solve these problems, Lin and Suslick[242] reported a new method for detection and quantification of TATP vapor using a colorimetric sensing approach. The TATP vapor in the gas stream is decomposed by a solid acid catalyst contained in the sensor spot (Amberlyst 15), and the resulting H_2O_2 vapor, being kinetically much more reactive, immediately responds to redox indicators. TATP is detectable even at very low concentrations down to 2 ppb (i.e., <0.02% of its saturation vapor pressure). The array could also differentiate TATP from other chemical oxidants (e.g., hydrogen peroxide, bleach, *tert*-butylhydroperoxide, peracetic acid), and the sensor response is independent of the presence of common potential interferences (e.g., humidity, perfume, personal hygiene products, laundry supplies, volatile organic compounds).

Microfluidic paper-based analytical devices (μPADs) stand for a class of easy-to-use sensing platforms particularly for liquid analyte detection and have reached a wide popularity both in academia and in industry. The large variety of relevant studies used in optical sensing has been elaborately reviewed.[382−385] Peters et al.[386] demonstrated a (μPAD) for rapid and field detection of both inorganic and organic explosives, including NO_3^-, ClO_4^-, RDX, H_2O_2, and urea nitrate. The microfluidic

DOI: 10.1021/acs.chemrev.8b00226
Chem. Rev. 2019, 119, 231−292

device was fabricated with wax to generate five hydrophobic channels and prepared on chromatography paper for aqueous sample detection. Each channel contains colorimetric agents that are able to interact with one or more explosive components leading to a specific color change.

In real-world applications, the identification of explosives using a sensor array is primarily based on the recognition of "chemical bouquets", i.e., degradation products or impurities that can be potentially fingerprinted. In order to identify such complicated explosive mixtures, the chemical diversity of the array becomes particularly critical. Askim et al.[32] reported a 40-element sensor array capable of detecting and differentiating among several explosives and related compounds, including a range of amines, nitroaromatic compounds, peroxides, and characteristic contaminants (e.g., cyclohexanone, a major solvent used for RDX purification). The sensor array incorporates a broad range of chemical sensors including traditional pH indicators, redox probes, strong nucleophiles, and a novel class of metal−dye chromogens that are sensitive to nitroaromatics. A set of distinctive color difference patterns from each explosive analyte is shown in Figure 48. Scree plots from

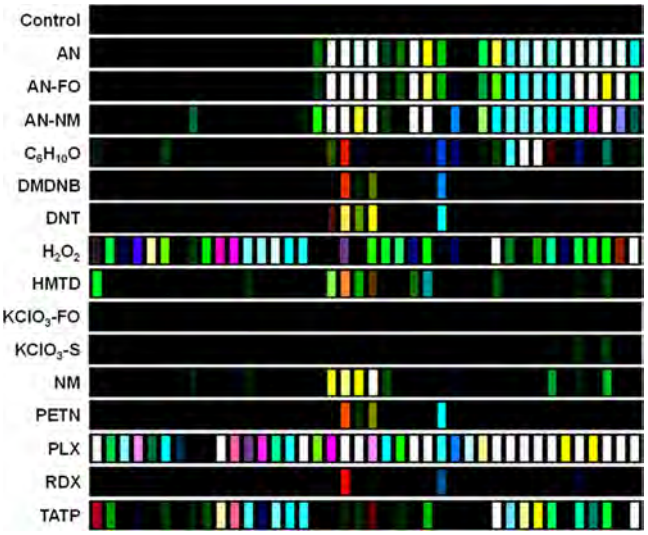

Figure 48. Color difference maps of the 40-element linearized colorimetric sensor array with bar spots showing signal-to-noise ratios of 16 explosives, related analytes, and the control. Reproduced with permission from ref 32. Copyright 2016 Royal Society of Chemistry.

the PCA of results obtained by the array show a high dimensionality in overall response probed by the sensor array; it requires 16 dimensions to account for over 95% of the total variance. As shown in Figure 49, HCA shows that the 16 analytes were separable into 13 groups: two $KClO_3$-containing mixtures were grouped together, along with 2,3-dimethyl-2,3-dinitrobutane (DMDNB), PETN, and RDX (weakly responding nitro-based explosives). Interestingly, application of SVMs used with cross-validation enables the separation of RDX from the group of nitro compounds, and the resulting 14 out of 16 groups had 100% cross-validation accuracy.

In a follow-up study, Li et al.[31] reported that this array was capable of discriminating subtle differences among types of TATP and HMTD prepared by different sources of acids or oxidants, in large part due to the presence of impurities left over from synthesis and degradation products during storage (Figure 50). The colorimetric array was integrated with a field-

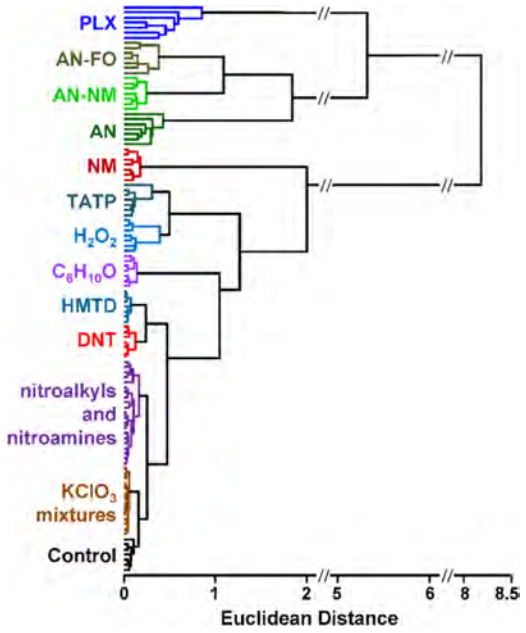

Figure 49. HCA dendrogram of normalized difference vectors for 16 explosives, related analytes, and the control: 112 trials in total. All species were clearly differentiable except among members of two groups: $KClO_3$ mixtures ($KClO_3$−sugar and $KClO_3$−fuel oil) and nitroalkyls/nitroamines (DMDNB, PETN, and RDX). Reproduced with permission from ref 32. Copyright 2016 Royal Society of Chemistry.

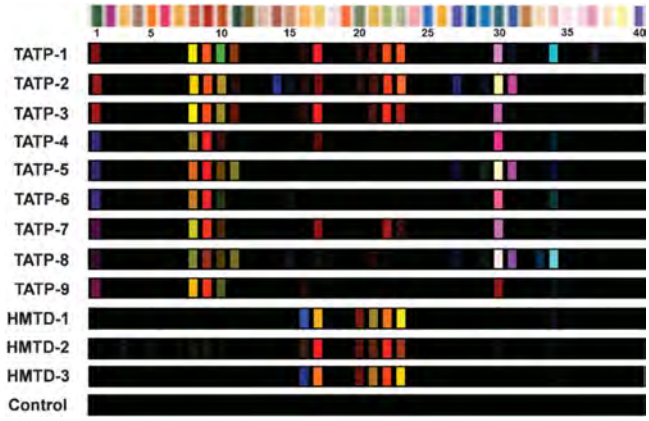

Figure 50. Scaled difference maps of the 40-element colorimetric sensor array showing signal-to-noise ratios of nine TATPs and three HMTDs and a control. TATP and HMTD were synthesized using different peroxide and acid sources. Reproduced with permission from ref 31. Copyright 2015 Royal Society of Chemistry.

deployable handheld reader for real-time analysis of different variations of peroxy explosives, which can be clearly differentiated against each other and against possible interferents found at a typical airport security checkpoint.

Printing quality (e.g., the uniformity of color across an individual sensor spot or from one array to another) of a sensor array is a major factor in its sensitivity and accuracy. Even using the difference maps of digital images before vs during exposure cannot eliminate completely the variation created by non-reproducibility in printing.[169] Improvement in print quality is a perennial challenge, and several methods have been attempted. In one such example, Berliner et al. used photolithographic patterning of a porous membrane to create well-defined polymer

DOI: 10.1021/acs.chemrev.8b00226
Chem. Rev. 2019, 119, 231−292

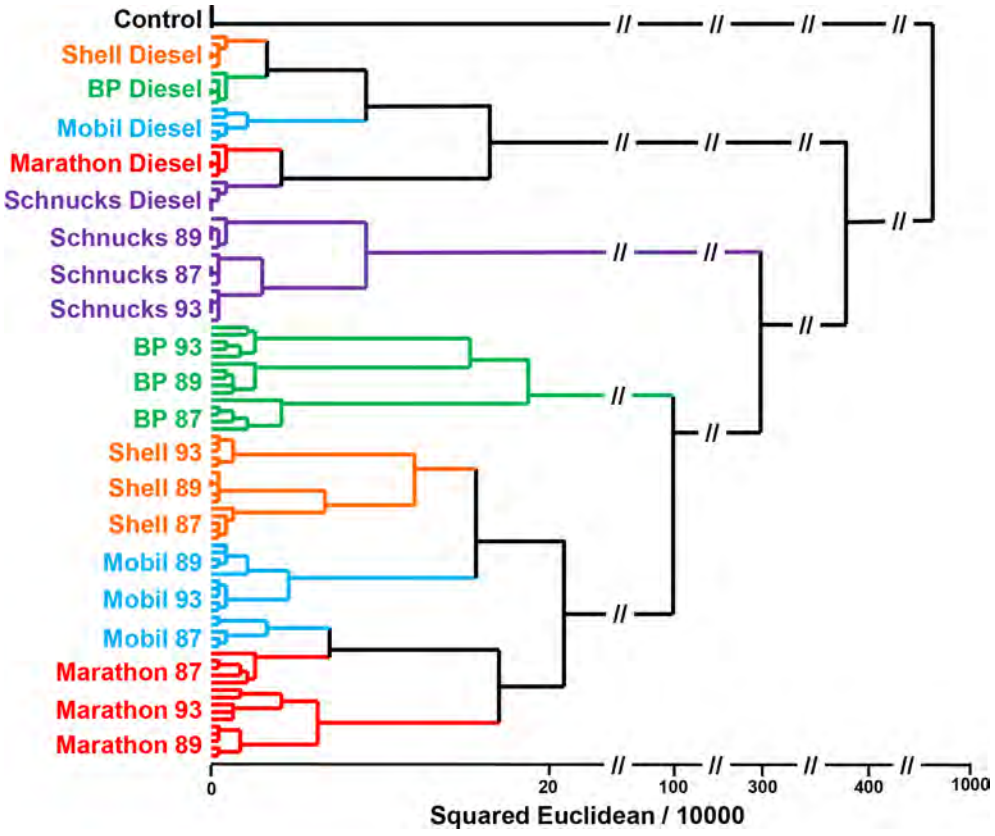

Figure 51. Hierarchical cluster analysis (HCA) for 20 separate automotive fuels and one control. Each analyte name represents quintuplicate trials after 1 min exposure at 1% saturated vapor pressure. No misclassifications or confusions were observed out of 105 total trials. Reproduced with permission from ref 298. Copyright 2015 Royal Society of Chemistry.

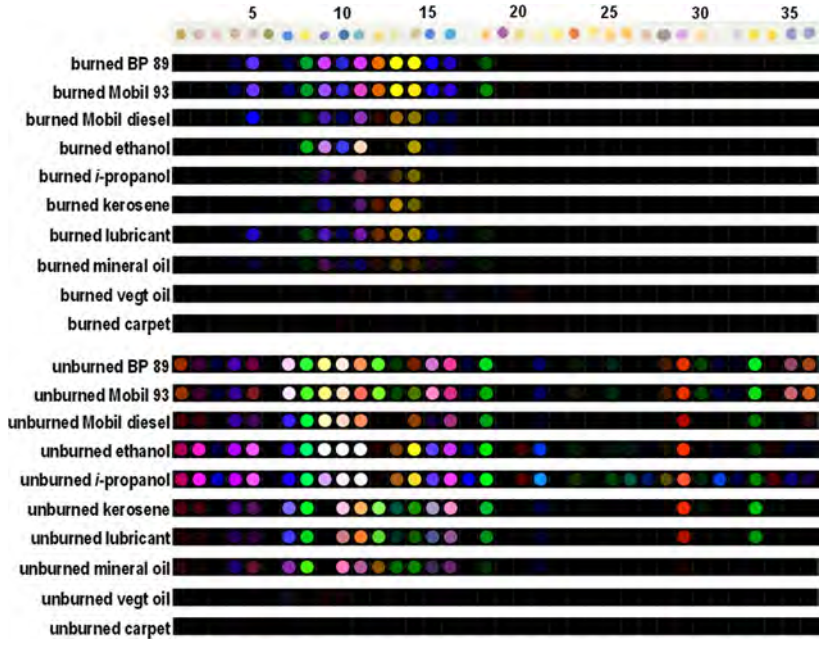

Figure 52. Representative color difference maps showing quintuplicate analyses of multiple accelerants after preoxidation and a control. Reproduced with permission from ref 298. Copyright 2015 Royal Society of Chemistry.

walls that improve the printability of arrays. The resulting array demonstrated highly selective detection of TNT vapor and other nitroaromatic compounds for rapid detection even at parts per trillion levels.[387]

5.1.5. Accelerants and Postcombustion Residues. Automotive fuels and other petroleum products, including gasoline, diesel, kerosene, and lubricants, comprise a class of hazardous chemicals commonly used as accelerants in cases of arson. Chemical sensor arrays have recently shown promising

DOI: 10.1021/acs.chemrev.8b00226
Chem. Rev. 2019, 119, 231−292

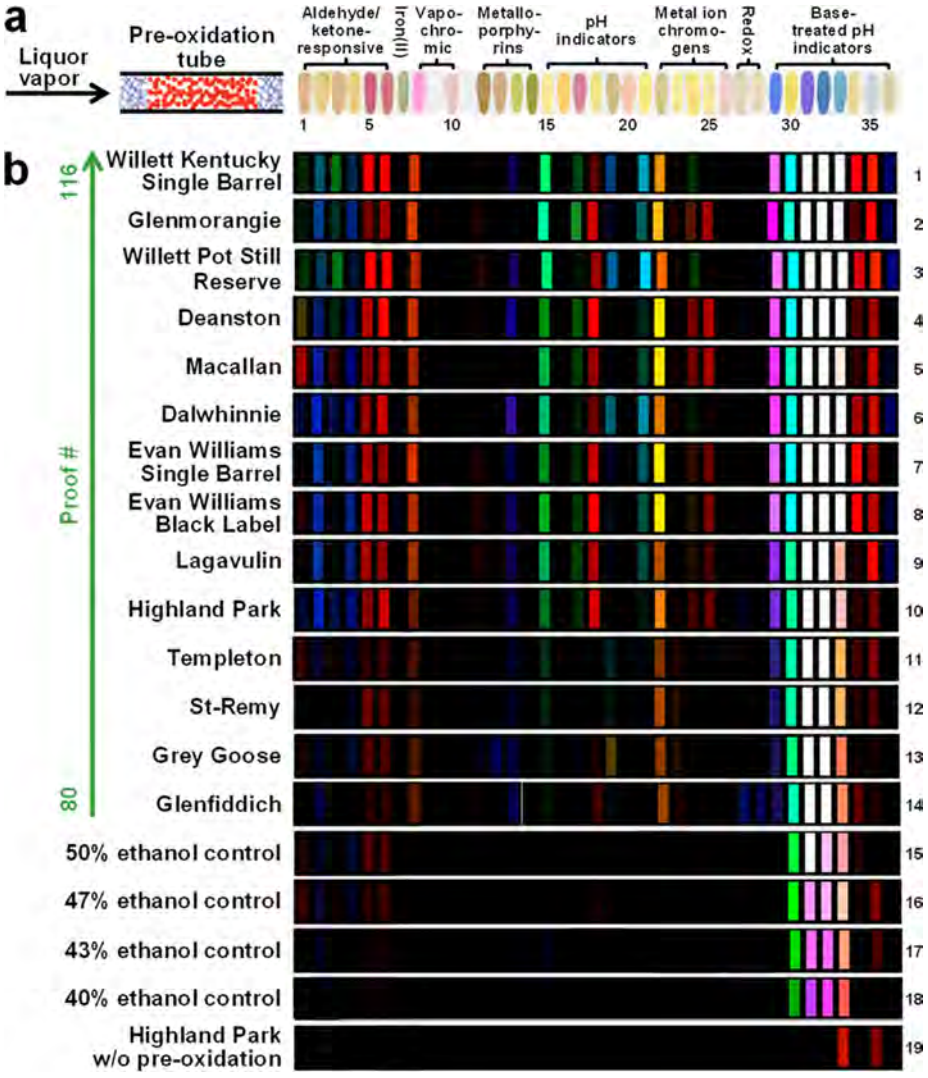

Figure 53. (a) Scheme of preoxidation of liquor vapors before exposure to the 36-element colorimetric sensor array. (b) Sensor array response to 14 liquor samples, four ethanol controls at relevant concentrations, and the control without preoxidation. Reproduced from ref 390. Copyright 2018 American Chemical Society.

applications in forensic identification of those accelerants for both pre- and postcombustion samples; this also has implications in other areas where one may want to identify hydrocarbon samples, such as product analysis and studies of air pollution.

Although colorimetric sensor arrays have traditionally performed well in identifying reactive volatiles, they have low sensitivity toward inert gases such as halocarbons and most hydrocarbons. This is obviously a problem for an array designed to work with precombustion accelerants; common accelerants universally consist of a mixture of alkanes, alkenes, and aromatic hydrocarbons. Suslick and co-workers addressed this problem by employing a pretreatment technique in which the vaporized hydrocarbons are first exposed to a strong oxidant in order to produce more reactive oxidation products (i.e., aldehydes, ketones, and carboxylic acids).[60]

This preoxidation technique was used to discriminate among various types of petroleum products that could act as accelerants both before and after their combustion. Samples included multiple brands of gasoline, common lubricants, and common fuels.[298] The array was able to discriminate even among different brands of gasoline, and further by octane rating. HCA of these data shows complete discrimination with no errors after 1 min of exposure to analytes at 1% of the saturated vapor pressures (Figure 51). Limit of recognition is also well below 1% of saturated vapor pressure for the library consisting of 20 separate automotive fuels plus the control.

Averaged color difference maps showing the sensor responses to both burned and unburned hydrocarbon products are shown in Figure 52. From these difference maps, it is evident that the preoxidation technique significantly enhances the sensor response and the uncombusted samples give more complicated patterns of array response than burned materials, probably due both to analyte evaporation (i.e., reduced analyte concentration during combustion) and to the formation of gaseous combustion products (i.e., CO_2 or CO) to which the sensor array is weakly responsive. The somewhat strong responses observed from some of the burned accelerants (i.e., burned BP 89 or Mobil 93) are attributed to the trace amounts of unburned volatiles or other byproducts from incomplete combustion of the accelerants.

DOI: 10.1021/acs.chemrev.8b00226
Chem. Rev. 2019, 119, 231−292

5.2. Applications to Complex Mixtures

For complex mixtures, chemists often assume that the ultimate goal is a complete quantitative component-by-component analysis. In truth, however, one seldom really wants to know the many hundreds of compounds present in a complex mixture, be it coffee, liquor, soil, bacteria, or exhaled breath. Instead, useful goals are better fulfilled by a highly discriminant fingerprinting of the entire mixture. Such a fingerprinting permits comparison to standards (e.g., quality control/quality assurance), identification of chemical class, origin, or manufacturer, and correlation of the fingerprint to properties measured by other, often less reproducible means (e.g., human sensory evaluation panels, so-called organoleptic analysis). In the cases where component-by-component analysis is required, "hyphenation" is the usual approach,[388] combining a separation technique (e.g., various chromatographies or electrophoresis) with an analysis technique. Sensor arrays are most commonly used for fingerprinting of complex mixtures, although there has been some preliminary exploration of their combination with disposable gas chromatography microcolumns.[389]

5.2.1. Foods and Beverages. The discrimination among highly similar complex mixtures often remains problematic even using the most sophisticated analytical techniques. A great number of foods and beverages are known for their complexity in chemical composition, and a component-by-component analysis is generally impractical, given the thousands of different compounds present in edible materials. On the other hand, quality control or assurance of foods and beverages has become increasingly imperative for regulation of the food industry, and the ability to differentiate adulterated food or beverage samples from the real ones is highly desirable. For these two reasons, the sort of fingerprinting that sensor arrays are able to achieve can prove extremely useful.

Li et al.[390] developed a 36-element colorimetric sensor array composed of a wide range of chemoresponsive indicators for quality control and assurance of alcoholic beverages. In combination with an aforementioned reagent (i.e., chromic acid on alumina support) for the preoxidation of liquor vapors, those alcoholic beverages become more responsive to the sensor array due to the increased levels of aldehydes, acids, and other oxidized products. This generalized sensor array is highly responsive to key components in liquors including aldehydes/ketones, carboxylic acids, polyphenols, sulfides, ethanol, and various other VOCs. Color difference patterns based on 2 min vapor exposure were unique to each of the 14 liquors or controls at relevant ethanol concentrations, and could be readily discriminated even by the naked eye (Figure 53). Sensor responses to real liquor samples were far more complicated than aqueous ethanol controls over a wide range of ethanol concentrations, which demonstrated the high chemical complexity of liquors and provided an effective approach to distinguish real liquors from counterfeited ones.

Han et al.[391] demonstrated a hypothesis-free (i.e., nonspecific interactions involved), three-element array consisting of either fluorescent polyelectrolytes or chimeric green fluorescent proteins (GFPs) for the discrimination of over 30 kinds of whiskies according to their country of origin, brand, blend status, taste, and age. Those fluorescent sensor arrays were based on differential quenching of the fluorescence by the complex mixture of analytes extracted from the oak barrels, including vanillin, vanillic acid, oak lactones, tannins, etc. The differential binding of the analytes to polymers or proteins originated from nonspecific interactions, such as hydrophobicity or electrostatic interactions. LDA showed accurate classification of (Figure 54). These fluorescent probes proved equal or even superior to state-of-the-art mass spectrometry in terms of the speed, resolution, and discriminatory powder.

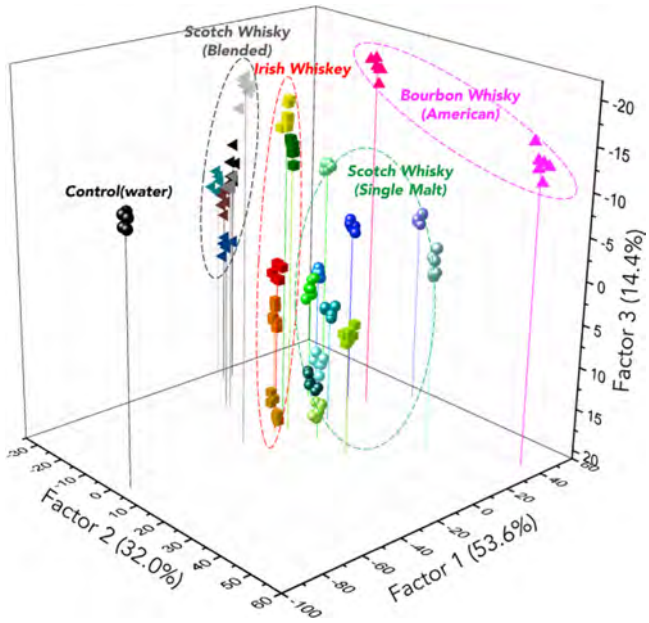

Figure 54. LDA plot of the fluorescence modulation data obtained with an array of selected polyelectrolytes treated with all of the whiskies investigated. The jackknifed classification matrix with cross-validation reveals 99% accuracy. Reproduced with permission from ref 391. Copyright 2017 Elsevier.

Jia-wei Li et al.[392] used a colorimetric sensor array consisting of four chemical reagents to analyze multiple Chinese liquors. Based on PCA, HCA, and LDA using "leave-one-out" cross-validation, the colorimetric sensor array was able to distinguish four types of Chinese base liquors from a famous liquor brand, "Luzhou Laojiao", nine Chinese liquors with different flavor types, and seven Chinese liquors from different geographical origins.

Colorimetric sensors have also shown useful applications in other common alcoholic drinks. Zhang et al.[40] reported an earlier version of colorimetric sensor arrays that enabled the differentiation among 18 brands of beer. Accurate results of differentiation between ales and lagers were obtained, and even among very similar beers the classification was still able to achieve an accuracy rate of >97%. In addition, differentiation of pristine beer from the effects of watering or decarbonation proved possible. As another example in beer quality screening, Rico-Yuste et al.[393] reported a disposable polymeric film for quantification of furfural, as an indicator of beer freshness. The designed colorimetric reaction between aniline-derived polymers and furfural based on the Stenhouse reaction was monitored using a portable fiber optic spectrophotometer or the built-in camera of a smartphone. The sensor film allowed for sensitive detection of furfural with a linear response range of 39–500 $\mu g\ L^{-1}$ and a detection limit of 12 $\mu g\ L^{-1}$, both of which were superior to other available colorimetric or chromatographic methods.

Coffee provides another prototype of highly multicomponent systems of beverages. While there are about 300 volatile compounds in unroasted and green coffee, over 1000 volatile

DOI: 10.1021/acs.chemrev.8b00226
Chem. Rev. 2019, 119, 231–292

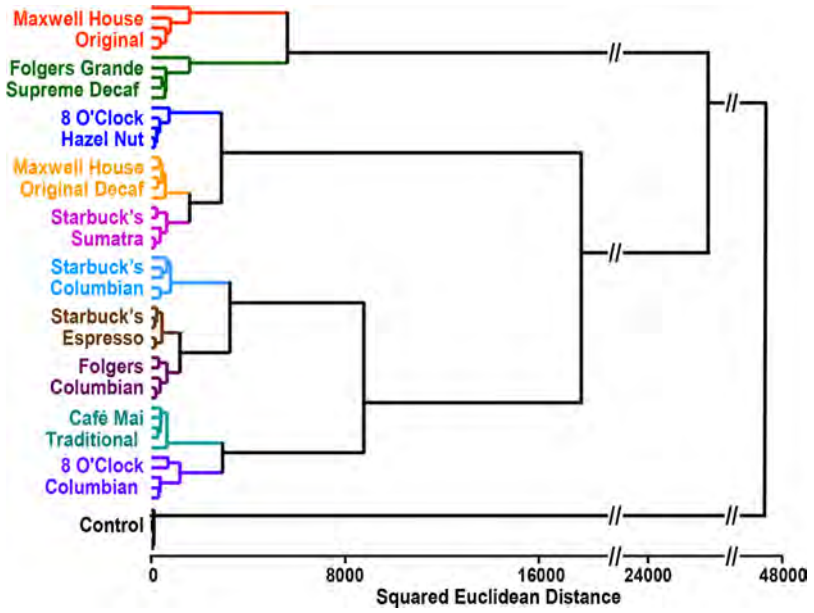

Figure 55. HCA for 10 commercial coffees and a control, with all analytes run in quintuplicate. Adapted from ref 397. Copyright 2010 American Chemical Society.

compounds have been identified for roasted coffee including carboxylic acids, alcohols, aldehydes, alkanes, alkenes, aromatics, esters, furans, ketones, lactones, oxazoles, phenols, pyridines, thiazoles, and thiophenes.[394−396] Moreover, the roasting of coffee beans is highly dynamic, and the processes that develop the flavor and aroma of coffee are largely dependent on the time and temperature. Suslick et al.[397] made use of the same sensor array developed for TIC identification for the measurement of coffee aromas. The color changes of the sensor array were used as a digital representation of the array response and analyzed with standard statistical methods. In quintuplicate runs of 10 commercial coffees and controls, HCA gave tight clustering of all analyte and control groups with no confusions or errors out of 55 trials (Figure 55). PCA revealed that the sensor array has extraordinarily high dimensionality with 25 dimensions to account for >95% of the total variance. In addition, the effects of time and temperature on the roasting of green coffee beans were readily observed and distinguishable with a resolution of 5 min and 10 °C, respectively.

The nutritional value of milk is primarily determined by its fat amount, and a rapid and sensitive fat sensor is therefore in high demand for the quality control of dairy products. Chang and co-workers have developed a fluorometric microplate assay for quantification of milk fat using bodipy-based sensors that rely on disaggregation-induced fluorescence emission.[398] By monitoring the fluorescence spectra of the microwell plate, the assay was able to quantitatively measure the fat amount of different milk samples and to classify them based on their fat content, thus proving useful in a milk quality control process.

Monitoring the freshness of meat products, including pork, beef, poultry, and fish, is a potential application of colorimetric and fluorometric sensor arrays in food inspection. Chen et al.[399] constructed a paper-based colorimetric sensor array with cross-reactive dyes encapsulated in resin microbeads. These dyes were sensitive to volatile amines produced during spoilage of chicken. A low-cost smartphone camera was used to obtain color information on the sensor array pattern for quantitative estimate of chicken aging and eventual spoilage under different temperature conditions. Salinas et al.[400] reported an optoelectronic nose constructed from 16 pigments (pH indicators, Lewis acids, hydrogen-bonding derivatives, selective probes, and natural dyes) incorporated into porous silica or alumina for identification of the age of chicken meat, again based only on detection of biogenic amines. Li and Suslick most recently have expanded the range of analytes used for meat spoilage detection.[312] They made use of a disposable array combined with a handheld device for on-site assessment and monitoring of the freshness of five meat products: beef, chicken, fish, pork, and shrimp. The sensor array showed excellent sensitivity to gaseous analytes, especially amines and sulfides at low parts per billion levels; excellent discrimination among meat volatiles in terms of meat type and storage time was demonstrated with multiple chemometric approaches including PCA, HCA (Figure 56), and SVM analysis.

Detection and quantification of saccharides is of great importance in real-time monitoring of food quality. Lim, Musto, and Suslick[342,401,402] have developed colorimetric sensor arrays for detection and quantification of saccharides and artificial sweeteners using a 4 × 4 colorimetric sensor array. The chemoresponsive colorants used were immobilized in hydrophobic nanoporous organosilanes as host matrices. Based on the color difference patterns generated from the array, the sensor was able to accurately determine 14 sugars and sweeteners at millimolar concentrations in buffered solution (pH 7.4). The concentrations of sugars and sweeteners could be determined over at least a 5-fold range, and glucose concentrations were measurable over the full range of clinically significant levels for blood sugar determinations.

Anslyn and co-workers have developed a general displacement strategy using a series of serum albumins and three fluorophores as sensing ensembles that can selectively respond to a variety of nonpolar analytes, including fatty acids,[279] terpenes,[403] plasticizers,[404] and glycerides.[273] For their applications in food chemistry, the resultant probe was able to differentiate among four fatty acids (palmitic acid, oleic acid, stearic acid, and linoleic acid) and among five edible oils (sunflower oil, hazelnut oil, canola oil, extra virgin olive oil, and peanut oil). PCA of the data library shows clear clustering

DOI: 10.1021/acs.chemrev.8b00226
Chem. Rev. 2019, 119, 231−292

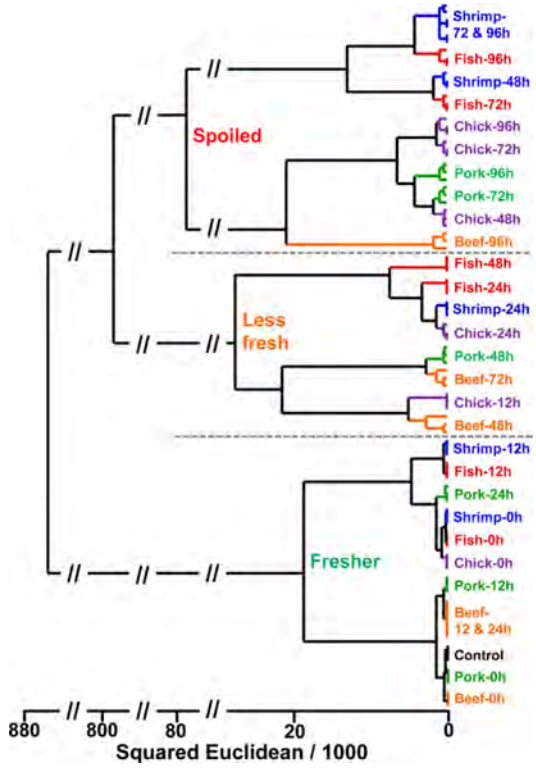

Figure 56. Dendrogram showing hierarchical cluster analysis of the spoilage of five meat products stored at 25 °C with 0, 24, 48, 72, and 96 h plus an ambient air control; 93 trials in triplicate replicates. Reproduced with permission from ref 312. Copyright 2016 American Chemical Society.

among all analyte species. It is noteworthy that the PCA is heavily dominated by a single component (~90% of total variance), and that dimension essentially represents the hydrophobicity of the analytes (which is determined by carbon chain length and degree of unsaturation of different fatty acids involved).

In a similar concept, Anslyn and co-workers used the definition of the indicator displacement assay (IDA) by designing a set of peptide-based ternary sensing ensembles to discriminate among polyphenol-based flavonoids and red wine varietals.[405] In the designed IDA, the probes were based on replacement of a catechol dye from a cation center bound to the peptide; the designed strategy (Figure 57) is quite straightforward and specific due to significant structural similarities between the indicator dye and chosen analytes. The method was also successfully employed for the prediction of the composition of red wine blends[277] and differentiation of wood extracts of Cachaça,[278] the most popular alcoholic beverage in Brazil, which is made from distilled and fermented sugarcane juice. The discrimination pattern was accurate and reproducible for Cachaça extracts of oaks obtained from different countries and of Brazilian woods (as alternatives to oaks for aging Cachaça) from different regions (Figure 58).

Colorimetric sensor arrays have successfully been applied in wine discrimination. Using a diversified set of synthetic boronic acid and guanidinium-functionalized receptors, the Anslyn group designed a 3 × 3 array sensitive to organic acids in wine.[406] The authors showed the ability of the array to discriminate malate, tartrate, and citrate based on spectrophotometric data at three wavelengths (the indicator maxima); using this data, the array was able to discriminate accurately among six different red wines. These more chemically diverse displacement assays provide a much higher dimensionality of data (three dimensions include 88% of the discriminatory power) as demonstrated by the LDA, and a much improved distinction between the wine varietals compared to their prior publication.[405]

5.2.2. Proteins. Developing an economically accessible, high-throughput sensing technique for identification of proteins is of substantial importance in medical diagnostics, especially in the area of proteomics. There have been several recent studies reported on the use of optical sensor arrays for sensing individual proteins in solution,[407,408] some of which have been further applied to the detection of real biological samples, including bacteria and cancer cells.[409,410] One may hope that such arrays might prove useful for detecting specific proteins in blood or urine that could be associated with pathogen diagnosis or health monitoring.

Li et al.[409] reported the applications of unmodified noble metal nanoparticles in the detection of proteins. In this work, five gold nanoparticles and two silver nanoparticles with different sizes constructed the colorimetric sensor array, which could selectively interact with proteins and show distinct color change patterns. The array was able to discriminate 10 different proteins at 0.5, 5, and 50 μM each without errors based on LDA results (Figure 59). Wang et al.[411] demonstrated a fluorescent turn-on array consisting of several combinations of nanoparticles and CdSe quantum dots for sensitive detection of proteins. The addition of proteins disrupted interactions between nanoparticles and quantum dots, thus restoring distinct fluorescence responses. A linear dynamic range of 2−50 μM was obtained, and LODs were generally below 2 μM for all tested proteins. Hou et al.[407] tested an artificial tongue modeled closely on Suslick's work using a series of metalloporphyrins and indicator dyes capable of rapid interaction with proteins. The array produced distinct patterns in response to each protein which permitted accurate identification of the pure and mixed proteins as well as denatured proteins at 10 μM. Two-dimensional PCA plots showed excellent discrimination

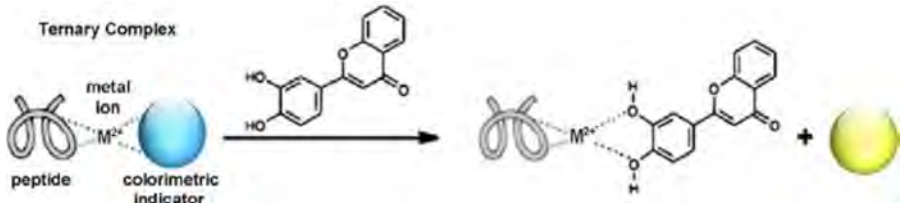

Figure 57. General scheme of a peptide-based ternary sensing ensemble for the discrimination of wine flavonoids. Differential sensing ability is provided by several peptide sequences used with an indicator displacement strategy. Reproduced with permission from ref 405. Copyright 2011 Royal Society of Chemistry.

DOI: 10.1021/acs.chemrev.8b00226
Chem. Rev. 2019, 119, 231−292

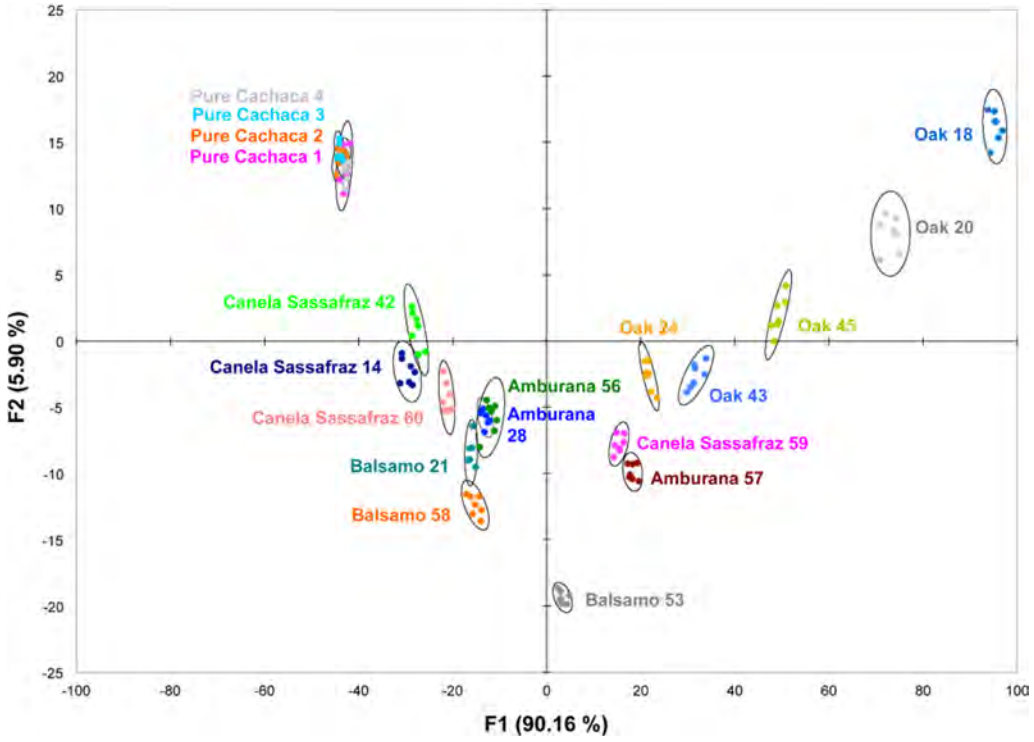

Figure 58. LDA score plot of UV−vis responses of the peptide-based ternary sensor array to Cachaça extracts of oaks and Brazilian woods (Amburana, Balsamo, and Canela-Sassafras) in comparison to pure samples. The numbers for oak samples represent different countries of origin, while different numbers associated with Brazilian woods represent different regions within each country. Reproduced from ref 278. Copyright 2017 American Chemical Society.

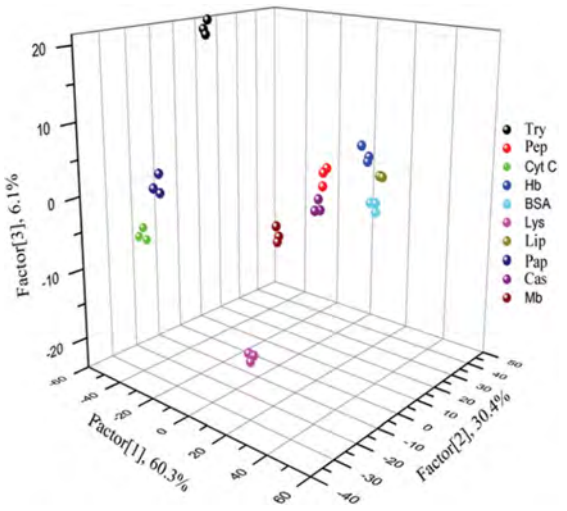

Figure 59. Canonical score plot for the first three components (factors) from LDA of simplified absorbance response patterns obtained with the noble metal nanoparticle-based array against 5 μM proteins. Reproduced with permission from ref 409. Copyright 2015 Royal Society of Chemistry.

among all tested proteins, especially given that only ~64% of the total variance is captured for pure and mixed proteins and 82% of total variance for natural and denatured protein clusters in a two-dimensional plot. Remarkably, one is able to distinguish thermally denatured proteins from the native form rather easily using this approach.

Fluorometric sensor arrays using displacement or differential assays also show significant capability in the differentiation of proteins with complicated structures. Of special interest, the Rotello group has extensively worked on creating multiple differential sensor arrays using engineered gold nanoparticles with the goal of discriminating among a variety of biological samples; this area of work has been both concisely[412,413] and exhaustively reviewed.[414−416] The analytes competitively bind to gold nanoparticles with fluorophores, which adds additional unique characteristics to the selectivity of sensor arrays, as shown schematically in Figure 60. Different types of fluorophores as capping agents have been used in their studies, including synthesized polymers,[417−419] green fluorescent proteins (GFPs),[343] and enzymes[420] that catalyze the generation of new fluorophores.

In one of their representative publications, Rotello and co-workers used a gold nanoparticle−fluorophore system made from gold nanoparticles conjugated to green fluorescent protein (GFP−NP) to act as the displaced indicator. Using a protein as the displaced indicator is a straightforward method of discriminating among peptide-based analytes due to the molecular similarity between the incoming analyte and the displaced probe. This method allowed for the discrimination among several types of human serum proteins including fibrinogen, HSA, α-antitrypsin, transferrin, and IgG (Figure 33),[343] which was then reported in a subsequent publication for the detection of mammalian cells.[421]

In another work, Rotello and co-workers used a set of functionalized Fe_3O_4 nanoparticles to discriminate among several proteins, which utilizes the interactions between proteins and cationic Fe_3O_4 nanoparticles that enable the modulation of their peroxidase-like activity in response to H_2O_2.[417] This work used only two probes for discrimination, which unavoidably leads to low dimensionality. In practice, the variance of data is dominated by a single dimension, as shown in Figure 61. The

DOI: 10.1021/acs.chemrev.8b00226
Chem. Rev. 2019, 119, 231−292

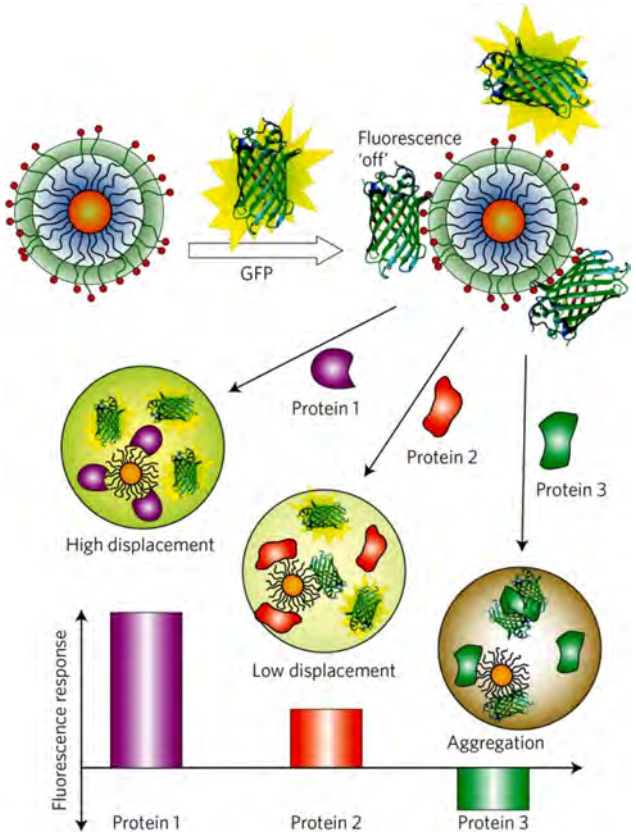

Figure 60. Schematic representation of competitive binding between protein and quenched green fluorescent protein (GFP)−gold nanoparticle complexes and protein aggregation, which leads to restored fluorescence or further quenching with distinct responses. Reproduced with permission from ref 343. Copyright 2009 Nature.

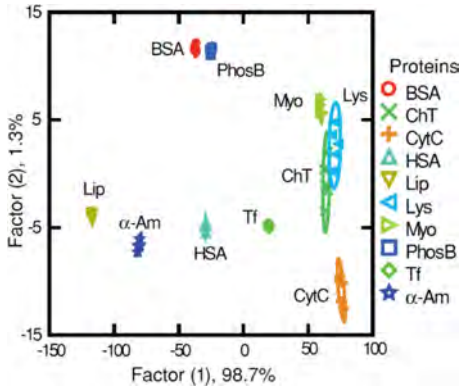

Figure 61. LDA score plot showing discrimination among 10 separate proteins using cationic Fe_3O_4 nanoparticles. Note the complete dominance by one dimension (factor 1). Reproduced with permission from ref 417. Copyright 2012 Wiley.

authors state that surface charge, protein size, and surface hydrophobicity all play roles in discrimination of these species; they may all contribute in a composite sense to the principal component, but the low dimensionality of the data means that one is likely to encounter overlaps in clustering due to changes in concentration or other factors, and the ability to discriminate one cluster of analytes from another is heavily limited by the S/N in the two dimensions (i.e., the width or length of the ellipsoids marking out one cluster from another). The origin of the specificity is not clear; proteins with very similar p*I* values are differentiated, and there is no correlation with protein size or surface charge. More detailed data about surface hydrophobicity may provide some further insight.

Anslyn and co-workers also reported a set of 30 aptamers for fluorescent discrimination of protein variations of HIV-1 reverse transcriptase with a few substitutions in amino acids (WT, M3, M5, and M9, as shown in Table 3), based upon the differential

Table 3. Amino Acid Identity for Protein Variants of Wild-Type (WT) or Drug-Resistant Variant (M3, M5, and M9) of HIV-1 Reverse Transcriptase (Reproduced with Permission from Ref 422. Copyright 2011 Wiley.)

no.	WT	M3	M5	M9	no.	WT	M3	M5	M9
41	M	L	M	M	44	E	D	E	E
67	D	N	N	D	69	T	D	D	T
70	K	K	R	K	75	V	V	V	I
77	F	F	F	L	116	F	F	F	Y
118	V	I	V	V	151	Q	Q	Q	M
184	M	V	V	M	210	L	W	L	L
215	T	Y	Y	T	219	K	K	Q	K

sensing protocols.[422] The three-dimensional (3D) LDA plot showed that clusters were separated in the vector space defined by the three most important components (Figure 62). Leave-

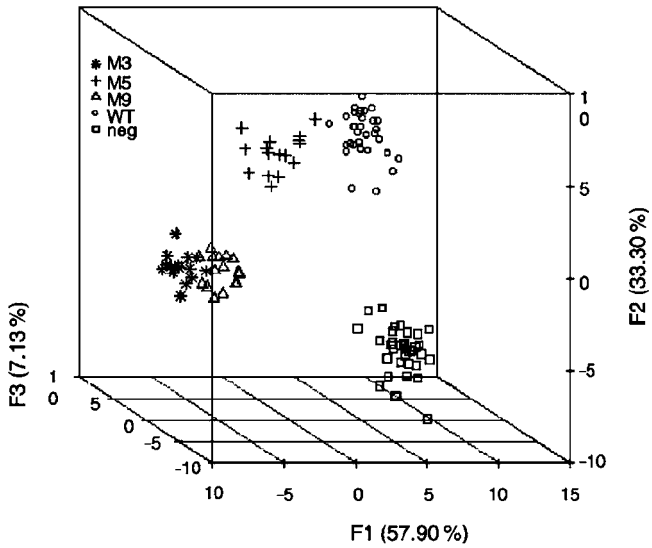

Figure 62. Normalized 3D LDA of 30 aptamers set for the discrimination of four protein variants plus the negative controls; 98.3% of total variance captured. Reproduced with permission from ref 422. Copyright 2011 Wiley.

one-out cross-validation revealed that M9, WT, and the negative controls could all be predicted with 100% accuracy, while an overall accuracy of ~85% was obtained for M5 and ~73% was obtained for M3. This work proved the hypothesis that an array of cross-reactive aptamers could act as an effective tool for discriminating proteins that are structurally similar without the efforts to create specific receptors for each variant.

5.2.3. Ratiometric Fluorometry for Intracellular Sensing. In a sense, the incorporation of two or more fluorophores in a single probe constitutes a special class of low-dimensionality optical sensor arrays: ratiometric fluorescent probes with multiple fluorophores (which display either dual-excitation or dual-emission behaviors) can provide an array-like, self-

DOI: 10.1021/acs.chemrev.8b00226
Chem. Rev. 2019, 119, 231−292

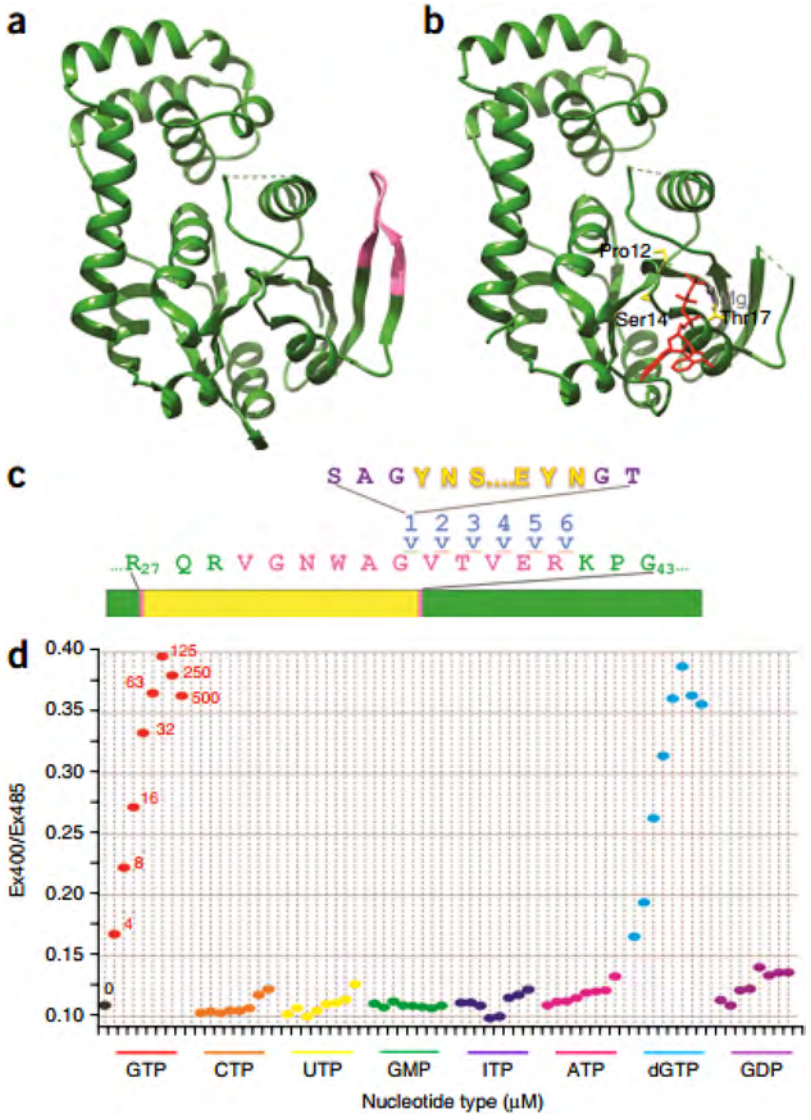

Figure 63. Construction and nucleotide selectivity of a GTP sensor. (a) G protein domain of *E. coli* FeoB without ligand. (b) G protein domain of *E. coli* FeoB protein with a bound GTP analogue (shown in red with the Mg^{2+} ion). (c) Creation of the sensor by inserting cpYFP (yellow) at six different positions within the switch I region (pink) of the FeoB G-protein domain (green), either with or without a Ser-Ala-Gly linker (purple) at the N-terminal fusion point and either with or without a Gly-Thr linker (purple) at the C-terminal fusion point. (d) Ex405/Ex485 ratio for the designed sensor in the absence or presence of nucleotides in the concentration range 4−500 μM. Reproduced with permission from ref 427. Copyright 2017 Nature.

calibrated sensor response. Ratiometric fluorometry has been extensively applied to the detection or quantitation of different biochemical parameters in living cells, such as intracellular pH, cations/anions, biomolecules, and cellular viability.[207,229,423−426]

Phosphate is critical to cellular function and skeletal mineralization, and the quantitative evaluation of biologically relevant phosphate has drawn tremendous attention in recent years. Bianchi-Smiraglia et al.[427] reported a ratiometric sensor for measuring cellular concentration of guanosine triphosphate (GTP), which relates to a series of human diseases and, most remarkably, cancers. Using genetically encoded circularly permuted yellow fluorescent proteins (cpYFPs), the sensor undergoes conformational change and exhibits a rapid, internally normalized ratiometric signal in response to GTP at different concentrations ranging from 4 to 500 μM, both in vitro and in vivo (Figure 63). The sensor also enables detection of intracellular distribution of GTP within individual cells, which raises the possibility for high-throughput screening of molecules that modulate intracellular GTP levels.

Intracellular pH plays numerous key roles in cellular activities, and therefore monitoring pH in vitro or in vivo is of great importance for probing living cell functions.[428,429] Bao et al.[430] employed five tunable ratiometric fluorescent pH nanosensors that incorporate hyperbranched polymer nanoparticles with the combination of two different aggregation-induced emission-active fluorophores: a green emissive naphthalimide indicator as the pH probe and a blue emissive naphthalimide indicator as the reference (Figure 64). The resultant probes exhibit a wide range of emission intensity ratio (I_{520}/I_{450}) values from 0.4 to 1.9 as pH changes from 8.1 to 5.0, thus allowing for quantitative analysis of intracellular pH values (Figure 65). These polymer ratiometric nanosensors show great potential as an effective platform for sensing intracellular pH, as validated by the pH measurement of acidic organelles in HeLa cells. One may well imagine future intracellular probes of this sort that will report on the

DOI: 10.1021/acs.chemrev.8b00226
Chem. Rev. 2019, 119, 231−292

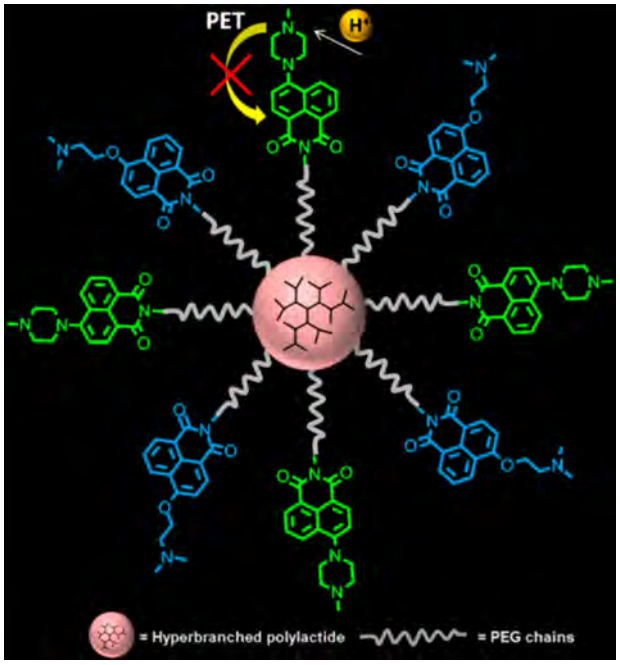

Figure 64. Construction of ratiometric pH nanosensors using hyperbranched polylactide nanoparticles functionalized with naphthalimide-based fluorophores N2 (green) as the pH probe and N1 (blue) as the reference. For five different nanosensors P1−P5, the molar ratios of N1 to N2 are 1:0, 3.3:1, 1:1, 1:2.5, and 0:1. Reproduced from ref 430. Copyright 2015 American Chemical Society.

concentration of multiple critical molecular or ionic species inside living cells.

Nanomaterial-based probes are also an actively pursued route for addressing the ratiometric detection of intracellular pH or O_2 concentrations.[431] Pan et al.[432] reported a series of fluorescent nanoprobes that combine aminofluorescein and ethidium bromide for subcellular pH imaging in cytoplasm, lysosomes, and mitochondria. Huang et al.[433] addressed the construction of AuNP-based nanoprobes integrated with single-stranded oligonucleotides and a dual-fluorophore-labeled i-motif, which generate high or low signal in fluorescence resonance energy transfer (FRET) at acidic or neutral pH. Näreoja et al.[434] demonstrated polyethylenimine-coated $NaYF_4$:Yb^{3+},Er^{3+} nanoparticles as the fluorescent molecular pH nanoprobe. All of these nanosensors show excellent spatial and temporal resolution in living cells or tissues, in part because as many as 20 000 nanosensors may be taken up by an individual cell.[435]

Intracellular temperature sensors are another interesting application of ratiometric fluometric sensors. As changes in the temperature of the cellular microenvironment can have a significant impact on signaling pathways and their nanoparticle uptakes,[436−438] the development of novel temperature nanoprobes could prove useful for intracellular imaging and monitoring. Homma et al.[439] reported a ratiometric fluorescent molecular probe that incorporates the thermally sensitive rhodamine B and a thermally insensitive NIR dye for the selective visualization of the temperature elevation (34−41 °C) in the mitochondria, which plays a key role in cellular activities related to homeostasis and energy balance. Han et al.[440] developed a diselenide ratiometric fluorescent probe based on a selenium−sulfur exchange reaction for the qualitative and quantitative detection of glutathione concentrations, which is an important index of hypothermia or hyperthermia that reflects the cell stressed states (Figure 66). The probe was successfully used to image the glutathione levels of HepG2 in vivo.

Ratiometric fluorescence sensors were also employed to detect oxygen levels in cytosol[431] and for the detection of hypoxia in tumor cells. Cui et al.[441] designed a *p*-nitrobenzyl probe that undergoes an evident blue to green fluorescent emission change catalyzed by nitroreductase at low oxygen levels (Figure 67). This probe was applied to in vitro imaging of hypoxia for solid tumors from A549 cell line, which displayed no cytotoxicity and interference. Similar probes were also developed and employed in the recent work for the hypoxia imaging of other cancer cells.[442−444]

5.2.4. Bacteria and Fungi. Effective methods for detection and discrimination of bacteria are highly desirable in both medicine and industy. Bacterial infections are widely involved in food poisoning, hospital-acquired infections, and many other areas that cause diseases and that are of great concern for the health of the general population.[445,446] In industry, many products have to be screened to avoid possible bacterial contamination before they may be released, and as a consequence regulation of the food industry must be particularly strict.[447,448] Challenges associated with the identification of pathogenic bacteria include the necessity of long culturing times, the need for highly trained laboratory personnel, the demand for

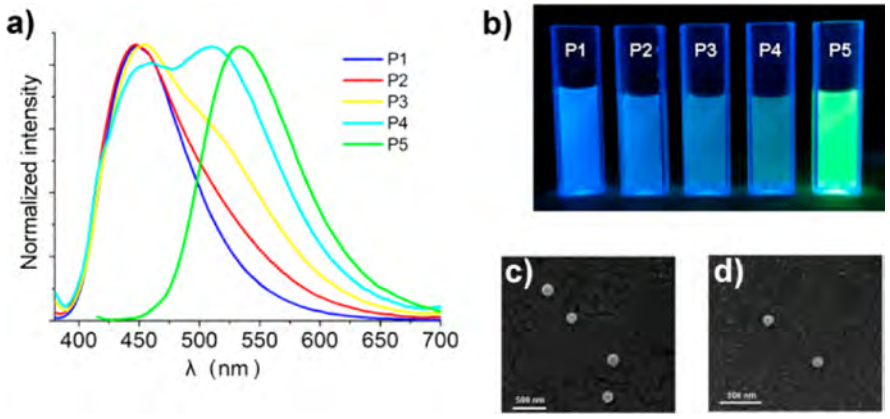

Figure 65. (a) Fluorescence emission spectra of P1−P5 in buffer solutions of pH 7.0. (b) Visible emission of P1−P5 observed under UV lamp excited at 365 nm. (c) SEM image of P2-based nanoparticles. (d) SEM image of P3-based nanoparticles. Reproduced from ref 430. Copyright 2015 American Chemical Society.

DOI: 10.1021/acs.chemrev.8b00226
Chem. Rev. 2019, 119, 231−292

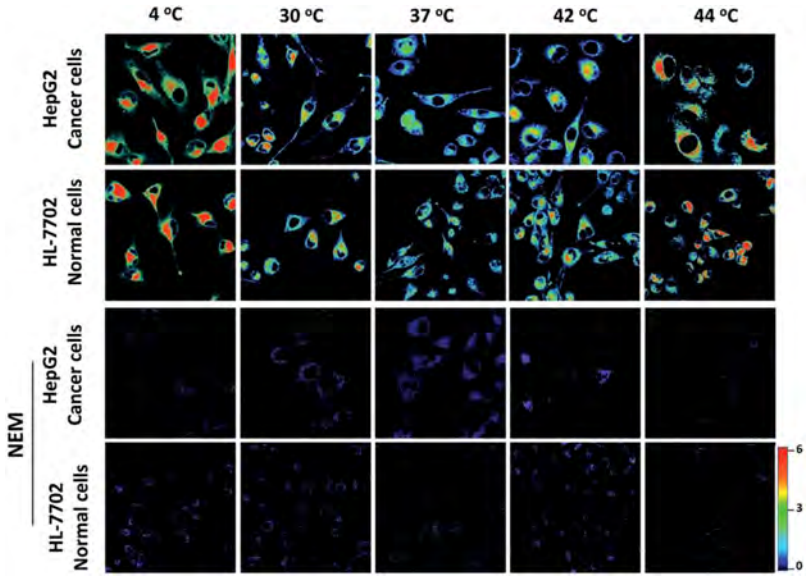

Figure 66. Pseudocolor ratio imaging showing the distribution of glutathione with addition of 10 mM probe in HepG2 and HL-7702 cells under hypothermic (4 and 30 °C) and hyperthermic (42 and 44 °C) conditions for 30 min, with or without 5 mM *N*-ethylmaleimide (NEM) treatment (to consume all the glutathione). Reproduced with permission from ref 440. Copyright 2017 Royal Society of Chemistry.

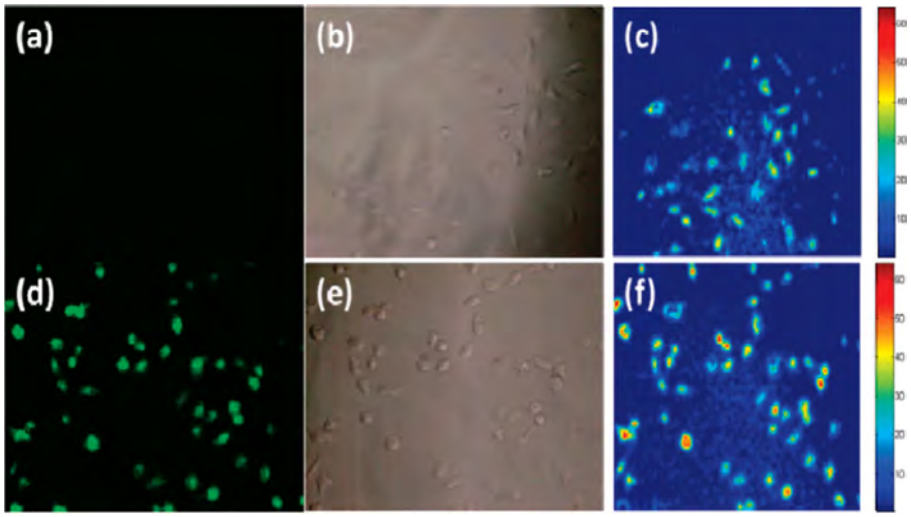

Figure 67. Fluorescence microphotographs of A549 cells incubated with 10 μM *p*-nitrobenzyl probe at 37 °C for 7 h. The top row was at aerobic conditions (a–c). The bottom row was under hypoxic conditions (d–f). (a) and (d) were taken in optical windows between 540 and 580 nm. (b) and (e) were phase contrasts; (c) and (f) were displayed in pseudocolor representing the ratio of emission intensities collected in optical windows between 540–580 and 430–495 nm. Reproduced from ref 441. Copyright 2011 American Chemical Society.

expensive and high-maintenance equipment, and the ineffectiveness caused by antibiotic resistance.[449−451]

Bacteria stink: i.e., the volatile organic compounds (VOCs) produced from bacteria metabolism to which the mammalian olfactory system is highly responsive. Consequently, an experienced microbiologist can readily identify many bacteria by smell. Applications of prior electronic nose technology, however, have been limited by the low dimensionality of traditional sensor arrays (e.g., conductive polymers or metal oxides) and have achieved only modest success, even when attempting to classify small numbers of bacterial variants.[452−456]

Disposable colorimetric sensor arrays have shown numerous successful applications in the identification of microbial species, especially for bacteria. Carey et al.[457] used the 6 × 6 array to recognize strains of human pathogenic bacteria grown on standard agar based on specific VOCs produced from different bacterial cultures. Through monitoring bacterial growth during 10 h of incubation time, 10 strains of bacteria including *Enterococcus faecalis* and *Staphylococcus aureus* as well as their antibiotic-resistant strains were identified with 98.8% accuracy out of 164 trials, as assessed by PCA (Figure 68), HCA, and leave-one-out LDA using time-stacked data.

Very recently, Lim and co-workers have developed an 8 × 10 colorimetric sensor array for screening of other specific classes of bacteria,[458−462] e.g., *Yersinia pestis* and *Bacillus anthracis*, that feature on the Center for Disease Control and Prevention's list of potential biothreats.[458] Via headspace gas analysis of bacteria incubated in Petri dishes, the sensor array was capable of distinguishing four different bacterial species and five strains of *Y. pestis* and *B. anthracis*, with the detection limit as low as 8 CFU/plate for several strains (Figure 69). In addition to the promising results demonstrated in the work, the authors also

DOI: 10.1021/acs.chemrev.8b00226
Chem. Rev. 2019, 119, 231−292

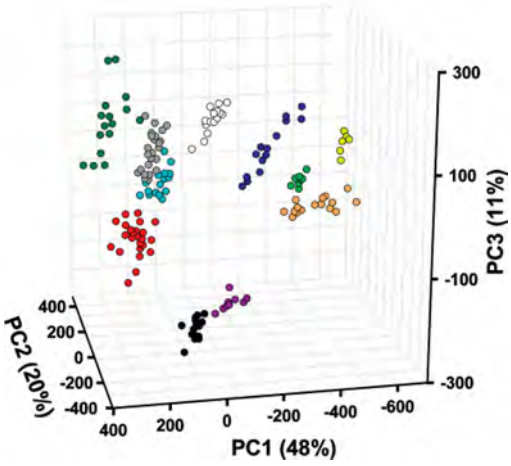

Figure 68. Three-dimensional PCA score plot of 10 bacterial strains and controls. First three principal components account for only 79% of the total variance; 164 trials in total. Color code: black, *S. aureus*; red, MRSA; dark green, *S. epidermidis*; purple, *S. sciuri*; orange, *P. aeruginosa*; white, *E. faecium*; light blue, *E. faecalis*; gray, *E. faecalis* VRE; yellow, *E. coli* 25922; light green, *E. coli* 53502; dark blue, control. Reproduced from ref 457. Copyright 2011 American Chemical Society.

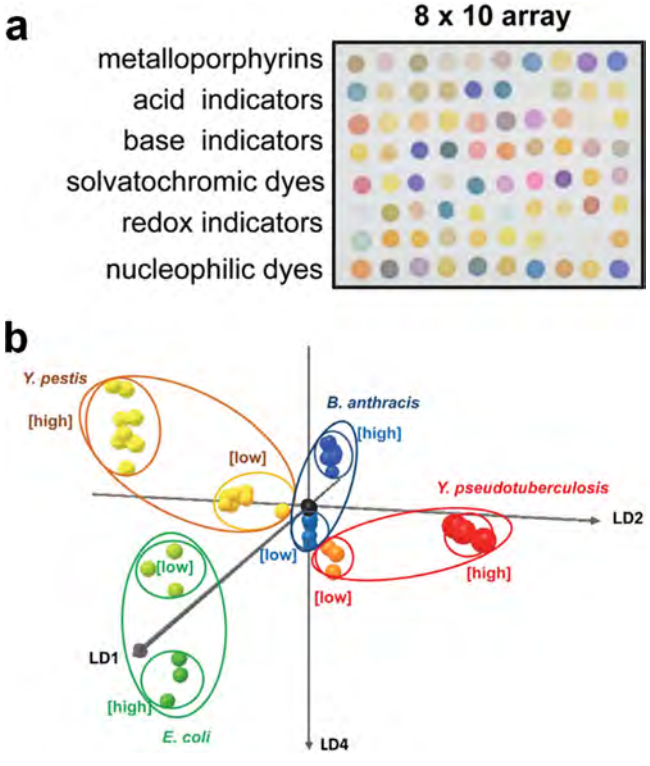

Figure 69. (a) An 8 × 10 colorimetric sensor array comprising 80 different chemically responsive nanoporous dyes. (b) Species concentration trajectories in LDA multidimensional space. All species can be identified independent of inoculum concentration. Six control trials (black) are located at the origin. Reproduced with permission from ref 458. Copyright 2013 Lonsdale et al.

suggested several aspects of considerations for the future improvement of array-based sensing techniques, in terms of the array sensitivity, selectivity, incubation volume, data analysis, and portability of the imaging device.

Rotello, Bunz, and co-workers employed a displacement assay consisting of hydrophobically functionalized AuNPs and a conjugated polymer, poly(*p*-phenyleneethynylene) (PPE), to identify several different bacteria in liquid growth media based on the fluorescence quenching of fluorophores attached to gold nanoparticles.[463] In this method, the negatively charged conjugated polymer fluorophore is replaced by negatively charged bacteria on the surface of positively charged AuNPs, generating a differential fluorescence probe whose response is dictated by the binding strength of each specific bacterium. By diversifying the surface chemistry of AuNPs and the structure of the conjugated polymer, they generated array-like data that provided high dimensionality (albeit one solution at a time). Nine bacterial species and three strains of *E. coli* were examined in 64 trials with a 95% accuracy of classification using LDA.

Furthermore, Bunz and co-workers have very recently reported a similar fluorescent array by combining PPE with four variants of antimicrobial peptides (AMP), for the identification of 14 different bacteria based on their Gram status and genetic relationship (Figure 70);[464] the array showed 100% discrimination accuracy using LDA with leave-one-out cross-validation. This chemical sensor was also successfully applied to target relevant microbes in urine and serum samples, which enabled the discrimination of all bacteria at the upper ranges of their clinically relevant concentrations.

Detection of infectious bacteria on biofilms is a great challenge due to the complexity and heterogeneity of biofilm matrices. Li et al.[465] used a AuNP-based multichannel sensor for the in situ, real-time monitoring of different biofilms based on their physicochemical properties, as an important complement to the currently available methods for early infection detection and antibiotic treatment. Through the selective binding between the AuNP−fluorescent protein conjugates and biofilms, the authors were able to discriminate six types of bacterial biofilms including two uropathogenic bacteria. The sensor array was further proven effective in vitro, that it worked perfectly in a mixed bacteria−mammalian cell coculture wound model.

The immobilized fluorescent bead strategy that Walt and co-workers developed for use with microbead optical fiber bundles has also been recently applied to bacterial identification. Fixed arrays of this sort are difficult to reuse multiple times, in part due to photobleaching. Walt and co-workers have attempted to resolve this issue by using time-shared optical tweezers to dynamically create sensing materials.[466] The quantum-dot-encoded microbead arrays were able to collect fluorescence signals from biological samples in real time. A false color image showing raw data output using this method is shown as Figure 71 for the detection and pattern discrimination of four different strains of *E. coli*.

Especially for human immunocompromised patients, fungal infections are a serious worldwide problem and have gained recent notoriety following contamination of pharmaceuticals in the compounding process. As with any rapidly growing cells, fungi produce volatile organic compounds, and these provide an alternative diagnostic approach for identification of fungal strains. Suslick and co-workers made use of their disposable colorimetric sensor array and demonstrated rapid differentiation and identification of pathogenic fungi based on their metabolic profiles of emitted volatiles.[467] Twelve human pathogenic fungal strains grown on standard agar medium were tested (Figure 72). All fungal strains gave unique composite responses within 3 h and were correctly clustered using hierarchical cluster analysis. Classification analysis using a tensor discriminant analysis, which takes better advantage of the high dimensionality of the sensor array data, gave a classification accuracy of 98% for 155

DOI: 10.1021/acs.chemrev.8b00226
Chem. Rev. 2019, 119, 231−292

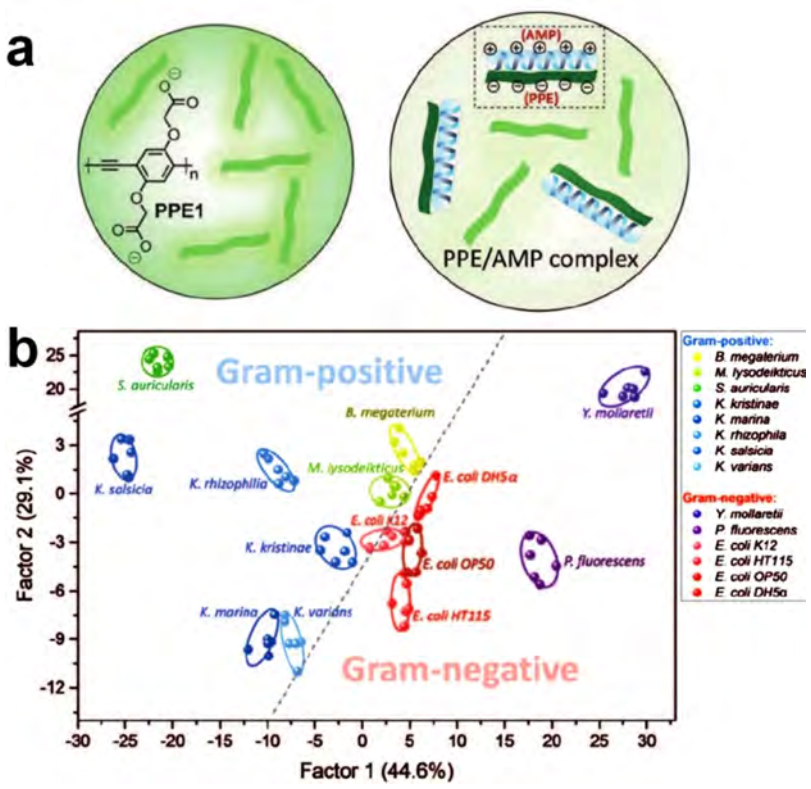

Figure 70. (a) Structure of PPE and electrostatic complex formed between negatively charged PPE and positively charged AMP. (b) Two-dimensional canonical score plot obtained from fluorescence response patterns. In the score plot, 95% confidence ellipses were depicted for the individual bacteria. Reproduced with permission from ref 464. Copyright 2017 Wiley.

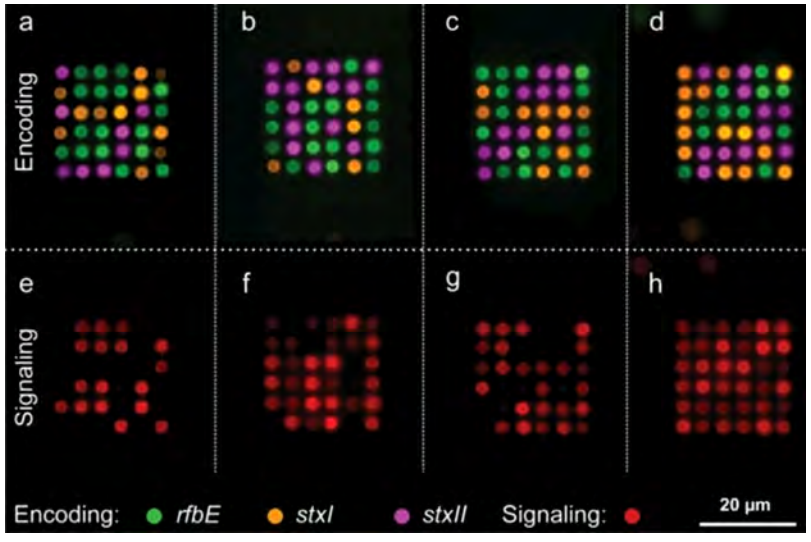

Figure 71. False color images of microbead array in response to four strains of *E. coli*: (a) and (e), strain 43888; (b) and (f), strain 43889; (c) and (g), strain 43890; (d) and (h), strain 43894. Top row (a–d) are the encoding images showing the identity of the beads, while bottom row (e–h) are the signaling images showing the intensity of responses to the bacteria. Adapted with permission from ref 466. Copyright 2013 Royal Society of Chemistry.

trials. The sensor array is also able to observe metabolic changes in growth patterns upon the addition of fungicides, and this provides a facile screening tool for determining fungicide efficacy for various fungal strains in real time. Further work has proven the utility of this technique for identification of clinically important pathogenic yeasts in standard blood cultures.[468]

5.2.5. Cancer and Disease Biomarkers. Optical array sensing has begun to find applications in the area of cancer diagnosis of biomarker detection.[419,469−471] Different cell lines produce different types of VOCs as featured metabolites; this applies to any rapidly growing cells, and in principle the breath composition is consistent with the volatiles produced in the body. Breath analysis has a long history as an underutilized diagnostic approach;[36,472,473] limitations in traditional analytical tools that are insufficiently sensitive, selective, or inexpensive have restricted the use of these methods in clinical or hospital settings. Electronic noses have certainly been evaluated for breath analysis, especially for diagnosis of lung cancer and of

DOI: 10.1021/acs.chemrev.8b00226
Chem. Rev. 2019, 119, 231−292

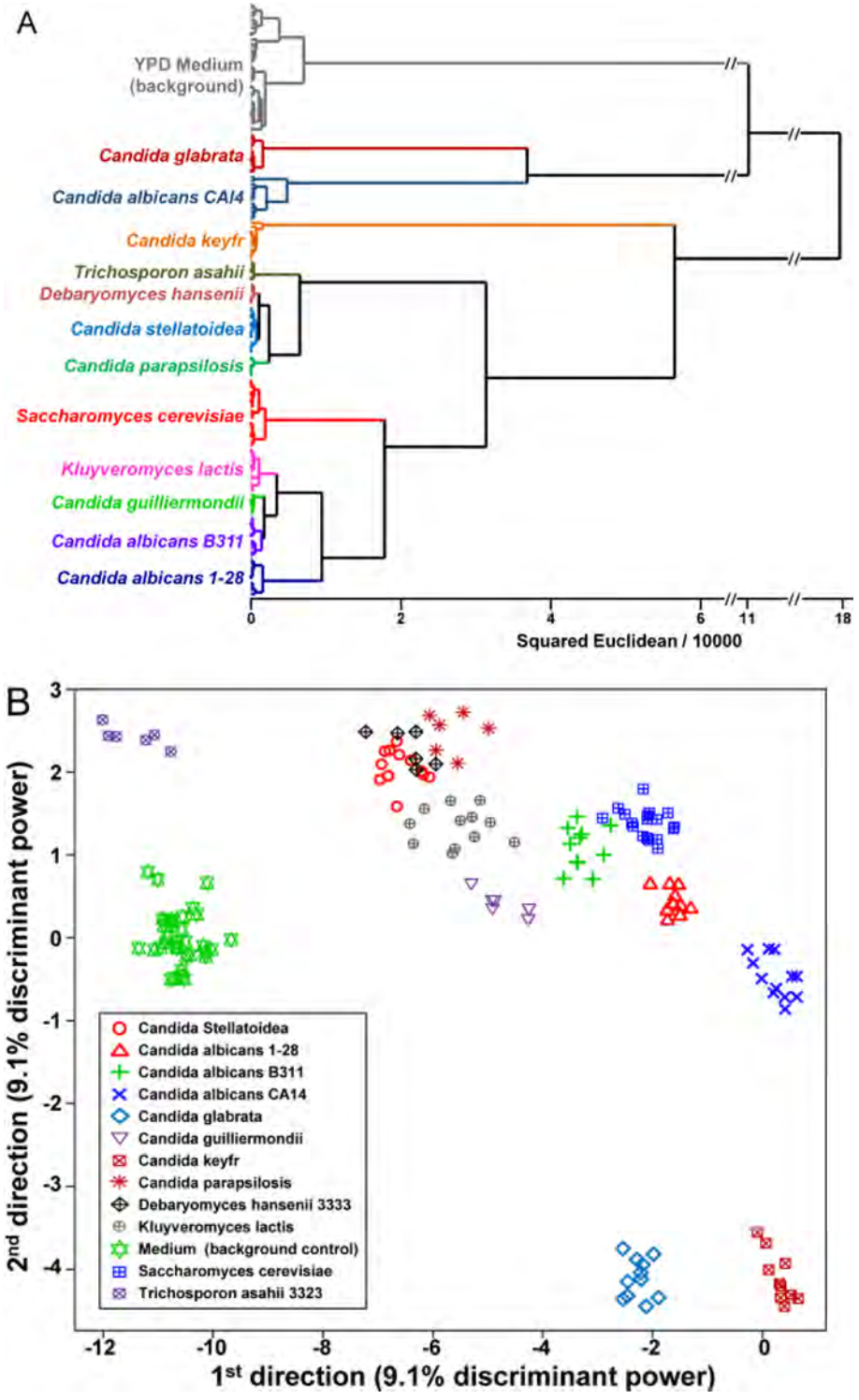

Figure 72. Classification analysis of colorimetric sensor array response to cultured pathogenic fungi. (A) Hierarchical cluster analysis dendrogram of 12 fungal strains and YPD medium background at 180 min with 2.4×10^7 colony forming units of inoculation; no errors in clustering were observed among a total of 155 trials. (B) Scatter plot of the first two directions from the tensor discriminant analysis. Surprisingly good discrimination of the fungal strains is achieved even with only two TDA directions, which account for only 18.2% of the total discriminant power. Reproduced with permission from ref 467. Copyright 2014 Royal Society of Chemistry.

respiratory infections, albeit with inadequate success. The prototype colorimetric sensor arrays developed by the Suslick group for fungal[467] and bacterial[457] identification have shown some preliminary clinical success for breath diagnosis. Lim et al.[474,475] designed a tuberculosis testing tool that incorporated a 73-indicator colorimetric sensor array for fingerprinting VOC signatures of human urine samples. Sensor array responses to 22 tuberculosis urine samples and the other 41 symptomatic controls were collected under different sample treatment conditions, which proved that basified condition was able to provide the best accuracy of >85% sensitivity and >79% specificity of all samples. The urine assay using a colorimetric

DOI: 10.1021/acs.chemrev.8b00226
Chem. Rev. 2019, 119, 231−292

sensor array offers a powerful tool for a quick and simple diagnosis of tuberculosis in low resource settings.

Lung cancer detection via breath analysis using colorimetric sensing techniques has also been elucidated by Mazzone et al.[476,477] at the Cleveland Clinic with promising classification results. The test revealed that, based on exhaled breath screening of 229 study subjects (92 with lung cancer and 137 as controls), lung cancer patients can be distinguished from control subjects with high accuracy (*C*-statistic 0.889 for adenocarcinoma vs squamous cell carcinoma), and the accuracy for identification of lung cancer can be further improved by adjusting clinical and breath predictors.[477]

The direct analysis of nonvolatile cancer cells or disease biomarkers in aqueous biological samples is also highly desirable. In an entirely different approach to cell differentiation, it is not surprising that different cell lines interact differently with different nanoparticles[478,479] and that those interactions are strongly affected by the chemical nature of the nanoparticle surfaces, particularly as biomolecules adsorb onto nanoparticle surfaces forming a "protein corona".[480−483]

Taking advantage of interactions between polymers/AuNPs and various biomolecules, the parallel soluble fluorescent displacement assays developed by Rotello and co-workers[421,484−486] for protein detection have also been extended to identification of cancer cells. Very recently, they reported a nanosensor using cell lysates to rapidly profile the tumorigenicity of cancer cells.[487] In addition to the aforementioned approach involving differential probes, this sensing platform used a host−guest interaction between the macrocyclic cucurbit[7]uril (CB[7]) and the ammonium head of gold nanoparticles to build the second recognition receptor that extends the number of dimensions within each sensor element from three to six (Figure 73). The overall accuracy in classification accordingly increased from 63% of using only three channels of the composite without the supramolecular assembly to 95% when taking all six channels into account (Figure 74). More significantly, this method required the minimal sample quantity of ∼200 ng (∼1000 cells) for analysis and could become an ideal tool for microbiopsy-based cancer diagnosis.

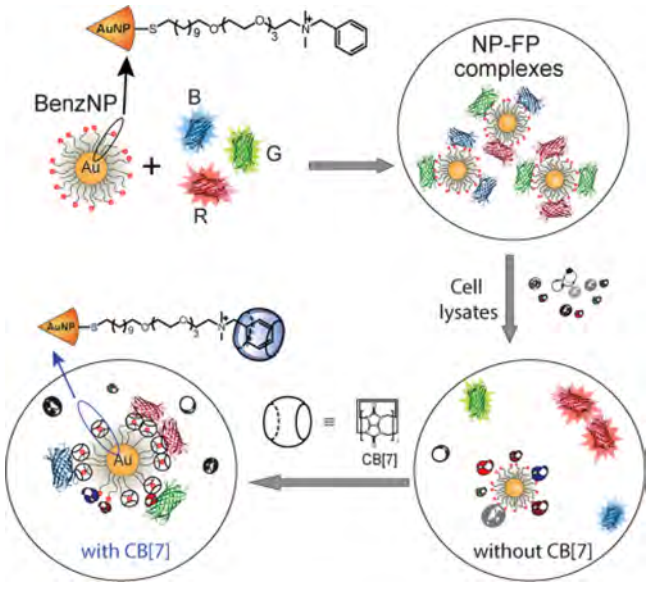

Figure 73. Construction of a six-channel sensor in a single well. Quenched AuNP−fluorescent protein (BenzNP−FP) conjugates serve as differential probes for the detection of cell lysates, based on fluorescence signal changes in three emission channels. CB[7] is then added to the same well to gain three additional fluorescent channels based on the interactions between the analytes and newly formed composites incorporating CB[7]. Reproduced from ref 487. Copyright 2017 American Chemical Society.

6. CONCLUSIONS AND FUTURE CHALLENGES

During the last decade, chemical sensing has witnessed rapid development in both sensing materials and analytical techniques. Array-based optical sensing has demonstrated its usefulness in addressing a wide range of analytical challenges. By using chemically diverse chemoresponsive dyes or biological receptors in combination with chemometric analysis, arrays can be designed to discriminate various structurally similar analytes and analyte mixtures. While many biological systems employ a lock-and-key method for molecular recognition (e.g., enzymes and antibodies), which requires a highly specific receptor for each substrate, this approach is not used by the olfactory system and does not work for artificial olfaction. Using customized receptors (biological or synthetic) is simply impractical for the overwhelming number of volatiles and volatile mixtures that one would like to detect. Instead, sensor arrays provide an alternative means of creating specificity through pattern recognition of the response of an array of highly cross-reactive sensors. With recent advances in optical array sensing, sensitive and reliable fingerprinting of both single compounds and complex mixtures has become possible over a wide range of analyte types. Sensor arrays comprising a number of different sensor elements have been employed for detection of both gaseous and aqueous samples. The primary feature of an advanced sensor array, as an analogue to the mammalian nose, is that it gives a composite response to mixtures, but one that provides discrimination even between highly similar complex mixtures.

Another essential feature of colorimetric or fluorometric sensor arrays is that they probe chemical properties of analytes, rather than physical properties, giving highly discriminatory, specific responses to an enormous range of analytes. The result is high-dimensional data that cannot be reduced to just two or three dominant coordinates. The advances in chemometric analysis of high-dimensional data provide new methods for the optimal use of high-dimensional sensor arrays. These developments parallel the advances in pattern recognition demanded by the burgeoning fields of artificial intelligence and machine learning.

Probing chemical properties for chemical sensing is a "good news/bad news" story. The good news is that most analytes of concern (e.g., toxic industrial chemicals) are, essentially by definition, highly reactive and therefore readily detected, even at sub parts per million concentration; this resolves some issues in false positives associated with traditional electronic nose and solid state chemical sensors. The bad news, nevertheless, is that some targeted analytes are less reactive and could not reach ideal sensitivity using chemical methods. One solution is to pretreat the analyte stream to produce, for example, partial oxidation products that are more reactive and more easily detectable by cross-reactive sensors. More selective methods of "activating" these analytes, especially in the presence of a considerable concentration of interferents, would greatly improve the sensing capability of current sensor arrays.

The primary limitation of array-based sensing, however, is that it does not offer a component-by-component analysis for

DOI: 10.1021/acs.chemrev.8b00226
Chem. Rev. 2019, 119, 231−292

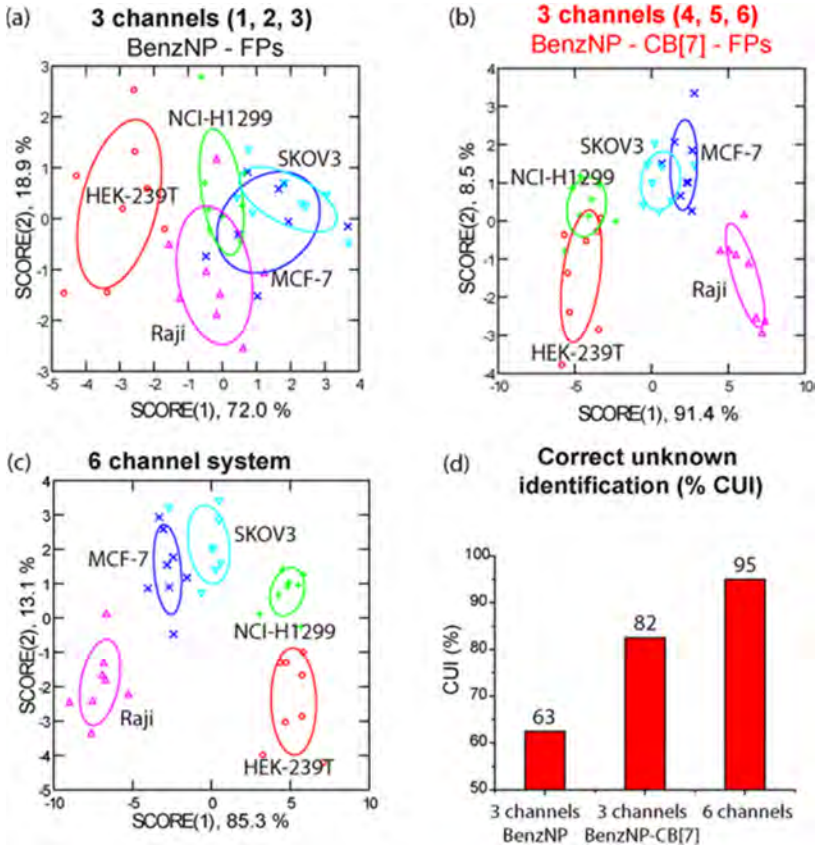

Figure 74. LDA classification of five human cancerous cell lines based on (a) only three channels of BenzNP−FPs, (b) only three channels of BenzNP−CB[7], and (c) the combinatory classification with all six channels. (d) Overall classification accuracy of three sensing systems. Reproduced from ref 487. Copyright 2017 American Chemical Society.

composite mixtures. Most chemists naturally assume that the goal with any complex mixture is to obtain a complete quantitative analysis of each component, which, in some cases, is difficult to be accomplished using either a colorimetric or fluorometric sensor array. In practice, however, one seldom really wants to know, for example, what the thousand different components are in a cup of coffee.[488] What one often wants to know is whether the coffee is roasted properly or burnt, its place of origin, and other issues of quality control and quality assurance: array-based sensing proves to be an excellent technique for those goals.

The other great challenge of optical array sensing lies in its performance in practical applications. Despite the success of colorimetric or fluorometric array sensing achieved in controlled laboratory environments, there are still challenges to overcome before these methods become common in field use. In order to create array-based assays that can accurately predict the identity of unknown analytes, the response of unknown analytes to the array should be reproducible; the system has to be able to match responses from unknowns to responses from a training set of analytes; disturbances from possible interferents should be effectively eliminated. The development of portable, low-noise, and accurate optical instrumentation with the capability of onboard and real-time analysis has shown substantial progress over the past few years and begins to match the increasing pressure for real-world use.

AUTHOR INFORMATION

Corresponding Author

*E-mail: ksuslick@illinois.edu.

ORCID

Zheng Li: 0000-0001-9066-5791
Kenneth S. Suslick: 0000-0001-5422-0701

Notes

The authors declare no competing financial interest.

Biographies

Zheng Li was born and grew up in Wuhu, Auhui Province, China. He received his B.S. in chemistry from Nanjing University in 2012, and his Ph.D. in chemistry from the University of Illinois at Urbana−Champaign in 2017 under the guidance of Prof. Kenneth S. Suslick. His research interests include the development of new chromogenic or fluorometric materials and the design of portable sensing devices for a wide range of applications in health diagnosis, security screening, and environmental monitoring as well as agricultural and food inspection. He is currently a postdoctoral scholar from Prof. Qingshan Wei's group at the North Carolina State University.

Jon R. Askim received his Ph.D. in chemistry from the University of Illinois in 2015 under the supervision of Prof. Kenneth S. Suslick, where he worked to develop novel optical sensor arrays as well as instrumentation and techniques for their application. He is currently a postdoctoral fellow at the National Institute of Standards and Technology in Gaithersburg, MD, where he is working on developing new sensor fusion techniques for imaging-based methods.

DOI: 10.1021/acs.chemrev.8b00226
Chem. Rev. 2019, 119, 231−292

Kenneth S. Suslick is the Marvin T. Schmidt Research Professor of Chemistry at the University of Illinois at Urbana−Champaign and the George Eastman Professor at the University of Oxford for 2018−2019. Prof. Suslick received his B.S. from Caltech in 1974 and his Ph.D. from Stanford in 1978, and came to the University of Illinois immediately thereafter. Among his awards are the Centenary Prize and the Sir George Stokes Medal of the RSC, the MRS Medal, the ACS Nobel Laureate Signature and Cope Scholar Awards, the Helmholtz−Rayleigh Silver Medal of the Acoustical Society of America, and the Chemical Pioneer Award of the American Institute of Chemists. He is a Fellow of the National Academy of Inventors.

ACKNOWLEDGMENTS

Z.L. acknowledges the postdoctoral fellowship from the Procter & Gamble Foundation. K.S.S. acknowledges past funding in this research area by NIH, DHS, NSF, and DoD.

REFERENCES

(1) Janata, J. *Principles of Chemical Sensors*, 2nd ed.; Springer: New York, 2009.
(2) Gründler, P. *Chemical Sensors, an Introduction for Scientists and Engineers*; Springer-Verlag: Berlin, 2007.
(3) Banica, F.-G. *Chemical Sensors and Biosensors: Fundamentals and Applications*; John Wiley and Sons: Chichester, U.K., 2012.
(4) Buck, L.; Axel, R. A Novel Multigene Family May Encode Odorant Receptors: A Molecular Basis for Odor Recognition. *Cell* **1991**, *65*, 175−187.
(5) Bushdid, C.; Magnasco, M. O.; Vosshall, L. B.; Keller, A. Humans Can Discriminate More Than 1 Trillion Olfactory Stimuli. *Science* **2014**, *343*, 1370−1372.
(6) Mombaerts, P. Seven-Transmembrane Proteins as Odorant and Chemosensory Receptors. *Science* **1999**, *286*, 707−711.
(7) Hawkes, C. H.; Doty, R. L. *The Neurology of Olfaction*; Cambridge University Press: 2009.
(8) Buck, L. B. Unraveling the Sense of Smell (Nobel Lecture). *Angew. Chem., Int. Ed.* **2005**, *44*, 6128−6140.
(9) McGann, J. P. Poor Human Olfaction Is a 19th-Century Myth. *Science* **2017**, *356*, eaam7263.
(10) Wang, J.; Luthey-Schulten, Z. A.; Suslick, K. S. Is the Olfactory Receptor a Metalloprotein? *Proc. Natl. Acad. Sci. U. S. A.* **2003**, *100*, 3035−3039.
(11) Block, E.; Batista, V. S.; Matsunami, H.; Zhuang, H.; Ahmed, L. The Role of Metals in Mammalian Olfaction of Low Molecular Weight Organosulfur Compounds. *Nat. Prod. Rep.* **2017**, *34*, 529−557.
(12) Duan, X.; Block, E.; Li, Z.; Connelly, T.; Zhang, J.; Huang, Z.; Su, X.; Pan, Y.; Wu, L.; Chi, Q.; et al. Crucial Role of Copper in Detection of Metal-Coordinating Odorants. *Proc. Natl. Acad. Sci. U. S. A.* **2012**, *109*, 3492−3497.
(13) Zarzo, M. The Sense of Smell: Molecular Basis of Odorant Recognition. *Biological Reviews* **2007**, *82*, 455−479.
(14) Rock, F.; Barsan, N.; Weimar, U. Electronic Nose: Current Status and Future Trends. *Chem. Rev.* **2008**, *108*, 705−725.
(15) Jurs, P. C.; Bakken, G. A.; McClelland, H. E. Computational Methods for the Analysis of Chemical Sensor Array Data from Volatile Analytes. *Chem. Rev.* **2000**, *100*, 2649−2678.
(16) Wilson, A. D.; Baietto, M. Applications and Advances in Electronic-Nose Technologies. *Sensors* **2009**, *9*, 5099−5148.
(17) Loutfi, A.; Coradeschi, S.; Mani, G. K.; Shankar, P.; Rayappan, J. B. B. Electronic Noses for Food Quality: A Review. *J. Food Eng.* **2015**, *144*, 103−111.
(18) Broza, Y. Y.; Haick, H. Nanomaterial-Based Sensors for Detection of Disease by Volatile Organic Compounds. *Nanomedicine* **2013**, *8*, 785−806.
(19) Zhang, C. C.; Chen, P. L.; Hu, W. P. Organic Field-Effect Transistor-Based Gas Sensors. *Chem. Soc. Rev.* **2015**, *44*, 2087−2107.
(20) Montuschi, P.; Mores, N.; Trove, A.; Mondino, C.; Barnes, P. J. The Electronic Nose in Respiratory Medicine. *Respiration* **2013**, *85*, 72−84.
(21) Di Natale, C.; Paolesse, R.; Martinelli, E.; Capuano, R. Solid-State Gas Sensors for Breath Analysis: A Review. *Anal. Chim. Acta* **2014**, *824*, 1−17.
(22) Capelli, L.; Sironi, S.; Del Rosso, R. Electronic Noses for Environmental Monitoring Applications. *Sensors* **2014**, *14*, 19979−20007.
(23) Albert, K. J.; Lewis, N. S.; Schauer, C. L.; Sotzing, G. A.; Stitzel, S. E.; Vaid, T. P.; Walt, D. R. Cross-Reactive Chemical Sensor Arrays. *Chem. Rev.* **2000**, *100*, 2595−2626.
(24) Persaud, K.; Dodd, G. Analysis of Discrimination Mechanisms in the Mammalian Olfactory System Using a Model Nose. *Nature* **1982**, *299*, 352−355.
(25) Mirica, K. A.; Azzarelli, J. M.; Weis, J. G.; Schnorr, J. M.; Swager, T. M. Rapid Prototyping of Carbon-Based Chemiresistive Gas Sensors on Paper. *Proc. Natl. Acad. Sci. U. S. A.* **2013**, *110*, E3265−E3270.
(26) Jayawardane, B. M.; McKelvie, I. D.; Kolev, S. D. Development of a Gas-Diffusion Microfluidic Paper-Based Analytical Device (Mpad) for the Determination of Ammonia in Wastewater Samples. *Anal. Chem.* **2015**, *87*, 4621−4626.
(27) Lim, S. H.; Feng, L.; Kemling, J. W.; Musto, C. J.; Suslick, K. S. An Optoelectronic Nose for the Detection of Toxic Gases. *Nat. Chem.* **2009**, *1*, 562−567.
(28) Prasad, R. M.; Lauterbach, S.; Kleebe, H.-J.; Merdrignac-Conanec, O.; Barsan, N.; Weimar, U.; Gurlo, A. Response of Gallium Nitride Chemiresistors to Carbon Monoxide Is Due to Oxygen Contamination. *ACS Sens.* **2017**, *2*, 713−717.
(29) Su, S.; Wu, W.; Gao, J.; Lu, J.; Fan, C. Nanomaterials-Based Sensors for Applications in Environmental Monitoring. *J. Mater. Chem.* **2012**, *22*, 18101−18110.
(30) Bright, C. J.; Nallon, E. C.; Polcha, M. P.; Schnee, V. P. Quantum Dot and Polymer Composite Cross-Reactive Array for Chemical Vapor Detection. *Anal. Chem.* **2015**, *87*, 12270−12275.
(31) Li, Z.; Bassett, W. P.; Askim, J. R.; Suslick, K. S. Differentiation among Peroxide Explosives with an Optoelectronic Nose. *Chem. Commun.* **2015**, *51*, 15312−15315.
(32) Askim, J. R.; Li, Z.; LaGasse, M. K.; Rankin, J. M.; Suslick, K. S. An Optoelectronic Nose for Identification of Explosives. *Chem. Sci.* **2016**, *7*, 199−206.
(33) Hu, Z.; Deibert, B. J.; Li, J. Luminescent Metal-Organic Frameworks for Chemical Sensing and Explosive Detection. *Chem. Soc. Rev.* **2014**, *43*, 5815−5840.
(34) Le, N. D. B.; Yazdani, M.; Rotello, V. M. Array-Based Sensing Using Nanoparticles: An Alternative Approach for Cancer Diagnostics. *Nanomedicine (London, U. K.)* **2014**, *9*, 1487−1498.
(35) Tisch, U.; Haick, H. Chemical Sensors for Breath Gas Analysis: The Latest Developments at the Breath Analysis Summit 2013. *J. Breath Res.* **2014**, *8*, 027103.
(36) Konvalina, G.; Haick, H. Sensors for Breath Testing: From Nanomaterials to Comprehensive Disease Detection. *Acc. Chem. Res.* **2014**, *47*, 66−76.
(37) Tomita, S.; Niwa, O.; Kurita, R. Artificial Modification of an Enzyme for Construction of Cross-Reactive Polyion Complexes to Fingerprint Signatures of Proteins and Mammalian Cells. *Anal. Chem.* **2016**, *88*, 9079−9086.
(38) De Luna, P.; Mahshid, S. S.; Das, J.; Luan, B.; Sargent, E. H.; Kelley, S. O.; Zhou, R. High-Curvature Nanostructuring Enhances Probe Display for Biomolecular Detection. *Nano Lett.* **2017**, *17*, 1289−1295.
(39) Huang, W.; Diallo, A. K.; Dailey, J. L.; Besar, K.; Katz, H. E. Electrochemical Processes and Mechanistic Aspects of Field-Effect Sensors for Biomolecules. *J. Mater. Chem. C* **2015**, *3*, 6445−6470.
(40) Zhang, C.; Bailey, D. P.; Suslick, K. S. Colorimetric Sensor Arrays for the Analysis of Beers: A Feasibility Study. *J. Agric. Food Chem.* **2006**, *54*, 4925−4931.
(41) Maynor, M. S.; Nelson, T. L.; O'Sulliva, C.; Lavigne, J. J. A Food Freshness Sensor Using the Multistate Response from Analyte-Induced

DOI: 10.1021/acs.chemrev.8b00226
Chem. Rev. 2019, 119, 231−292

Aggregation of a Cross-Reactive Poly(Thiophene). *Org. Lett.* **2007**, *9*, 3217−3220.
(42) Narsaiah, K.; Jha, S. N.; Bhardwaj, R.; Sharma, R.; Kumar, R. Optical Biosensors for Food Quality and Safety Assurance—a Review. *J. Food Sci. Technol.* **2012**, *49*, 383−406.
(43) Zhang, C.; Suslick, K. S. Colorimetric Sensor Array for Soft Drink Analysis. *J. Agric. Food Chem.* **2007**, *55*, 237−242.
(44) Borisov, S. M.; Wolfbeis, O. S. Optical Biosensors. *Chem. Rev.* **2008**, *108*, 423−461.
(45) Diehl, K. L.; Anslyn, E. V. Array Sensing Using Optical Methods for Detection of Chemical and Biological Hazards. *Chem. Soc. Rev.* **2013**, *42*, 8596−8611.
(46) You, L.; Zha, D.; Anslyn, E. V. Recent Advances in Supramolecular Analytical Chemistry Using Optical Sensing. *Chem. Rev.* **2015**, *115*, 7840−7892.
(47) Nakamoto, T.; Ishida, H. Chemical Sensing in Spatial/Temporal Domains. *Chem. Rev.* **2008**, *108*, 680−704.
(48) Wu, J.; Kwon, B.; Liu, W.; Anslyn, E. V.; Wang, P.; Kim, J. S. Chromogenic/Fluorogenic Ensemble Chemosensing Systems. *Chem. Rev.* **2015**, *115*, 7893−7943.
(49) McDonagh, C.; Burke, C. S.; MacCraith, B. D. Optical Chemical Sensors. *Chem. Rev.* **2008**, *108*, 400−422.
(50) Rakow, N. A.; Suslick, K. S. A Colorimetric Sensor Array for Odour Visualization. *Nature* **2000**, *406*, 710−713.
(51) Anker, J. N.; Hall, W. P.; Lyandres, O.; Shah, N. C.; Zhao, J.; Van Duyne, R. P. Biosensing with Plasmonic Nanosensors. *Nat. Mater.* **2008**, *7*, 442−453.
(52) Jeon, S.; Ahn, S. E.; Song, I.; Kim, C. J.; Chung, U. I.; Lee, E.; Yoo, I.; Nathan, A.; Lee, S.; Robertson, J.; et al. Gated Three-Terminal Device Architecture to Eliminate Persistent Photoconductivity in Oxide Semiconductor Photosensor Arrays. *Nat. Mater.* **2012**, *11*, 301−305.
(53) Wang, S.; Ota, S.; Guo, B.; Ryu, J.; Rhodes, C.; Xiong, Y.; Kalim, S.; Zeng, L.; Chen, Y.; Teitell, M. A.; et al. Subcellular Resolution Mapping of Endogenous Cytokine Secretion by Nano-Plasmonic-Resonator Sensor Array. *Nano Lett.* **2011**, *11*, 3431−3434.
(54) Goossens, S.; Navickaite, G.; Monasterio, C.; Gupta, S.; Piqueras, J. J.; Pérez, R.; Burwell, G.; Nikitskiy, I.; Lasanta, T.; Galán, T.; et al. Broadband Image Sensor Array Based on Graphene−Cmos Integration. *Nat. Photonics* **2017**, *11*, 366−371.
(55) Peng, M.; Li, Z.; Liu, C.; Zheng, Q.; Shi, X.; Song, M.; Zhang, Y.; Du, S.; Zhai, J.; Wang, Z. L. High-Resolution Dynamic Pressure Sensor Array Based on Piezo-Phototronic Effect Tuned Photoluminescence Imaging. *ACS Nano* **2015**, *9*, 3143−3150.
(56) Laborde, C.; Pittino, F.; Verhoeven, H. A.; Lemay, S. G.; Selmi, L.; Jongsma, M. A.; Widdershoven, F. P. Real-Time Imaging of Microparticles and Living Cells with Cmos Nanocapacitor Arrays. *Nat. Nanotechnol.* **2015**, *10*, 791−795.
(57) Chen, Q.; Hu, X.; Wen, L.; Yu, Y.; Cumming, D. R. S. Nanophotonic Image Sensors. *Small* **2016**, *12*, 4922−4935.
(58) Askim, J. R.; Suslick, K. S. Hand-Held Reader for Colorimetric Sensor Arrays. *Anal. Chem.* **2015**, *87*, 7810−7816.
(59) Suslick, K. S. Synesthesia in Science and Technology: More Than Making the Unseen Visible. *Curr. Opin. Chem. Biol.* **2012**, *16*, 557−563.
(60) Lin, H.; Jang, M.; Suslick, K. S. Preoxidation for Colorimetric Sensor Array Detection of Vocs. *J. Am. Chem. Soc.* **2011**, *133*, 16786−16789.
(61) Suslick, K. S. An Optoelectronic Nose: "Seeing" Smells by Means of Colorimetric Sensor Arrays. *MRS Bull.* **2004**, *29*, 720−725.
(62) Askim, J. R.; Mahmoudi, M.; Suslick, K. S. Optical Sensor Arrays for Chemical Sensing: The Optoelectronic Nose. *Chem. Soc. Rev.* **2013**, *42*, 8649−8682.
(63) Janata, J.; Josowicz, M.; Vanýsek, P.; DeVaney, D. M. Chemical Sensors. *Anal. Chem.* **1998**, *70*, 179−208.
(64) Privett, B. J.; Shin, J. H.; Schoenfisch, M. H. Electrochemical Sensors. *Anal. Chem.* **2008**, *80*, 4499−4517.
(65) Privett, B. J.; Shin, J. H.; Schoenfisch, M. H. Electrochemical Sensors. *Anal. Chem.* **2010**, *82*, 4723−4741.
(66) Kaushik, A.; Kumar, R.; Arya, S. K.; Nair, M.; Malhotra, B. D.; Bhansali, S. Organic−Inorganic Hybrid Nanocomposite-Based Gas Sensors for Environmental Monitoring. *Chem. Rev.* **2015**, *115*, 4571−4606.
(67) Assen, A. H.; Yassine, O.; Shekhah, O.; Eddaoudi, M.; Salama, K. N. MOFs for the Sensitive Detection of Ammonia: Deployment of Fcu-MOF Thin Films as Effective Chemical Capacitive Sensors. *ACS Sens.* **2017**, *2*, 1294.
(68) Carminati, M. Advances in High-Resolution Microscale Impedance Sensors. *J. Sens.* **2017**, *2017* (15), 7638389.
(69) Maeng, S.; Kim, S.-W.; Lee, D.-H.; Moon, S.-E.; Kim, K.-C.; Maiti, A. Sno2 Nanoslab as No2 Sensor: Identification of the No2 Sensing Mechanism on a Sno2 Surface. *ACS Appl. Mater. Interfaces* **2014**, *6*, 357−363.
(70) Zou, Y.; Chen, S.; Sun, J.; Liu, J.; Che, Y.; Liu, X.; Zhang, J.; Yang, D. Highly Efficient Gas Sensor Using a Hollow Sno2Microfiber for Triethylamine Detection. *ACS Sens.* **2017**, *2*, 897−902.
(71) Potyrailo, R. A.; Surman, C.; Nagraj, N.; Burns, A. Materials and Transducers toward Selective Wireless Gas Sensing. *Chem. Rev.* **2011**, *111*, 7315−7354.
(72) Ford, M. J.; Wang, M.; Patel, S. N.; Phan, H.; Segalman, R. A.; Nguyen, T.-Q.; Bazan, G. C. High Mobility Organic Field-Effect Transistors from Majority Insulator Blends. *Chem. Mater.* **2016**, *28*, 1256−1260.
(73) Mei, J.; Diao, Y.; Appleton, A. L.; Fang, L.; Bao, Z. Integrated Materials Design of Organic Semiconductors for Field-Effect Transistors. *J. Am. Chem. Soc.* **2013**, *135*, 6724−6746.
(74) Krivitsky, V.; Zverzhinetsky, M.; Patolsky, F. Antigen-Dissociation from Antibody-Modified Nanotransistor Sensor Arrays as a Direct Biomarker Detection Method in Unprocessed Biosamples. *Nano Lett.* **2016**, *16*, 6272−6281.
(75) Zanardi, C.; Terzi, F.; Seeber, R. Polythiophenes and Polythiophene-Based Composites in Amperometric Sensing. *Anal. Bioanal. Chem.* **2013**, *405*, 509−531.
(76) Wang, M.; Duan, X.; Xu, Y.; Duan, X. Functional Three-Dimensional Graphene/Polymer Composites. *ACS Nano* **2016**, *10*, 7231−7247.
(77) Salavagione, H. J.; Diez-Pascual, A. M.; Lazaro, E.; Vera, S.; Gomez-Fatou, M. A. Chemical Sensors Based on Polymer Composites with Carbon Nanotubes and Graphene: The Role of the Polymer. *J. Mater. Chem. A* **2014**, *2*, 14289−14328.
(78) Fennell, J. F.; Liu, S. F.; Azzarelli, J. M.; Weis, J. G.; Rochat, S.; Mirica, K. A.; Ravnsbæk, J. B.; Swager, T. M. Nanowire Chemical/Biological Sensors: Status and a Roadmap for the Future. *Angew. Chem., Int. Ed.* **2016**, *55*, 1266−1281.
(79) Azzarelli, J. M.; Mirica, K. A.; Ravnsbæk, J. B.; Swager, T. M. Wireless Gas Detection with a Smartphone Via Rf Communication. *Proc. Natl. Acad. Sci. U. S. A.* **2014**, *111*, 18162−18166.
(80) Pedrero, M.; Campuzano, S.; Pingarrón, J. M. Magnetic Beads-Based Electrochemical Sensors Applied to the Detection and Quantification of Bioterrorism/Biohazard Agents. *Electroanalysis* **2012**, *24*, 470−482.
(81) Zhu, C.; Yang, G.; Li, H.; Du, D.; Lin, Y. Electrochemical Sensors and Biosensors Based on Nanomaterials and Nanostructures. *Anal. Chem.* **2015**, *87*, 230−249.
(82) Shiddiky, M. J. A.; Torriero, A. A. J. Application of Ionic Liquids in Electrochemical Sensing Systems. *Biosens. Bioelectron.* **2011**, *26*, 1775−1787.
(83) Yang, L.; Huang, N.; Huang, L.; Liu, M.; Li, H.; Zhang, Y.; Yao, S. An Electrochemical Sensor for Highly Sensitive Detection of Copper Ions Based on a New Molecular Probe Pi-a Decorated on Graphene. *Anal. Methods* **2017**, *9*, 618−624.
(84) Ng, B. Y. C.; Wee, E. J. H.; West, N. P.; Trau, M. Naked-Eye Colorimetric and Electrochemical Detection of Mycobacterium Tuberculosis—toward Rapid Screening for Active Case Finding. *ACS Sens.* **2016**, *1*, 173−178.
(85) Serra, B.; Reviejo, Á. J.; Pingarrón, J. M. Application of Electrochemical Enzyme Biosensors for Food Quality Control. *Compr. Anal. Chem.* **2007**, *49*, 255−298.

DOI: 10.1021/acs.chemrev.8b00226
Chem. Rev. 2019, 119, 231−292

(86) Yang, J.; Wang, P.; Zhang, X.; Wu, K. Electrochemical Sensor for Rapid Detection of Triclosan Using a Multiwall Carbon Nanotube Film. *J. Agric. Food Chem.* **2009**, *57*, 9403−9407.
(87) Lozano, J.; Arroyo, T.; Santos, J. P.; Cabellos, J. M.; Horrillo, M. C. Electronic Nose for Wine Ageing Detection. *Sens. Actuators, B* **2008**, *133*, 180−186.
(88) Kimmel, D. W.; LeBlanc, G.; Meschievitz, M. E.; Cliffel, D. E. Electrochemical Sensors and Biosensors. *Anal. Chem.* **2012**, *84*, 685−707.
(89) Tiwari, J. N.; Vij, V.; Kemp, K. C.; Kim, K. S. Engineered Carbon-Nanomaterial-Based Electrochemical Sensors for Biomolecules. *ACS Nano* **2016**, *10*, 46−80.
(90) O'Mahony, A. M.; Wang, J. Nanomaterial-Based Electrochemical Detection of Explosives: A Review of Recent Developments. *Anal. Methods* **2013**, *5*, 4296−4309.
(91) Yu, H. A.; Lee, J.; Lewis, S. W.; Silvester, D. S. Detection of 2,4,6-Trinitrotoluene Using a Miniaturized, Disposable Electrochemical Sensor with an Ionic Liquid Gel-Polymer Electrolyte Film. *Anal. Chem.* **2017**, *89*, 4729−4736.
(92) Wohltjen, H.; Barger, W. R.; Snow, A. W.; Jarvis, N. L. A Vapor-Sensitive Chemiresistor Fabricated with Planar Microelectrodes and a Langmuir-Blodgett Organic Semiconductor Film. *IEEE Trans. Electron Devices* **1985**, *32*, 1170−1174.
(93) Stitzel, S. E.; Aernecke, M. J.; Walt, D. R. Artificial Noses. *Annu. Rev. Biomed. Eng.* **2011**, *13*, 1−25.
(94) Lange, U.; Roznyatovskaya, N. V.; Mirsky, V. M. Conducting Polymers in Chemical Sensors and Arrays. *Anal. Chim. Acta* **2008**, *614*, 1−26.
(95) Panasyuk, T. L.; Mirsky, V. M.; Piletsky, S. A.; Wolfbeis, O. S. Electropolymerized Molecularly Imprinted Polymers as Receptor Layers in a Capacitive Chemical Sensors. *Anal. Chem.* **1999**, *71*, 4609−4613.
(96) Chen, L. X.; Wang, X. Y.; Lu, W. H.; Wu, X. Q.; Li, J. H. Molecular Imprinting: Perspectives and Applications. *Chem. Soc. Rev.* **2016**, *45*, 2137−2211.
(97) Blanco-Lopez, M. C.; Lobo-Castanon, M. J.; Miranda-Ordieres, A. J.; Tunon-Blanco, P. Electrochemical Sensors Based on Molecularly Imprinted Polymers. *TrAC, Trends Anal. Chem.* **2004**, *23*, 36−48.
(98) Famulok, M.; Mayer, G. Aptamer Modules as Sensors and Detectors. *Acc. Chem. Res.* **2011**, *44*, 1349−1358.
(99) Li, D.; Song, S. P.; Fan, C. H. Target-Responsive Structural Switching for Nucleic Acid-Based Sensors. *Acc. Chem. Res.* **2010**, *43*, 631−641.
(100) Cho, E. J.; Lee, J. W.; Ellington, A. D. Applications of Aptamers as Sensors. *Annu. Rev. Anal. Chem.* **2009**, *2*, 241−264.
(101) Willner, I.; Zayats, M. Electronic Aptamer-Based Sensors. *Angew. Chem., Int. Ed.* **2007**, *46*, 6408−6418.
(102) Nihtianov, S.; Luque, A. *Smart Sensors and Mems: Intelligent Devices and Microsystems for Industrial Applications*; Woodhead Publishing: Cambridge, 2014.
(103) Cheng, C. I.; Chang, Y. P.; Chu, Y. H. Biomolecular Interactions and Tools for Their Recognition: Focus on the Quartz Crystal Microbalance and Its Diverse Surface Chemistries and Applications. *Chem. Soc. Rev.* **2012**, *41*, 1947−1971.
(104) Atay, S.; Piskin, K.; Yilmaz, F.; Cakir, C.; Yavuz, H.; Denizli, A. Quartz Crystal Microbalance Based Biosensors for Detecting Highly Metastatic Breast Cancer Cells Via Their Transferrin Receptors. *Anal. Methods* **2016**, *8*, 153−161.
(105) Henry, C. Product Review: Measuring the Masses: Quartz Crystal Microbalances. *Anal. Chem.* **1996**, *68*, 625A−628A.
(106) Ogi, H.; Motoshisa, K.; Matsumoto, T.; Hatanaka, K.; Hirao, M. Isolated Electrodeless High-Frequency Quartz Crystal Microbalance for Immunosensors. *Anal. Chem.* **2006**, *78*, 6903−6909.
(107) Afzal, A.; Iqbal, N.; Mujahid, A.; Schirhagl, R. Advanced Vapor Recognition Materials for Selective and Fast Responsive Surface Acoustic Wave Sensors: A Review. *Anal. Chim. Acta* **2013**, *787*, 36−49.
(108) Devkota, J.; Ohodnicki, P. R.; Greve, D. W. Saw Sensors for Chemical Vapors and Gases. *Sensors* **2017**, *17*, 801.
(109) Mujahid, A.; Dickert, F. L. Surface Acoustic Wave (Saw) for Chemical Sensing Applications of Recognition Layers. *Sensors* **2017**, *17*, 2716.
(110) Martin, S. J.; Frye, G. C.; Wessendorf, K. O. Sensing Liquid Properties with Thickness-Shear Mode Resonators. *Sens. Actuators, A* **1994**, *44*, 209−218.
(111) Kankare, J.; Loikas, K.; Salomäki, M. Method for Measuring the Losses and Loading of a Quartz Crystal Microbalance. *Anal. Chem.* **2006**, *78*, 1875−1882.
(112) Webster, A.; Vollmer, F.; Sato, Y. Probing Biomechanical Properties with a Centrifugal Force Quartz Crystal Microbalance. *Nat. Commun.* **2014**, *5*, 5284.
(113) Tang, D.; Zhang, B.; Tang, J.; Hou, L.; Chen, G. Displacement-Type Quartz Crystal Microbalance Immunosensing Platform for Ultrasensitive Monitoring of Small Molecular Toxins. *Anal. Chem.* **2013**, *85*, 6958−6966.
(114) Abad, J. M.; Pariente, F.; Hernández, L.; Abruña, H. D.; Lorenzo, E. Determination of Organophosphorus and Carbamate Pesticides Using a Piezoelectric Biosensor. *Anal. Chem.* **1998**, *70*, 2848−2855.
(115) Bender, F.; Mohler, R. E.; Ricco, A. J.; Josse, F. Identification and Quantification of Aqueous Aromatic Hydrocarbons Using Sh-Surface Acoustic Wave Sensors. *Anal. Chem.* **2014**, *86*, 1794−1799.
(116) Ayad, M. M.; El-Hefnawey, G.; Torad, N. L. Quartz Crystal Microbalance Sensor Coated with Polyaniline Emeraldine Base for Determination of Chlorinated Aliphatic Hydrocarbons. *Sens. Actuators, B* **2008**, *134*, 887−894.
(117) Kumar, A.; Brunet, J.; Varenne, C.; Ndiaye, A.; Pauly, A. Phthalocyanines Based Qcm Sensors for Aromatic Hydrocarbons Monitoring: Role of Metal Atoms and Substituents on Response to Toluene. *Sens. Actuators, B* **2016**, *230*, 320−329.
(118) Zhang, Z.; Fan, J.; Yu, J.; Zheng, S.; Chen, W.; Li, H.; Wang, Z.; Zhang, W. New Poly(N,N-Dimethylaminoethyl Methacrylate)/Polyvinyl Alcohol Copolymer Coated Qcm Sensor for Interaction with Cwa Simulants. *ACS Appl. Mater. Interfaces* **2012**, *4*, 944−949.
(119) Yang, M.; He, J.; Hu, X.; Yan, C.; Cheng, Z. Cuo Nanostructures as Quartz Crystal Microbalance Sensing Layers for Detection of Trace Hydrogen Cyanide Gas. *Environ. Sci. Technol.* **2011**, *45*, 6088−6094.
(120) Liu, L.-S.; Kim, J.-M.; Kim, W.-S. Quartz Crystal Microbalance Technique for in Situ Analysis of Supersaturation in Cooling Crystallization. *Anal. Chem.* **2016**, *88*, 5718−5724.
(121) Olsson, A. L. J.; Quevedo, I. R.; He, D.; Basnet, M.; Tufenkji, N. Using the Quartz Crystal Microbalance with Dissipation Monitoring to Evaluate the Size of Nanoparticles Deposited on Surfaces. *ACS Nano* **2013**, *7*, 7833−7843.
(122) Zaera, F. Probing Liquid/Solid Interfaces at the Molecular Level. *Chem. Rev.* **2012**, *112*, 2920−2986.
(123) Wang, X.-d.; Wolfbeis, O. S. Fiber-Optic Chemical Sensors and Biosensors (2013−2015). *Anal. Chem.* **2016**, *88*, 203−227.
(124) Caucheteur, C.; Guo, T.; Liu, F.; Guan, B.-O.; Albert, J. Ultrasensitive Plasmonic Sensing in Air Using Optical Fibre Spectral Combs. *Nat. Commun.* **2016**, *7*, 13371.
(125) Walt, D. R. Fibre Optic Microarrays. *Chem. Soc. Rev.* **2010**, *39*, 38−50.
(126) Ma, H.; Jen, A. K. Y.; Dalton, L. R. Polymer-Based Optical Waveguides: Materials, Processing, and Devices. *Adv. Mater.* **2002**, *14*, 1339−1365.
(127) Schlücker, S. Surface-Enhanced Raman Spectroscopy: Concepts and Chemical Applications. *Angew. Chem., Int. Ed.* **2014**, *53*, 4756−4795.
(128) Haynes, C. L.; McFarland, A. D.; Van Duyne, R. P. Surface-Enhanced Raman Spectroscopy. *Anal. Chem.* **2005**, *77*, 338 A−346 A.
(129) Ding, S.-Y.; You, E.-M.; Tian, Z.-Q.; Moskovits, M. Electromagnetic Theories of Surface-Enhanced Raman Spectroscopy. *Chem. Soc. Rev.* **2017**, *46*, 4042−4076.
(130) Khansili, N.; Rattu, G.; Krishna, P. M. Label-Free Optical Biosensors for Food and Biological Sensor Applications. *Sens. Actuators, B* **2018**, *265*, 35−49.

DOI: 10.1021/acs.chemrev.8b00226
Chem. Rev. 2019, 119, 231−292

(131) Valenti, G.; Rampazzo, E.; Kesarkar, S.; Genovese, D.; Fiorani, A.; Zanut, A.; Palomba, F.; Marcaccio, M.; Paolucci, F.; Prodi, L. Electrogenerated Chemiluminescence from Metal Complexes-Based Nanoparticles for Highly Sensitive Sensors Applications. *Coord. Chem. Rev.* **2018**, *367*, 65−81.
(132) Zhang, L. C.; Hu, J.; Lv, Y.; Hou, X. D. Recent Progress in Chemiluminescence for Gas Analysis. *Appl. Spectrosc. Rev.* **2010**, *45*, 474−489.
(133) Lakowicz, J. R. *Principles of Fluorescence Spectroscopy*, 3rd ed.; Springer: New York, 2006.
(134) Podbielska, H.; Ulatowska-Jarza, A.; Muller, G.; Eichler, H. J. *Sol-Gels for Optical Sensors*; Springer: Erice, Italy, 2006.
(135) dos Santos, C. M. G.; Harte, A. J.; Quinn, S. J.; Gunnlaugsson, T. Recent Developments in the Field of Supramolecular Lanthanide Luminescent Sensors and Self-Assemblies. *Coord. Chem. Rev.* **2008**, *252*, 2512−2527.
(136) Bonacchi, S.; Genovese, D.; Juris, R.; Montalti, M.; Prodi, L.; Rampazzo, E.; Sgarzi, M.; Zaccheroni, N. Luminescent Chemosensors Based on Silica Nanoparticles. *Top. Curr. Chem.* **2010**, *300*, 93−138.
(137) del Mercato, L. L.; Pompa, P. P.; Maruccio, G.; Torre, A. D.; Sabella, S.; Tamburro, A. M.; Cingolani, R.; Rinaldi, R. Charge Transport and Intrinsic Fluorescence in Amyloid-Like Fibrils. *Proc. Natl. Acad. Sci. U. S. A.* **2007**, *104*, 18019−18024.
(138) Newman, R. H.; Fosbrink, M. D.; Zhang, J. Genetically Encodable Fluorescent Biosensors for Tracking Signaling Dynamics in Living Cells. *Chem. Rev.* **2011**, *111*, 3614−3666.
(139) Svendsen, A.; Kiefer, H. V.; Pedersen, H. B.; Bochenkova, A. V.; Andersen, L. H. Origin of the Intrinsic Fluorescence of the Green Fluorescent Protein. *J. Am. Chem. Soc.* **2017**, *139*, 8766−8771.
(140) Swain, J.; Kumar Mishra, A. Location, Partitioning Behavior, and Interaction of Capsaicin with Lipid Bilayer Membrane: Study Using Its Intrinsic Fluorescence. *J. Phys. Chem. B* **2015**, *119*, 12086−12093.
(141) Wen, X.; Yu, P.; Toh, Y.-R.; Hao, X.; Tang, J. Intrinsic and Extrinsic Fluorescence in Carbon Nanodots: Ultrafast Time-Resolved Fluorescence and Carrier Dynamics. *Adv. Opt. Mater.* **2013**, *1*, 173−178.
(142) Lee, J. Y.; Kim, S. K.; Jung, J. H.; Kim, J. S. Bifunctional Fluorescent Calix[4]Arene Chemosensor for Both a Cation and an Anion. *J. Org. Chem.* **2005**, *70*, 1463−1466.
(143) Zamora-Olivares, D.; Kaoud, T. S.; Dalby, K. N.; Anslyn, E. V. In-Situ Generation of Differential Sensors That Fingerprint Kinases and the Cellular Response to Their Expression. *J. Am. Chem. Soc.* **2013**, *135*, 14814−14820.
(144) Wright, A. T.; Anslyn, E. V. Differential Receptor Arrays and Assays for Solution-Based Molecular Recognition. *Chem. Soc. Rev.* **2006**, *35*, 14−28.
(145) Nassau, K. *The Physics and Chemistry of Color*; Wiley: New York, 2001.
(146) Kong, H.; Ma, Z. R.; Wang, S.; Gong, X. Y.; Zhang, S. C.; Zhang, X. R. Hydrogen Sulfide Detection Based on Reflection: From a Poison Test Approach of Ancient China to Single-Cell Accurate Localization. *Anal. Chem.* **2014**, *86*, 7734−7739.
(147) Suslick, K.; Rakow, N.; Sen, A. U.S. Patent 6,495,102, 2002.
(148) Kolthoff, I. M. *Acid Base Indicators*; Macmillan: New York, 1937.
(149) Sabnis, R. S. *Handbook of Acid-Base Indicators*; CRC Press: Boca Raton, FL, 2008.
(150) Green, F. J. *The Sigma-Aldrich Handbook of Stains, Dyes and Indicators*; Aldrich Chemical Co.: Milwaukee, WI, 1990.
(151) Kemling, J. W.; Qavi, A. J.; Bailey, R. C.; Suslick, K. S. Nanostructured Substrates for Optical Sensing. *J. Phys. Chem. Lett.* **2011**, *2*, 2934−2944.
(152) Kemling, J. W.; Suslick, K. S. Nanoscale Porosity in Pigments for Chemical Sensing. *Nanoscale* **2011**, *3*, 1971−1973.
(153) Lim, S. H.; Kemling, J. W.; Feng, L.; Suslick, K. S. A Colorimetric Sensor Array of Porous Pigments. *Analyst* **2009**, *134*, 2453−2457.
(154) Bang, J. H.; Lim, S. H.; Park, E.; Suslick, K. S. Chemically Responsive Nanoporous Pigments: Colorimetric Sensor Arrays and the Identification of Aliphatic Amines. *Langmuir* **2008**, *24*, 13168−13172.
(155) Atwood, J. L.; Davies, J. E. D.; MacNicol, D. D.; Vogtle, F. In *Comprehensive Supramolecular Chemistry*; Atwood, J. L., Davies, J. E. D., MacNicol, D. D., Vogtle, F., Eds.; Pergamon: Oxford, 1996.
(156) Pinalli, R.; Dalcanale, E. Supramolecular Sensing with Phosphonate Cavitands. *Acc. Chem. Res.* **2013**, *46*, 399−411.
(157) Barrow, S. J.; Kasera, S.; Rowland, M. J.; del Barrio, J.; Scherman, O. A. Cucurbituril-Based Molecular Recognition. *Chem. Rev.* **2015**, *115*, 12320−12406.
(158) Citterio, D.; Takeda, J.; Kosugi, M.; Hisamoto, H.; Sasaki, S.-i.; Komatsu, H.; Suzuki, K. Ph-Independent Fluorescent Chemosensor for Highly Selective Lithium Ion Sensing. *Anal. Chem.* **2007**, *79*, 1237−1242.
(159) Su, C.-Y.; Menuz, K.; Carlson, J. R. Olfactory Perception: Receptors, Cells, and Circuits. *Cell* **2009**, *139*, 45−59.
(160) Müller-Dethlefs, K.; Hobza, P. Noncovalent Interactions: A Challenge for Experiment and Theory. *Chem. Rev.* **2000**, *100*, 143−168.
(161) Hunter, C. A. Quantifying Intermolecular Interactions: Guidelines for the Molecular Recognition Toolbox. *Angew. Chem., Int. Ed.* **2004**, *43*, 5310−5324.
(162) Zhang, X.; Wang, C. Supramolecular Amphiphiles. *Chem. Soc. Rev.* **2011**, *40*, 94−101.
(163) Jungreis, E. *Spot Test Analysis*, 2nd ed.; Wiley: New York, 1997.
(164) Feigle, F.; Anger, V. *Spot Tests in Organic Analysis*, 7th ed.; Elsevier: New York, 1966.
(165) Feigle, F.; Anger, V. *Spot Tests in Inorganic Analysis*, 6th ed.; Elsevier: New York, 1972.
(166) El-Desouki, M.; Deen, M. J.; Fang, Q. Y.; Liu, L.; Tse, F.; Armstrong, D. CMOS Image Sensors for High Speed Applications. *Sensors* **2009**, *9*, 430−444.
(167) Paolesse, R.; Monti, D.; Dini, F.; Di Natale, C. Fluorescence Based Sensor Arrays. *Top. Curr. Chem.* **2010**, *300*, 139−174.
(168) Meier, R. J.; Fischer, L. H.; Wolfbeis, O. S.; Schaferling, M. Referenced Luminescent Sensing and Imaging with Digital Color Cameras: A Comparative Study. *Sens. Actuators, B* **2013**, *177*, 500−506.
(169) Janzen, M. C.; Ponder, J. B.; Bailey, D. P.; Ingison, C. K.; Suslick, K. S. Colorimetric Sensor Arrays for Volatile Organic Compounds. *Anal. Chem.* **2006**, *78*, 3591−3600.
(170) Hsieh, M. D.; Zellers, E. T. Limits of Recognition for Simple Vapor Mixtures Determined with a Microsensor Array. *Anal. Chem.* **2004**, *76*, 1885.
(171) Wade, A.; Lovera, P.; O'Carroll, D.; Doyle, H.; Redmond, G. Luminescent Optical Detection of Volatile Electron Deficient Compounds by Conjugated Polymer Nanofibers. *Anal. Chem.* **2015**, *87*, 4421−4428.
(172) Li, X.; Zamora-Olivares, D.; Diehl, K. L.; Tian, W.; Anslyn, E. V. Differential Sensing of Oils by Conjugates of Serum Albumins and 9,10-Distyrylanthracene Probes: A Cautionary Tale. *Supramol. Chem.* **2017**, *29*, 308−314.
(173) Rakow, N. A.; Sen, A.; Janzen, M. C.; Ponder, J. B.; Suslick, K. S. Molecular Recognition and Discrimination of Amines with a Colorimetric Array. *Angew. Chem., Int. Ed.* **2005**, *44*, 4528−4532.
(174) Feng, L.; Musto, C. J.; Kemling, J. W.; Lim, S. H.; Suslick, K. S. A Colorimetric Sensor Array for Identification of Toxic Gases Below Permissible Exposure Limits. *Chem. Commun.* **2010**, *46*, 2037−2039.
(175) Feng, L.; Musto, C. J.; Kemling, J. W.; Lim, S. H.; Zhong, W.; Suslick, K. S. Colorimetric Sensor Array for Determination and Identification of Toxic Industrial Chemicals. *Anal. Chem.* **2010**, *82*, 9433−9440.
(176) Rankin, J. M.; Zhang, Q.; LaGasse, M. K.; Zhang, Y.; Askim, J. R.; Suslick, K. S. Solvatochromic Sensor Array for the Identification of Common Organic Solvents. *Analyst* **2015**, *140*, 2613−2617.
(177) Paolesse, R.; Nardis, S.; Monti, D.; Stefanelli, M.; Di Natale, C. Porphyrinoids for Chemical Sensor Applications. *Chem. Rev.* **2017**, *117*, 2517−2583.
(178) Lemon, C. M.; Karnas, E.; Han, X.; Bruns, O. T.; Kempa, T. J.; Fukumura, D.; Bawendi, M. G.; Jain, R. K.; Duda, D. G.; Nocera, D. G.

DOI: 10.1021/acs.chemrev.8b00226
Chem. Rev. 2019, 119, 231−292

Micelle-Encapsulated Quantum Dot-Porphyrin Assemblies as in Vivo Two-Photon Oxygen Sensors. *J. Am. Chem. Soc.* **2015**, *137*, 9832−9842.
(179) Ding, Y.; Zhu, W.-H.; Xie, Y. Development of Ion Chemosensors Based on Porphyrin Analogues. *Chem. Rev.* **2017**, *117*, 2203−2256.
(180) Suslick, K. S.; Rakow, N. A.; Sen, A. Colorimetric Sensor Arrays for Molecular Recognition. *Tetrahedron* **2004**, *60*, 11133−11138.
(181) Collman, J. P.; Fu, L. Synthetic Models for Hemoglobin and Myoglobin. *Acc. Chem. Res.* **1999**, *32*, 455−463.
(182) Suslick, K. S.; Reinert, T. J. The Synthetic Analogs of O2-Binding Heme-Proteins. *J. Chem. Educ.* **1985**, *62*, 974−983.
(183) Fang, M.; Wilson, S. R.; Suslick, K. S. A Four-Coordinate Fe(I I I) Porphyrin Cation. *J. Am. Chem. Soc.* **2008**, *130*, 1134−1135.
(184) Sen, J.; Suslick, K. S. Shape-Selective Discrimination of Small Organic Molecules. *J. Am. Chem. Soc.* **2000**, *122*, 11565−11566.
(185) Suslick, K. S.; Van Deusen-Jeffries, S. Shape Selective Biomimetic Oxidation Catalysis. In *Comprehensive Supramolecular Chemistry: Bioinorganic Systems*; Atwood, J. L., Davies, J. E. D., MacNicol, D. D., Vogtle, F., Eds.; Pergamon: Oxford, 1996; Vol. *5*, pp 141−170.
(186) Cook, B. R.; Reinert, T. J.; Suslick, K. S. Shape Selective Alkane Hydroxylation by Metalloporphyrin Catalysts. *J. Am. Chem. Soc.* **1986**, *108*, 7281−7286.
(187) Suslick, K.; Cook, B.; Fox, M. Shape-Selective Alkane Hydroxylation. *J. Chem. Soc., Chem. Commun.* **1985**, 580−582.
(188) Suslick, K. S.; Cook, B. R. Regioselective Epoxidations of Dienes with Manganese(Iii) Porphyrin Catalysts. *J. Chem. Soc., Chem. Commun.* **1987**, 200−202.
(189) Bhyrappa, P.; Vaijayanthimala, G.; Suslick, K. S. Shape-Selective Ligation to Dendrimer-Metalloporphyrins. *J. Am. Chem. Soc.* **1999**, *121*, 262−263.
(190) Dunbar, A. D. F.; Brittle, S.; Richardson, T. H.; Hutchinson, J.; Hunter, C. A. Detection of Volatile Organic Compounds Using Porphyrin Derivatives. *J. Phys. Chem. B* **2010**, *114*, 11697−11702.
(191) Cai, W.-R.; Zhang, G.-Y.; Lu, K.-K.; Zeng, H.-B.; Cosnier, S.; Zhang, X.-J.; Shan, D. Enhanced Electrochemiluminescence of One-Dimensional Self-Assembled Porphyrin Hexagonal Nanoprisms. *ACS Appl. Mater. Interfaces* **2017**, *9*, 20904−20912.
(192) Sessler, J. L.; Gale, P. A.; Cho, W.-S. *Anion Receptor Chemistry*; RSC Publishing: Cambridge, U.K., 2006.
(193) Rhee, H.-W.; Lee, S. W.; Lee, J.-S.; Chang, Y.-T.; Hong, J.-I. Focused Fluorescent Probe Library for Metal Cations and Biological Anions. *ACS Comb. Sci.* **2013**, *15*, 483−490.
(194) Chifotides, H. T.; Dunbar, K. R. Anion-Pi Interactions in Supramolecular Architectures. *Acc. Chem. Res.* **2013**, *46*, 894−906.
(195) Liu, Z. P.; He, W. J.; Guo, Z. J. Metal Coordination in Photoluminescent Sensing. *Chem. Soc. Rev.* **2013**, *42*, 1568−1600.
(196) Du, J. J.; Hu, M. M.; Fan, J. L.; Peng, X. J. Fluorescent Chemodosimeters Using "Mild" Chemical Events for the Detection of Small Anions and Cations in Biological and Environmental Media. *Chem. Soc. Rev.* **2012**, *41*, 4511−4535.
(197) Busschaert, N.; Caltagirone, C.; Van Rossom, W.; Gale, P. A. Applications of Supramolecular Anion Recognition. *Chem. Rev.* **2015**, *115*, 8038−8155.
(198) Langton, M. J.; Serpell, C. J.; Beer, P. D. Anion Recognition in Water: Recent Advances from a Supramolecular and Macromolecular Perspective. *Angew. Chem., Int. Ed.* **2016**, *55*, 1974−1987.
(199) Gale, P. A.; Busschaert, N.; Haynes, C. J. E.; Karagiannidis, L. E.; Kirby, I. L. Anion Receptor Chemistry: Highlights from 2011 and 2012. *Chem. Soc. Rev.* **2014**, *43*, 205−241.
(200) Sakai, R. Conjugated Polymers Applicable to Colorimetric and Fluorescent Anion Detection. *Polym. J.* **2016**, *48*, 59−65.
(201) Evans, N. H.; Beer, P. D. Advances in Anion Supramolecular Chemistry: From Recognition to Chemical Applications. *Angew. Chem., Int. Ed.* **2014**, *53*, 11716−11754.
(202) Gale, P. A.; Howe, E. N. W.; Wu, X. Anion Receptor Chemistry. *Chem* **2016**, *1*, 351−422.
(203) Zhou, Y.; Zhang, J. F.; Yoon, J. Fluorescence and Colorimetric Chemosensors for Fluoride-Ion Detection. *Chem. Rev.* **2014**, *114*, 5511−5571.
(204) Kang, S. O.; Llinares, J. M.; Day, V. W.; Bowman-James, K. Cryptand-Like Anion Receptors. *Chem. Soc. Rev.* **2010**, *39*, 3980−4003.
(205) He, Q.; Tu, P. Y.; Sessler, J. L. Supramolecular Chemistry of Anionic Dimers, Trimers, Tetramers, and Clusters. *Chem.* **2018**, *4*, 46−93.
(206) Kim, D. S.; Sessler, J. L. Calix 4 Pyrroles: Versatile Molecular Containers with Ion Transport, Recognition, and Molecular Switching Functions. *Chem. Soc. Rev.* **2015**, *44*, 532−546.
(207) Lee, M. H.; Kim, J. S.; Sessler, J. L. Small Molecule-Based Ratiometric Fluorescence Probes for Cations, Anions, and Biomolecules. *Chem. Soc. Rev.* **2015**, *44*, 4185−4191.
(208) Sessler, J. L.; Gross, Z.; Furuta, H. Introduction: Expanded, Contracted, and Isomeric Porphyrins. *Chem. Rev.* **2017**, *117*, 2201−2202.
(209) Minami, T.; Liu, Y.; Akdeniz, A.; Koutnik, P.; Esipenko, N. A.; Nishiyabu, R.; Kubo, Y.; Anzenbacher, P. Intramolecular Indicator Displacement Assay for Anions: Supramolecular Sensor for Glyphosate. *J. Am. Chem. Soc.* **2014**, *136*, 11396−11401.
(210) Schiller, J.; Pérez-Ruiz, R.; Sampedro, D.; Marqués-López, E.; Herrera, R.; Díaz Díaz, D. Fluoride Anion Recognition by a Multifunctional Urea Derivative: An Experimental and Theoretical Study. *Sensors* **2016**, *16*, 658.
(211) Pérez-Ruiz, R.; Griesbeck, A. G.; Sampedro, D. Computational Study on Fluoride Recognition by an Urea-Activated Phthalimide Chemosensor. *Tetrahedron* **2012**, *68*, 5724−5729.
(212) Singh, J.; Yadav, M.; Singh, A.; Singh, N. Zinc Metal Complex as a Sensor for Simultaneous Detection of Fluoride and Hso4- Ions. *Dalton Transactions* **2015**, *44*, 12589−12597.
(213) Sakai, R.; Nagai, A.; Tago, Y.; Sato, S.-i.; Nishimura, Y.; Arai, T.; Satoh, T.; Kakuchi, T. Fluorescence Turn-on Sensing of Anions Based on Disassembly Process of Urea-Functionalized Poly(Phenylenebutadiynylene) Aggregates. *Macromolecules* **2012**, *45*, 4122−4127.
(214) Bharadwaj, P. K. Metal Ion Binding by Laterally Non-Symmetric Macrobicyclic Oxa-Aza Cryptands. *Dalton Transactions* **2017**, *46*, 5742−5775.
(215) Xu, M.; Wu, S.; Zeng, F.; Yu, C. Cyclodextrin Supramolecular Complex as a Water-Soluble Ratiometric Sensor for Ferric Ion Sensing. *Langmuir* **2010**, *26*, 4529−4534.
(216) Wang, X.; Qin, Y.; Meyerhoff, M. E. Paper-Based Plasticizer-Free Sodium Ion-Selective Sensor with Camera Phone as a Detector. *Chem. Commun.* **2015**, *51*, 15176−15179.
(217) Spenst, P.; Würthner, F. A Perylene Bisimide Cyclophane as a "Turn-on" and "Turn-Off" Fluorescence Probe. *Angew. Chem., Int. Ed.* **2015**, *54*, 10165−10168.
(218) Flaschka, H.; Schwarzenbach, G. *Complexometric Titrations*; Methuen: London, 1969.
(219) Zhai, J. Y.; Bakker, E. Complexometric Titrations: New Reagents and Concepts to Overcome Old Limitations. *Analyst* **2016**, *141*, 4252−4261.
(220) Přibil, R. *Applied Complexometry: Pergamon Series in Analytical Chemistry*; Pergamon: Oxford, 1982.
(221) Santos-Figueroa, L. E.; Moragues, M. E.; Climent, E.; Agostini, A.; Martínez-Máñez, R.; Sancenón, F. Chromogenic and Fluorogenic Chemosensors and Reagents for Anions. *Chem. Soc. Rev.* **2013**, *42*, 3489−3613.
(222) Mayr, T.; Igel, C.; Liebsch, G.; Klimant, I.; Wolfbeis, O. S. Cross-Reactive Metal Ion Sensor Array in a Micro Titer Plate Format. *Anal. Chem.* **2003**, *75*, 4389−4396.
(223) Feng, L.; Zhang, Y.; Wen, L.; Chen, L.; Shen, Z.; Guan, Y. Discrimination of Trace Heavy-Metal Ions by Filtration on Sol−Gel Membrane Arrays. *Chem. - Eur. J.* **2011**, *17*, 1101−1104.
(224) Zhai, J.; Xie, X.; Bakker, E. Solvatochromic Dyes as Ph-Independent Indicators for Ionophore Nanosphere-Based Complexometric Titrations. *Anal. Chem.* **2015**, *87*, 12318−12323.

DOI: 10.1021/acs.chemrev.8b00226
Chem. Rev. 2019, 119, 231−292

(225) Zhai, J.; Bakker, E. Complexometric Titrations: New Reagents and Concepts to Overcome Old Limitations. *Analyst* **2016**, *141*, 4252−4261.
(226) Garfield, S. *Mauve: How One Man Invented a Color That Changed the World*; Faber and Faber: London, 2000.
(227) *Industrial Dyes. Chemistry, Properties, Applications*; Hunger, K., Ed.; Wiley-VCH: Weinheim, 2003.
(228) Zollinger, H. *Color Chemistry. Synthesis, Properties and Applications of Organic Dyes and Pigments*, 3rd ed.; Wiley-VCH: Weinheim, 2003.
(229) Schäferling, M. Nanoparticle-Based Luminescent Probes for Intracellular Sensing and Imaging of Ph. *WIREs Nanomed. Nanobiotechnol.* **2016**, *8*, 378−413.
(230) Aigner, D.; Ungerbock, B.; Mayr, T.; Saf, R.; Klimant, I.; Borisov, S. M. Fluorescent Materials for Ph Sensing and Imaging Based on Novel 1,4-Diketopyrrolo-[3,4-C]Pyrrole Dyes. *J. Mater. Chem. C* **2013**, *1*, 5685−5693.
(231) Deng, M.; Yang, C.; Gong, D.; Iqbal, A.; Tang, X.; Liu, W.; Qin, W. Bodipy-Derived Piperazidine Fluorescent near-Neutral Ph Indicator and Its Bioimaging. *Sens. Actuators, B* **2016**, *232*, 492−498.
(232) Hulanicki, A.; Glab, S. Redox Indicators: Characteristics and Applications. *Pure Appl. Chem.* **1978**, *50*, 463−498.
(233) Connelly, N. G.; Geiger, W. E. Chemical Redox Agents for Organometallic Chemistry. *Chem. Rev.* **1996**, *96*, 877−910.
(234) Hyman, L. M.; Franz, K. J. Probing Oxidative Stress: Small Molecule Fluorescent Sensors of Metal Ions, Reactive Oxygen Species, and Thiols. *Coord. Chem. Rev.* **2012**, *256*, 2333−2356.
(235) Okumoto, S.; Jones, A.; Frommer, W. B. Quantitative Imaging with Fluorescent Biosensors. *Annu. Rev. Plant Biol.* **2012**, *63*, 663−706.
(236) Martin, A.; Portaels, F.; Palomino, J. C. Colorimetric Redox-Indicator Methods for the Rapid Detection of Multidrug Resistance in Mycobacterium Tuberculosis: A Systematic Review and Meta-Analysis. *J. Antimicrob. Chemother.* **2007**, *59*, 175−183.
(237) Rozman, M.; Cerar, J.; Lukšič, M.; Uršič, M.; Mourtzikou, A.; Spreizer, H.; Škofic, I. K.; Stathatos, E. Electrochromic Properties of Thin Nanocrystalline Tio2 Films Coated Electrodes with Adsorbed Co(Ii) or Fe(Ii) 2,2′-Bipyridine Complexes. *Electrochim. Acta* **2017**, *238*, 278−287.
(238) Krumova, K.; Cosa, G. Bodipy Dyes with Tunable Redox Potentials and Functional Groups for Further Tethering: Preparation, Electrochemical, and Spectroscopic Characterization. *J. Am. Chem. Soc.* **2010**, *132*, 17560−17569.
(239) Farjami, E.; Clima, L.; Gothelf, K. V.; Ferapontova, E. E. DNA Interactions with a Methylene Blue Redox Indicator Depend on the DNA Length and Are Sequence Specific. *Analyst* **2010**, *135*, 1443−1448.
(240) Boens, N.; Leen, V.; Dehaen, W. Fluorescent Indicators Based on Bodipy. *Chem. Soc. Rev.* **2012**, *41*, 1130−1172.
(241) Passos, M. L. C.; Saraiva, M. L. M. F. S.; Lima, J. L. F. C. A Thionine-Based Reversible Redox Sensor in a Sequential Injection System. *Anal. Chim. Acta* **2010**, *668*, 41−46.
(242) Lin, H.; Suslick, K. S. A Colorimetric Sensor Array for Detection of Triacetone Triperoxide Vapor. *J. Am. Chem. Soc.* **2010**, *132*, 15519−15521.
(243) Li, Z.; Fang, M.; LaGasse, M. K.; Askim, J. R.; Suslick, K. S. Colorimetric Recognition of Aldehydes and Ketones. *Angew. Chem., Int. Ed.* **2017**, *56*, 9860−9863.
(244) Reichardt, C.; Welton, T. *Solvents and Solvent Effects in Organic Chemistry*, 4th ed.; Wiley-VCH: Weinheim, 2010.
(245) Reichardt, C. Solvatochromic Dyes as Solvent Polarity Indicators. *Chem. Rev.* **1994**, *94*, 2319−2358.
(246) Katritzky, A. R.; Fara, D. C.; Yang, H.; Tämm, K.; Tamm, T.; Karelson, M. Quantitative Measures of Solvent Polarity. *Chem. Rev.* **2004**, *104*, 175−198.
(247) Marini, A.; Muñoz-Losa, A.; Biancardi, A.; Mennucci, B. What Is Solvatochromism? *J. Phys. Chem. B* **2010**, *114*, 17128−17135.
(248) Gstrein, C.; Zhang, B.; Abdel-Rahman, M. A.; Bertran, O.; Aleman, C.; Wegner, G.; Schluter, A. D. Solvatochromism of Dye-Labeled Dendronized Polymers of Generation Numbers 1−4: Comparison to Dendrimers. *Chem. Sci.* **2016**, *7*, 4644−4652.
(249) Catalán, J. Toward a Generalized Treatment of the Solvent Effect Based on Four Empirical Scales: Dipolarity (Sdp, a New Scale), Polarizability (Sp), Acidity (Sa), and Basicity (Sb) of the Medium. *J. Phys. Chem. B* **2009**, *113*, 5951−5960.
(250) Yousefinejad, S.; Honarasa, F.; Chaabi, M. New Relationship Models for Solvent-Pyrene Solubility Based on Molecular Structure and Empirical Properties. *New J. Chem.* **2016**, *40*, 10197−10207.
(251) Yamashita, H.; Abe, J. Remarkable Solvatochromic Color Change Via Proton Tautomerism of a Phenol-Linked Imidazole Derivative. *J. Phys. Chem. A* **2014**, *118*, 1430−1438.
(252) Klymchenko, A. S. Solvatochromic and Fluorogenic Dyes as Environment-Sensitive Probes: Design and Biological Applications. *Acc. Chem. Res.* **2017**, *50*, 366−375.
(253) Wenger, O. S. Vapochromism in Organometallic and Coordination Complexes: Chemical Sensors for Volatile Organic Compounds. *Chem. Rev.* **2013**, *113*, 3686−3733.
(254) Kobayashi, A.; Kato, M. Vapochromic Platinum(Ii) Complexes: Crystal Engineering toward Intelligent Sensing Devices. *Eur. J. Inorg. Chem.* **2014**, *2014*, 4469−4483.
(255) Cich, M. J.; Hill, I. M.; Lackner, A. D.; Martinez, R. J.; Ruthenburg, T. C.; Takeshita, Y.; Young, A. J.; Drew, S. M.; Buss, C. E.; Mann, K. R. Enantiomerically Selective Vapochromic Sensing. *Sens. Actuators, B* **2010**, *149*, 199−204.
(256) Yang, K.; Li, S.-L.; Zhang, F.-Q.; Zhang, X.-M. Simultaneous Luminescent Thermochromism, Vapochromism, Solvatochromism, and Mechanochromism in a C3-Symmetric Cubane [Cu4i4p4] Cluster without Cu−Cu Interaction. *Inorg. Chem.* **2016**, *55*, 7323−7325.
(257) Mei, J.; Leung, N. L. C.; Kwok, R. T. K.; Lam, J. W. Y.; Tang, B. Z. Aggregation-Induced Emission: Together We Shine, United We Soar! *Chem. Rev.* **2015**, *115*, 11718−11940.
(258) Murphy, C. J.; Gole, A. M.; Stone, J. W.; Sisco, P. N.; Alkilany, A. M.; Goldsmith, E. C.; Baxter, S. C. Gold Nanoparticles in Biology: Beyond Toxicity to Cellular Imaging. *Acc. Chem. Res.* **2008**, *41*, 1721−1730.
(259) Zhao, W.; Brook, M. A.; Li, Y. F. Design of Gold Nanoparticle-Based Colorimetric Biosensing Assays. *ChemBioChem* **2008**, *9*, 2363−2371.
(260) Penn, S. G.; He, L.; Natan, M. J. Nanoparticles for Bioanalysis. *Curr. Opin. Chem. Biol.* **2003**, *7*, 609−615.
(261) Rosi, N. L.; Mirkin, C. A. Nanostructures in Biodiagnostics. *Chem. Rev.* **2005**, *105*, 1547−1562.
(262) Chinen, A. B.; Guan, C. M.; Ferrer, J. R.; Barnaby, S. N.; Merkel, T. J.; Mirkin, C. A. Nanoparticle Probes for the Detection of Cancer Biomarkers, Cells, and Tissues by Fluorescence. *Chem. Rev.* **2015**, *115*, 10530−10574.
(263) Wolfbeis, O. S. An Overview of Nanoparticles Commonly Used in Fluorescent Bioimaging. *Chem. Soc. Rev.* **2015**, *44*, 4743−4768.
(264) Lim, S. Y.; Ahn, J.; Lee, J. S.; Kim, M.-G.; Park, C. B. Graphene-Oxide-Based Immunosensing through Fluorescence Quenching by Peroxidase-Catalyzed Polymerization. *Small* **2012**, *8*, 1994−1999.
(265) Pang, X.; Li, J.; Zhao, Y.; Wu, D.; Zhang, Y.; Du, B.; Ma, H.; Wei, Q. Label-Free Electrochemiluminescent Immunosensor for Detection of Carcinoembryonic Antigen Based on Nanocomposites of G O/M W C N Ts-C O O H/Au@Ce O2. *ACS Appl. Mater. Interfaces* **2015**, *7*, 19260−19267.
(266) Farka, Z.; Juřík, T.; Kovář, D.; Trnková, L.; Skládal, P. Nanoparticle-Based Immunochemical Biosensors and Assays: Recent Advances and Challenges. *Chem. Rev.* **2017**, *117*, 9973−10042.
(267) Roark, B.; Tan, J. A.; Ivanina, A.; Chandler, M.; Castaneda, J.; Kim, H. S.; Jawahar, S.; Viard, M.; Talic, S.; Wustholz, K. L.; et al. Fluorescence Blinking as an Output Signal for Biosensing. *ACS Sens.* **2016**, *1*, 1295−1300.
(268) Huang, C.-C.; Chang, H.-T. Selective Gold-Nanoparticle-Based "Turn-on" Fluorescent Sensors for Detection of Mercury(Ii) in Aqueous Solution. *Anal. Chem.* **2006**, *78*, 8332−8338.

DOI: 10.1021/acs.chemrev.8b00226
Chem. Rev. 2019, 119, 231−292

(269) Yang, X.; Yang, M.; Pang, B.; Vara, M.; Xia, Y. Gold Nanomaterials at Work in Biomedicine. *Chem. Rev.* **2015**, *115*, 10410−10488.
(270) Guo, Y.; Cao, F.; Lei, X.; Mang, L.; Cheng, S.; Song, J. Fluorescent Copper Nanoparticles: Recent Advances in Synthesis and Applications for Sensing Metal Ions. *Nanoscale* **2016**, *8*, 4852−4863.
(271) Li, J.; Li, Y.; Shahzad, S. A.; Chen, J.; Chen, Y.; Wang, Y.; Yang, M.; Yu, C. Fluorescence Turn-on Detection of Glucose Via the Ag Nanoparticle Mediated Release of a Perylene Probe. *Chem. Commun.* **2015**, *51*, 6354−6356.
(272) Umali, A. P.; Anslyn, E. V. A General Approach to Differential Sensing Using Synthetic Molecular Receptors. *Curr. Opin. Chem. Biol.* **2010**, *14*, 685−692.
(273) Diehl, K. L.; Ivy, M. A.; Rabidoux, S.; Petry, S. M.; Müller, G.; Anslyn, E. V. Differential Sensing for the Regio- and Stereoselective Identification and Quantitation of Glycerides. *Proc. Natl. Acad. Sci. U. S. A.* **2015**, *112*, E3977−E3986.
(274) Dorh, N.; Zhu, S.; Dhungana, K. B.; Pati, R.; Luo, F.-T.; Liu, H.; Tiwari, A. BODIPY-Based Fluorescent Probes for Sensing Protein Surface-Hydrophobicity. *Sci. Rep.* **2016**, *5*, 18337.
(275) Liu, Y.; Perez, L.; Mettry, M.; Easley, C. J.; Hooley, R. J.; Zhong, W. Self-Aggregating Deep Cavitand Acts as a Fluorescence Displacement Sensor for Lysine Methylation. *J. Am. Chem. Soc.* **2016**, *138*, 10746−10749.
(276) Culver, H. R.; Sharma, I.; Wechsler, M. E.; Anslyn, E. V.; Peppas, N. A. Charged Poly(N-Isopropylacrylamide) Nanogels for Use as Differential Protein Receptors in a Turbidimetric Sensor Array. *Analyst* **2017**, *142*, 3183−3193.
(277) Ghanem, E.; Hopfer, H.; Navarro, A.; Ritzer, M.; Mahmood, L.; Fredell, M.; Cubley, A.; Bolen, J.; Fattah, R.; Teasdale, K.; et al. Predicting the Composition of Red Wine Blends Using an Array of Multicomponent Peptide-Based Sensors. *Molecules* **2015**, *20*, 9170.
(278) Ghanem, E.; Afsah, S.; Fallah, P. N.; Lawrence, A.; LeBovidge, E.; Raghunathan, S.; Rago, D.; Ramirez, M. A.; Telles, M.; Winkler, M.; et al. Differentiation and Identification of Cachaça Wood Extracts Using Peptide-Based Receptors and Multivariate Data Analysis. *ACS Sens.* **2017**, *2*, 641−647.
(279) Kubarych, C. J.; Adams, M. M.; Anslyn, E. V. Serum Albumins as Differential Receptors for the Discrimination of Fatty Acids and Oils. *Org. Lett.* **2010**, *12*, 4780−4783.
(280) Wackerlig, J.; Schirhagl, R. Applications of Molecularly Imprinted Polymer Nanoparticles and Their Advances toward Industrial Use: A Review. *Anal. Chem.* **2016**, *88*, 250−261.
(281) Chen, L.; Wang, X.; Lu, W.; Wu, X.; Li, J. Molecular Imprinting: Perspectives and Applications. *Chem. Soc. Rev.* **2016**, *45*, 2137−2211.
(282) Li, J.; Hu, X.; Guan, P.; Zhang, X.; Qian, L.; Song, R.; Du, C.; Wang, C. Preparation of Molecularly Imprinted Polymers Using Ion-Pair Dummy Template Imprinting and Polymerizable Ionic Liquids. *RSC Adv.* **2015**, *5*, 62697−62705.
(283) Zhang, W.; Liu, W.; Li, P.; Xiao, H.; Wang, H.; Tang, B. A Fluorescence Nanosensor for Glycoproteins with Activity Based on the Molecularly Imprinted Spatial Structure of the Target and Boronate Affinity. *Angew. Chem., Int. Ed.* **2014**, *53*, 12489−12493.
(284) Liang, J.; Wu, Y.; Deng, J. Construction of Molecularly Imprinted Polymer Microspheres by Using Helical Substituted Polyacetylene and Application in Enantio-Differentiating Release and Adsorption. *ACS Appl. Mater. Interfaces* **2016**, *8*, 12494−12503.
(285) Ahmad, R.; Griffete, N.; Lamouri, A.; Felidj, N.; Chehimi, M. M.; Mangeney, C. Nanocomposites of Gold Nanoparticles@Molecularly Imprinted Polymers: Chemistry, Processing, and Applications in Sensors. *Chem. Mater.* **2015**, *27*, 5464−5478.
(286) Xu, S.; Lu, H.; Li, J.; Song, X.; Wang, A.; Chen, L.; Han, S. Dummy Molecularly Imprinted Polymers-Capped Cdte Quantum Dots for the Fluorescent Sensing of 2,4,6-Trinitrotoluene. *ACS Appl. Mater. Interfaces* **2013**, *5*, 8146−8154.
(287) Zimmerman, S. C.; Wendland, M. S.; Rakow, N. A.; Zharov, I.; Suslick, K. S. Synthetic Hosts by Monomolecular Imprinting inside Dendrimers. *Nature* **2002**, *418*, 399−403.
(288) Zimmerman, S. C.; Zharov, I.; Wendland, M. S.; Rakow, N. A.; Suslick, K. S. Molecular Imprinting inside Dendrimers. *J. Am. Chem. Soc.* **2003**, *125*, 13504−13518.
(289) Zhang, C.; Suslick, K. S. A Colorimetric Sensor Array for Organics in Water. *J. Am. Chem. Soc.* **2005**, *127*, 11548−11549.
(290) Rottman, C.; Grader, G.; De Hazan, Y.; Melchior, S.; Avnir, D. Surfactant-Induced Modification of Dopants Reactivity in Sol−Gel Matrixes. *J. Am. Chem. Soc.* **1999**, *121*, 8533−8543.
(291) Dmitriev, A.; Hägglund, C.; Chen, S.; Fredriksson, H.; Pakizeh, T.; Käll, M.; Sutherland, D. S. Enhanced Nanoplasmonic Optical Sensors with Reduced Substrate Effect. *Nano Lett.* **2008**, *8*, 3893−3898.
(292) Podbielska, H.; Ulatowska-Jarza, A.; Muller, G.; Eichler, H. J. *Sol-Gels for Optical Sensors*; Springer: Erice, Italy, 2006.
(293) LaGasse, M. K.; Rankin, J. M.; Askim, J. R.; Suslick, K. S. Colorimetric Sensor Arrays: Interplay of Geometry, Substrate and Immobilization. *Sens. Actuators, B* **2014**, *197*, 116−122.
(294) Sannino, A.; Pappadà, S.; Giotta, L.; Valli, L.; Maffezzoli, A. Spin Coating Cellulose Derivatives on Quartz Crystal Microbalance Plates to Obtain Hydrogel-Based Fast Sensors and Actuators. *J. Appl. Polym. Sci.* **2007**, *106*, 3040−3050.
(295) Yamada, K.; Henares, T. G.; Suzuki, K.; Citterio, D. Paper-Based Inkjet-Printed Microfluidic Analytical Devices. *Angew. Chem., Int. Ed.* **2015**, *54*, 5294−5310.
(296) Zhan, Z.; An, J.; Wei, Y.; Tran, V. T.; Du, H. Inkjet-Printed Optoelectronics. *Nanoscale* **2017**, *9*, 965−993.
(297) Jerónimo, P. C. A.; Araújo, A. N.; Conceição B. S. M. Montenegro, M. Optical Sensors and Biosensors Based on Sol−Gel Films. *Talanta* **2007**, *72*, 13−27.
(298) Li, Z.; Jang, M.; Askim, J. R.; Suslick, K. S. Identification of Accelerants, Fuels and Post-Combustion Residues Using a Colorimetric Sensor Array. *Analyst* **2015**, *140*, 5929−5935.
(299) LaFratta, C. N.; Walt, D. R. Very High Density Sensing Arrays. *Chem. Rev.* **2008**, *108*, 614−637.
(300) Cohen, L.; Walt, D. R. Single-Molecule Arrays for Protein and Nucleic Acid Analysis. *Annu. Rev. Anal. Chem.* **2017**, *10*, 345−363.
(301) Carrasco, S.; Benito-Pena, E.; Walt, D. R.; Moreno-Bondi, M. C. Fiber-Optic Array Using Molecularly Imprinted Microspheres for Antibiotic Analysis. *Chem. Sci.* **2015**, *6*, 3139−3147.
(302) Walt, D. R. Fiber Optic Array Biosensors. *BioTechniques* **2006**, *41*, 529−535.
(303) Walt, D. R. Bead-Based Fiber-Optic Arrays. *Science* **2000**, *287*, 451−452.
(304) Nie, S.; Benito-Peña, E.; Zhang, H.; Wu, Y.; Walt, D. R. Multiplexed Salivary Protein Profiling for Patients with Respiratory Diseases Using Fiber-Optic Bundles and Fluorescent Antibody-Based Microarrays. *Anal. Chem.* **2013**, *85*, 9272−9280.
(305) Epstein, J. R.; Ferguson, J. A.; Lee, K. H.; Walt, D. R. Combinatorial Decoding: An Approach for Universal DNA Array Fabrication. *J. Am. Chem. Soc.* **2003**, *125*, 13753−13759.
(306) Kuang, Y.; Walt, D. R. Monitoring "Promiscuous" Drug Effects on Single Cells of Multiple Cell Types. *Anal. Biochem.* **2005**, *345*, 320−325.
(307) Schubert, S. M.; Walter, S. R.; Manesse, M.; Walt, D. R. Protein Counting in Single Cancer Cells. *Anal. Chem.* **2016**, *88*, 2952−2957.
(308) Dinh, T. L.; Ngan, K. C.; Shoemaker, C. B.; Walt, D. R. Using Antigen−Antibody Binding Kinetic Parameters to Understand Single-Molecule Array Immunoassay Performance. *Anal. Chem.* **2016**, *88*, 11335−11339.
(309) Wu, D.; Katilius, E.; Olivas, E.; Dumont Milutinovic, M.; Walt, D. R. Incorporation of Slow Off-Rate Modified Aptamers Reagents in Single Molecule Array Assays for Cytokine Detection with Ultrahigh Sensitivity. *Anal. Chem.* **2016**, *88*, 8385−8389.
(310) Schubert, S. M.; Arendt, L. M.; Zhou, W.; Baig, S.; Walter, S. R.; Buchsbaum, R. J.; Kuperwasser, C.; Walt, D. R. Ultra-Sensitive Protein Detection Via Single Molecule Arrays Towards Early Stage Cancer Monitoring. *Sci. Rep.* **2015**, *5*, 11034.
(311) Li, Z.; Li, H.; LaGasse, M. K.; Suslick, K. S. Rapid Quantification of Trimethylamine. *Anal. Chem.* **2016**, *88*, 5615−5620.

DOI: 10.1021/acs.chemrev.8b00226
Chem. Rev. 2019, 119, 231−292

(312) Li, Z.; Suslick, K. S. Portable Optoelectronic Nose for Monitoring Meat Freshness. *ACS Sens.* **2016**, *1*, 1330−1335.
(313) Kawazu, M.; Ogura, Y. Application of Gradient-Index Fiber Arrays to Copying Machines. *Appl. Opt.* **1980**, *19*, 1105−1112.
(314) Ohta, J. *Smart CMOS Image Sensors and Applications*; Taylor & Francis: Boca Raton, FL, 2008.
(315) Li, Z.; Suslick, K. S. Ultrasonic Preparation of Porous Silica-Dye Microspheres: Sensors for Quantification of Urinary Trimethylamine N-Oxide. *ACS Appl. Mater. Interfaces* **2018**, *10*, 15820−15828.
(316) Alkasir, R. S. J.; Rossner, A.; Andreescu, S. Portable Colorimetric Paper-Based Biosensing Device for the Assessment of Bisphenol a in Indoor Dust. *Environ. Sci. Technol.* **2015**, *49*, 9889−9897.
(317) Nikkhoo, N.; Cumby, N.; Gulak, P. G.; Maxwell, K. L. Rapid Bacterial Detection Via an All-Electronic Cmos Biosensor. *PLoS One* **2016**, *11*, e0162438.
(318) Estevez, M. C.; Alvarez, M.; Lechuga, L. M. Integrated Optical Devices for Lab-on-a-Chip Biosensing Applications. *Laser & Photonics Reviews* **2012**, *6*, 463−487.
(319) Zhang, W.; Guo, S.; Pereira Carvalho, W. S.; Jiang, Y.; Serpe, M. J. Portable Point-of-Care Diagnostic Devices. *Anal. Methods* **2016**, *8*, 7847−7867.
(320) Vashist, S. K.; van Oordt, T.; Schneider, E. M.; Zengerle, R.; von Stetten, F.; Luong, J. H. T. A Smartphone-Based Colorimetric Reader for Bioanalytical Applications Using the Screen-Based Bottom Illumination Provided by Gadgets. *Biosens. Bioelectron.* **2015**, *67*, 248−255.
(321) Long, K. D.; Woodburn, E. V.; Le, H. M.; Shah, U. K.; Lumetta, S. S.; Cunningham, B. T. Multimode Smartphone Biosensing: The Transmission, Reflection, and Intensity Spectral (Tri)-Analyzer. *Lab Chip* **2017**, *17*, 3246.
(322) Roda, A.; Michelini, E.; Zangheri, M.; Di Fusco, M.; Calabria, D.; Simoni, P. Smartphone-Based Biosensors: A Critical Review and Perspectives. *TrAC, Trends Anal. Chem.* **2016**, *79*, 317−325.
(323) Zhang, D.; Liu, Q. Biosensors and Bioelectronics on Smartphone for Portable Biochemical Detection. *Biosens. Bioelectron.* **2016**, *75*, 273−284.
(324) Lopez-Ruiz, N.; Curto, V. F.; Erenas, M. M.; Benito-Lopez, F.; Diamond, D.; Palma, A. J.; Capitan-Vallvey, L. F. Smartphone-Based Simultaneous Ph and Nitrite Colorimetric Determination for Paper Microfluidic Devices. *Anal. Chem.* **2014**, *86*, 9554−9562.
(325) Vashist, S. K.; Mudanyali, O.; Schneider, E. M.; Zengerle, R.; Ozcan, A. Cellphone-Based Devices for Bioanalytical Sciences. *Anal. Bioanal. Chem.* **2014**, *406*, 3263−3277.
(326) Berg, B.; Cortazar, B.; Tseng, D.; Ozkan, H.; Feng, S.; Wei, Q.; Chan, R. Y.-L.; Burbano, J.; Farooqui, Q.; Lewinski, M.; et al. Cellphone-Based Hand-Held Microplate Reader for Point-of-Care Testing of Enzyme-Linked Immunosorbent Assays. *ACS Nano* **2015**, *9*, 7857−7866.
(327) Ballard, Z. S.; Shir, D.; Bhardwaj, A.; Bazargan, S.; Sathianathan, S.; Ozcan, A. Computational Sensing Using Low-Cost and Mobile Plasmonic Readers Designed by Machine Learning. *ACS Nano* **2017**, *11*, 2266−2274.
(328) Wei, Q.; Qi, H.; Luo, W.; Tseng, D.; Ki, S. J.; Wan, Z.; Göröcs, Z.; Bentolila, L. A.; Wu, T.-T.; Sun, R.; et al. Fluorescent Imaging of Single Nanoparticles and Viruses on a Smart Phone. *ACS Nano* **2013**, *7*, 9147−9155.
(329) Wei, Q.; Luo, W.; Chiang, S.; Kappel, T.; Mejia, C.; Tseng, D.; Chan, R. Y. L.; Yan, E.; Qi, H.; Shabbir, F.; et al. Imaging and Sizing of Single DNA Molecules on a Mobile Phone. *ACS Nano* **2014**, *8*, 12725−12733.
(330) Kühnemund, M.; Wei, Q.; Darai, E.; Wang, Y.; Hernández-Neuta, I.; Yang, Z.; Tseng, D.; Ahlford, A.; Mathot, L.; Sjöblom, T.; et al. *Nat. Commun.* **2017**, *8*, 13913.
(331) Kong, J. E.; Wei, Q.; Tseng, D.; Zhang, J.; Pan, E.; Lewinski, M.; Garner, O. B.; Ozcan, A.; Di Carlo, D. Highly Stable and Sensitive Nucleic Acid Amplification and Cell-Phone-Based Readout. *ACS Nano* **2017**, *11*, 2934−2943.
(332) Koydemir, H. C.; Gorocs, Z.; Tseng, D.; Cortazar, B.; Feng, S.; Chan, R. Y. L.; Burbano, J.; McLeod, E.; Ozcan, A. Rapid Imaging, Detection and Quantification of Giardia Lamblia Cysts Using Mobile-Phone Based Fluorescent Microscopy and Machine Learning. *Lab Chip* **2015**, *15*, 1284−1293.
(333) Ludwig, S. K. J.; Tokarski, C.; Lang, S. N.; van Ginkel, L. A.; Zhu, H.; Ozcan, A.; Nielen, M. W. F. Calling Biomarkers in Milk Using a Protein Microarray on Your Smartphone. *PLoS One* **2015**, *10*, e0134360.
(334) Feng, S.; Tseng, D.; Di Carlo, D.; Garner, O. B.; Ozcan, A. High-Throughput and Automated Diagnosis of Antimicrobial Resistance Using a Cost-Effective Cellphone-Based Micro-Plate Reader. *Sci. Rep.* **2016**, *6*, 39203.
(335) Suslick, K. S.; Bailey, D. P.; Ingison, C. K.; Janzen, M.; Kosal, M. E.; McNamara, W. B., III; Rakow, N. A.; Sen, A.; Weaver, J. J.; Wilson, J. B.; et al. Seeing Smells: Development of an Optoelectronic Nose. *Quim. Nova* **2007**, *30*, 677−681.
(336) Haswell, S. J. *Practical Guide to Chemometrics*; CRC Press: 1992.
(337) Donoho, D. L. High-Dimensional Data Analysis: The Curses and Blessings of Dimensionality. Presented at Mathematical Challenges of the 21st Century; 2000; pp 1−32.
(338) Johnson, R. A.; Wichern, D. W. *Applied Multivariate Statistical Analysis*, 6th ed.; Prentice Hall: Upper Saddle River, NJ, 2007.
(339) Hair, J. F.; Black, B.; Babin, B.; Anderson, R. E.; Tatham, R. L. *Multivariate Data Analysis*, 6th ed.; Prentice Hall: Upper Saddle River, NJ, 2005.
(340) Massart, D. L.; Kaufman, L. *The Interpretation of Analytical Chemical Data by the Use of Cluster Analysis*; John Wiley & Sons: New York, 1983.
(341) Stewart, S.; Ivy, M. A.; Anslyn, E. V. The Use of Principal Component Analysis and Discriminant Analysis in Differential Sensing Routines. *Chem. Soc. Rev.* **2014**, *43*, 70−84.
(342) Musto, C. J.; Lim, S. H.; Suslick, K. S. Colorimetric Detection and Identification of Natural and Artificial Sweeteners. *Anal. Chem.* **2009**, *81*, 6526−6533.
(343) De, M.; Rana, S.; Akpinar, H.; Miranda, O. R.; Arvizo, R. R.; Bunz, U. H. F.; Rotello, V. M. Sensing of Proteins in Human Serum Using Conjugates of Nanoparticles and Green Fluorescent Protein. *Nat. Chem.* **2009**, *1*, 461−465.
(344) Zhong, W.; Suslick, K. S. Matrix Discriminant Analysis with Application to Colorimetric Sensor Array Data. *Technometrics* **2015**, *57*, 524−534.
(345) Zhong, W. X.; Xing, X.; Suslick, K. Tensor Sufficient Dimension Reduction. *Wiley Interdisciplinary Reviews-Computational Statistics* **2015**, *7*, 178−184.
(346) Li, B.; Kim, M. K.; Altman, N. On Dimension Folding of Matrix- or Array-Valued Statistical Objects. *Ann. Statist.* **2010**, *38*, 1094−1121.
(347) Yan, S. C.; Xu, D.; Yang, Q.; Zhang, L.; Tang, X. O.; Zhang, H. J. Discriminant Analysis with Tensor Representation. In *2005 IEEE Computer Society Conference on Computer Vision and Pattern Recognition, Proceedings*; Schmid, C., Soatto, S., Tomasi, C., Eds.; IEEE: 2005; Vol. *1*, pp 526−532. DOI: 10.1109/CVPR.2005.131.
(348) Chang, C.-C.; Lin, C.-J. Libsvm: A Library for Support Vector Machines. *ACM Trans. Intell. Syst. Technol.* **2011**, *2*, 1−27.
(349) Burns, J. A.; Whitesides, G. M. Feed-Forward Neural Networks in Chemistry: Mathematical Systems for Classification and Pattern Recognition. *Chem. Rev.* **1993**, *93*, 2583−2601.
(350) Peng, P.; Zhao, X.; Pan, X.; Ye, W. Gas Classification Using Deep Convolutional Neural Networks. *Sensors* **2018**, *18*, 157.
(351) Gardner, M. W.; Dorling, S. R. Artificial Neural Networks (the Multilayer Perceptron)—a Review of Applications in the Atmospheric Sciences. *Atmos. Environ.* **1998**, *32*, 2627−2636.
(352) Hornik, K.; Stinchcombe, M.; White, H. Multilayer Feedforward Networks Are Universal Approximators. *Neural Networks* **1989**, *2*, 359−366.
(353) Krizhevsky, A.; Sutskever, I.; Hinton, G. E. In *Proceedings of the 25th International Conference on Neural Information Processing Systems*; Curran Associates Inc.: Lake Tahoe, NV, 2012; Vol. *1*, pp 1097−1105.
(354) Rosenblatt, F. The Perceptron: A Probabilistic Model for Information Storage and Organization in the Brain. *Psychological Review* **1958**, *65*, 386−408.

DOI: 10.1021/acs.chemrev.8b00226
Chem. Rev. 2019, 119, 231−292

(355) Szegedy, C.; Wei, L.; Yangqing, J.; Sermanet, P.; Reed, S.; Anguelov, D.; Erhan, D.; Vanhoucke, V.; Rabinovich, A. In *2015 IEEE Conference on Computer Vision and Pattern Recognition (CVPR)*; IEEE: 2015; pp 1−9.
(356) Soga, T.; Jimbo, Y.; Suzuki, K.; Citterio, D. Inkjet-Printed Paper-Based Colorimetric Sensor Array for the Discrimination of Volatile Primary Amines. *Anal. Chem.* **2013**, *85*, 8973−8978.
(357) Feng, L.; Musto, C. J.; Suslick, K. S. A Simple and Highly Sensitive Colorimetric Detection Method for Gaseous Formaldehyde. *J. Am. Chem. Soc.* **2010**, *132*, 4046−4047.
(358) Byrnes, M. E.; King, D. A.; Tierno, P. M., Jr. *Nuclear, Chemical, and Biological Terrorism: Emergency Response and Public Protection*; CRC Press: 2003.
(359) Armour, S. J. *International Task Force 40: Toxic Industrial Chemicals (TICs)-Operational and Medical Concerns*; U.S. Government Printing Office: Washington, DC, 2001.
(360) Hoang, A. T.; Cho, Y. B.; Kim, Y. S. A Strip Array of Colorimetric Sensors for Visualizing a Concentration Level of Gaseous Analytes with Basicity. *Sens. Actuators, B* **2017**, *251*, 1089−1095.
(361) Sen, A.; Albarella, J. D.; Carey, J. R.; Kim, P.; McNamara, W. B., III. Low-Cost Colorimetric Sensor for the Quantitative Detection of Gaseous Hydrogen Sulfide. *Sens. Actuators, B* **2008**, *134*, 234−237.
(362) Kim, P.; Albarella, J. D.; Carey, J. R.; Placek, M. J.; Sen, A.; Wittrig, A. E.; McNamara, W. B., III. Towards the Development of a Portable Device for the Monitoring of Gaseous Toxic Industrial Chemicals Based on a Chemical Sensor Array. *Sens. Actuators, B* **2008**, *134*, 307−312.
(363) Koo, C.-K.; Samain, F.; Dai, N.; Kool, E. T. DNA Polyfluorophores as Highly Diverse Chemosensors of Toxic Gases. *Chem. Sci.* **2011**, *2*, 1910−1917.
(364) Feng, L.; Li, X.; Li, H.; Yang, W.; Chen, L.; Guan, Y. Enhancement of Sensitivity of Paper-Based Sensor Array for the Identification of Heavy-Metal Ions. *Anal. Chim. Acta* **2013**, *780*, 74−80.
(365) Sener, G.; Uzun, L.; Denizli, A. Colorimetric Sensor Array Based on Gold Nanoparticles and Amino Acids for Identification of Toxic Metal Ions in Water. *ACS Appl. Mater. Interfaces* **2014**, *6*, 18395−18400.
(366) Park, S. H.; Maruniak, A.; Kim, J.; Yi, G.-R.; Lim, S. H. Disposable Microfluidic Sensor Arrays for Discrimination of Antioxidants. *Talanta* **2016**, *153*, 163−169.
(367) Qian, S.; Lin, H. Colorimetric Sensor Array for Detection and Identification of Organophosphorus and Carbamate Pesticides. *Anal. Chem.* **2015**, *87*, 5395−5400.
(368) Corradini, R.; Paganuzzi, C.; Marchelli, R.; Pagliari, S.; Sforza, S.; Dossena, A.; Galaverna, G.; Duchateau, A. Fast Parallel Enantiomeric Analysis of Unmodified Amino Acids by Sensing with Fluorescent [Small Beta]-Cyclodextrins. *J. Mater. Chem.* **2005**, *15*, 2741−2746.
(369) Larkey, N. E.; Almlie, C. K.; Tran, V.; Egan, M.; Burrows, S. M. Detection of Mirna Using a Double-Strand Displacement Biosensor with a Self-Complementary Fluorescent Reporter. *Anal. Chem.* **2014**, *86*, 1853−1863.
(370) Mahmoudi, M.; Lohse, S. E.; Murphy, C. J.; Suslick, K. S. Identification of Nanoparticles with a Colorimetric Sensor Array. *ACS Sens.* **2016**, *1*, 17−21.
(371) Meher, N.; Iyer, P. K. Pendant Chain Engineering to Fine-Tune the Nanomorphologies and Solid State Luminescence of Naphthalimide Aieegens: Application to Phenolic Nitro-Explosive Detection in Water. *Nanoscale* **2017**, *9*, 7674−7685.
(372) Yang, J.; Wang, Z.; Hu, K.; Li, Y.; Feng, J.; Shi, J.; Gu, J. Rapid and Specific Aqueous-Phase Detection of Nitroaromatic Explosives with Inherent Porphyrin Recognition Sites in Metal−Organic Frameworks. *ACS Appl. Mater. Interfaces* **2015**, *7*, 11956−11964.
(373) Yao, R.-X.; Cui, X.; Jia, X.-X.; Zhang, F.-Q.; Zhang, X.-M. A Luminescent Zinc(Ii) Metal−Organic Framework (Mof) with Conjugated Π-Electron Ligand for High Iodine Capture and Nitro-Explosive Detection. *Inorg. Chem.* **2016**, *55*, 9270−9275.
(374) Krausa, M. In *Vapour and Trace Detection of Explosives for Anti-Terrorism Purposes*; Springer: New York, 2004.
(375) Zhang, K.; Zhou, H.; Mei, Q.; Wang, S.; Guan, G.; Liu, R.; Zhang, J.; Zhang, Z. Instant Visual Detection of Trinitrotoluene Particulates on Various Surfaces by Ratiometric Fluorescence of Dual-Emission Quantum Dots Hybrid. *J. Am. Chem. Soc.* **2011**, *133*, 8424−8427.
(376) Mosca, L.; Karimi Behzad, S.; Anzenbacher, P. Small-Molecule Turn-on Fluorescent Probes for Rdx. *J. Am. Chem. Soc.* **2015**, *137*, 7967−7969.
(377) Gopalakrishnan, D.; Dichtel, W. R. Direct Detection of Rdx Vapor Using a Conjugated Polymer Network. *J. Am. Chem. Soc.* **2013**, *135*, 8357−8362.
(378) Kangas, M. J.; Burks, R. M.; Atwater, J.; Lukowicz, R. M.; Williams, P.; Holmes, A. E. Colorimetric Sensor Arrays for the Detection and Identification of Chemical Weapons and Explosives. *Crit. Rev. Anal. Chem.* **2017**, *47*, 138−153.
(379) Peveler, W. J.; Roldan, A.; Hollingsworth, N.; Porter, M. J.; Parkin, I. P. Multichannel Detection and Differentiation of Explosives with a Quantum Dot Array. *ACS Nano* **2016**, *10*, 1139−1146.
(380) Laine, D. F.; Roske, C. W.; Cheng, I. F. Electrochemical Detection of Triacetone Triperoxide Employing the Electrocatalytic Reaction of Iron(Ii/Iii)-Ethylenediaminetetraacetate and Hydrogen Peroxide. *Anal. Chim. Acta* **2008**, *608*, 56−60.
(381) Dubnikova, F.; Kosloff, R.; Zeiri, Y.; Karpas, Z. Novel Approach to the Detection of Triacetone Triperoxide (Tatp): Its Structure and Its Complexes with Ions. *J. Phys. Chem. A* **2002**, *106*, 4951−4956.
(382) Lopez-Marzo, A. M.; Merkoci, A. Paper-Based Sensors and Assays: A Success of the Engineering Design and the Convergence of Knowledge Areas. *Lab Chip* **2016**, *16*, 3150−3176.
(383) Almeida, M. I. G. S.; Jayawardane, B. M.; Kolev, S. D.; McKelvie, I. D. Developments of Microfluidic Paper-Based Analytical Devices (Mpads) for Water Analysis: A Review. *Talanta* **2018**, *177*, 176−190.
(384) Cate, D. M.; Adkins, J. A.; Mettakoonpitak, J.; Henry, C. S. Recent Developments in Paper-Based Microfluidic Devices. *Anal. Chem.* **2015**, *87*, 19−41.
(385) Yang, Y.; Noviana, E.; Nguyen, M. P.; Geiss, B. J.; Dandy, D. S.; Henry, C. S. Paper-Based Microfluidic Devices: Emerging Themes and Applications. *Anal. Chem.* **2017**, *89*, 71−91.
(386) Peters, K. L.; Corbin, I.; Kaufman, L. M.; Zreibe, K.; Blanes, L.; McCord, B. R. Simultaneous Colorimetric Detection of Improvised Explosive Compounds Using Microfluidic Paper-Based Analytical Devices ([Small Mu]Pads). *Anal. Methods* **2015**, *7*, 63−70.
(387) Berliner, A.; Lee, M.-G.; Zhang, Y.; Park, S. H.; Martino, R.; Rhodes, P. A.; Yi, G.-R.; Lim, S. H. A Patterned Colorimetric Sensor Array for Rapid Detection of Tnt at Ppt Level. *RSC Adv.* **2014**, *4*, 10672−10675.
(388) *Hyphenated and Alternative Methods of Detection in Chromatography*; Shalliker, R. A., Ed.; CRC Press: Boca Raton, FL, 2012.
(389) Rankin, J. M.; Suslick, K. S. The Development of a Disposable Gas Chromatography Microcolumn. *Chem. Commun.* **2015**, *51*, 8920−8923.
(390) Li, Z.; Suslick, K. S. A Hand-Held Optoelectronic Nose for the Identification of Liquors. *ACS Sens.* **2018**, *3*, 121−127.
(391) Han, J.; Ma, C.; Wang, B.; Bender, M.; Bojanowski, M.; Hergert, M.; Seehafer, K.; Herrmann, A.; Bunz, U. H. F. A Hypothesis-Free Sensor Array Discriminates Whiskies for Brand, Age, and Taste. *Chem.* **2017**, *2*, 817−824.
(392) Jia-wei, L.; Chang-jun, H.; Dan-qun, H.; Mei, Y.; Su-yi, Z.; Yi, M.; Yang, L. A Minimalist Chinese Liquor Identification System Based on a Colorimetric Sensor Array with Multiple Applications. *Anal. Methods* **2017**, *9*, 141−148.
(393) Rico-Yuste, A.; González-Vallejo, V.; Benito-Peña, E.; de las Casas Engel, T.; Orellana, G.; Moreno-Bondi, M. C. Furfural Determination with Disposable Polymer Films and Smartphone-Based Colorimetry for Beer Freshness Assessment. *Anal. Chem.* **2016**, *88*, 3959−3966.
(394) Illy, E. The Complexity of Coffee. *Sci. Am.* **2002**, *286*, 86−91.
(395) Clarke, R. J.; Vitzthum, O. G. *Coffee: Recent Developments*; Blackwell Science: Oxford, 2001.

DOI: 10.1021/acs.chemrev.8b00226
Chem. Rev. 2019, 119, 231−292

(396) Flament, I. *Coffee Flavor Chemistry*; John Wiley & Sons: Chichester, U.K., 2002.
(397) Suslick, B. A.; Feng, L.; Suslick, K. S. Discrimination of Complex Mixtures by a Colorimetric Sensor Array: Coffee Aromas. *Anal. Chem.* **2010**, *82*, 2067−2073.
(398) Xu, W.; Bai, J.; Peng, J.; Samanta, A.; Divyanshu; Chang, Y.-T. Milk Quality Control: Instant and Quantitative Milk Fat Determination with a Bodipy Sensor-Based Fluorescence Detector. *Chem. Commun.* **2014**, *50*, 10398−10401.
(399) Chen, Y.; Fu, G.; Zilberman, Y.; Ruan, W.; Ameri, S. K.; Zhang, Y. S.; Miller, E.; Sonkusale, S. R. Low Cost Smart Phone Diagnostics for Food Using Paper-Based Colorimetric Sensor Arrays. *Food Control* **2017**, *82*, 227−232.
(400) Salinas, Y.; Ros-Lis, J. V.; Vivancos, J.-L.; Martinez-Manez, R.; Marcos, M. D.; Aucejo, S.; Herranz, N.; Lorente, I. Monitoring of Chicken Meat Freshness by Means of a Colorimetric Sensor Array. *Analyst* **2012**, *137*, 3635−3643.
(401) Lim, S. H.; Musto, C. J.; Park, E.; Zhong, W.; Suslick, K. S. A Colorimetric Sensor Array for Detection and Identification of Sugars. *Org. Lett.* **2008**, *10*, 4405−4408.
(402) Musto, C. J.; Suslick, K. S. Differential Sensing of Sugars by Colorimetric Arrays. *Curr. Opin. Chem. Biol.* **2010**, *14*, 758−766.
(403) Adams, M. M.; Anslyn, E. V. Differential Sensing Using Proteins: Exploiting the Cross-Reactivity of Serum Albumin to Pattern Individual Terpenes and Terpenes in Perfume. *J. Am. Chem. Soc.* **2009**, *131*, 17068−17069.
(404) Ivy, M. A.; Gallagher, L. T.; Ellington, A. D.; Anslyn, E. V. Exploration of Plasticizer and Plastic Explosive Detection and Differentiation with Serum Albumin Cross-Reactive Arrays. *Chem. Sci.* **2012**, *3*, 1773−1779.
(405) Umali, A. P.; LeBoeuf, S. E.; Newberry, R. W.; Kim, S.; Tran, L.; Rome, W. A.; Tian, T.; Taing, D.; Hong, J.; Kwan, M.; et al. Discrimination of Flavonoids and Red Wine Varietals by Arrays of Differential Peptidic Sensors. *Chem. Sci.* **2011**, *2*, 439−445.
(406) Gallagher, L. T.; Heo, J. S.; Lopez, M. A.; Ray, B. M.; Xiao, J.; Umali, A. P.; Zhang, A.; Dharmarajan, S.; Heymann, H.; Anslyn, E. V. Pattern-Based Discrimination of Organic Acids and Red Wine Varietals by Arrays of Synthetic Receptors. *Supramol. Chem.* **2012**, *24*, 143−148.
(407) Hou, C.; Dong, J.; Zhang, G.; Lei, Y.; Yang, M.; Zhang, Y.; Liu, Z.; Zhang, S.; Huo, D. Colorimetric Artificial Tongue for Protein Identification. *Biosens. Bioelectron.* **2011**, *26*, 3981−3986.
(408) Wang, F.; Lu, Y.; Yang, J.; Chen, Y.; Jing, W.; He, L.; Liu, Y. A Smartphone Readable Colorimetric Sensing Platform for Rapid Multiple Protein Detection. *Analyst* **2017**, *142*, 3177−3182.
(409) Li, D.; Dong, Y.; Li, B.; Wu, Y.; Wang, K.; Zhang, S. Colorimetric Sensor Array with Unmodified Noble Metal Nanoparticles for Naked-Eye Detection of Proteins and Bacteria. *Analyst* **2015**, *140*, 7672−7677.
(410) Li, B.; Li, X.; Dong, Y.; Wang, B.; Li, D.; Shi, Y.; Wu, Y. Colorimetric Sensor Array Based on Gold Nanoparticles with Diverse Surface Charges for Microorganisms Identification. *Anal. Chem.* **2017**, *89*, 10639−10643.
(411) Wang, K.; Dong, Y.; Li, B.; Li, D.; Zhang, S.; Wu, Y. Differentiation of Proteins and Cancer Cells Using Metal Oxide and Metal Nanoparticles-Quantum Dots Sensor Array. *Sens. Actuators, B* **2017**, *250*, 69−75.
(412) Miranda, O. R.; Creran, B.; Rotello, V. M. Array-Based Sensing with Nanoparticles: 'Chemical Noses' for Sensing Biomolecules and Cell Surfaces. *Curr. Opin. Chem. Biol.* **2010**, *14*, 728−736.
(413) Bunz, U. H. F.; Rotello, V. M. Gold Nanoparticle−Fluorophore Complexes: Sensitive and Discerning "Noses" for Biosystems Sensing. *Angew. Chem., Int. Ed.* **2010**, *49*, 3268−3279.
(414) Mout, R.; Moyano, D. F.; Rana, S.; Rotello, V. M. Surface Functionalization of Nanoparticles for Nanomedicine. *Chem. Soc. Rev.* **2012**, *41*, 2539−2544.
(415) Saha, K.; Agasti, S. S.; Kim, C.; Li, X.; Rotello, V. M. Gold Nanoparticles in Chemical and Biological Sensing. *Chem. Rev.* **2012**, *112*, 2739−2779.
(416) Moyano, D. F.; Rana, S.; Bunz, U. H. F.; Rotello, V. M. Gold Nanoparticle-Polymer/Biopolymer Complexes for Protein Sensing. *Faraday Discuss.* **2011**, *152*, 33−42.
(417) Li, X.; Wen, F.; Creran, B.; Jeong, Y.; Zhang, X.; Rotello, V. M. Colorimetric Protein Sensing Using Catalytically Amplified Sensor Arrays. *Small* **2012**, *8*, 3589−3592.
(418) You, C.-C.; Miranda, O. R.; Gider, B.; Ghosh, P. S.; Kim, I.-B.; Erdogan, B.; Krovi, S. A.; Bunz, U. H. F.; Rotello, V. M. Detection and Identification of Proteins Using Nanoparticle-Fluorescent Polymer 'Chemical Nose' Sensors. *Nat. Nanotechnol.* **2007**, *2*, 318−323.
(419) Creran, B.; Bunz, U. H. F.; Rotello, V. M. Polymer − Nanoparticle Assemblies for Array Based Sensing. *Curr. Org. Chem.* **2015**, *109*, 1054−1062.
(420) Miranda, O. R.; Chen, H.-T.; You, C.-C.; Mortenson, D. E.; Yang, X.-C.; Bunz, U. H. F.; Rotello, V. M. Enzyme-Amplified Array Sensing of Proteins in Solution and in Biofluids. *J. Am. Chem. Soc.* **2010**, *132*, 5285−5289.
(421) Rana, S.; Singla, A. K.; Bajaj, A.; Elci, S. G.; Miranda, O. R.; Mout, R.; Yan, B.; Jirik, F. R.; Rotello, V. M. Array-Based Sensing of Metastatic Cells and Tissues Using Nanoparticle−Fluorescent Protein Conjugates. *ACS Nano* **2012**, *6*, 8233−8240.
(422) Stewart, S.; Syrett, A.; Pothukuchy, A.; Bhadra, S.; Ellington, A.; Anslyn, E. Identifying Protein Variants with Cross-Reactive Aptamer Arrays. *ChemBioChem* **2011**, *12*, 2021−2024.
(423) Sun, W.; Guo, S.; Hu, C.; Fan, J.; Peng, X. Recent Development of Chemosensors Based on Cyanine Platforms. *Chem. Rev.* **2016**, *116*, 7768−7817.
(424) Ashton, T. D.; Jolliffe, K. A.; Pfeffer, F. M. Luminescent Probes for the Bioimaging of Small Anionic Species in Vitro and in Vivo. *Chem. Soc. Rev.* **2015**, *44*, 4547−4595.
(425) Wu, P.; Hou, X.; Xu, J.-J.; Chen, H.-Y. Ratiometric Fluorescence, Electrochemiluminescence, and Photoelectrochemical Chemo/Biosensing Based on Semiconductor Quantum Dots. *Nanoscale* **2016**, *8*, 8427−8442.
(426) Marquês, J. T.; de Almeida, R. F. M. Application of Ratiometric Measurements and Microplate Fluorimetry to Protein Denaturation: An Experiment for Analytical and Biochemistry Students. *J. Chem. Educ.* **2013**, *90*, 1522−1527.
(427) Bianchi-Smiraglia, A.; Rana, M. S.; Foley, C. E.; Paul, L. M.; Lipchick, B. C.; Moparthy, S.; Moparthy, K.; Fink, E. E.; Bagati, A.; Hurley, E.; et al. Internally Ratiometric Fluorescent Sensors for Evaluation of Intracellular Gtp Levels and Distribution. *Nat. Methods* **2017**, *14*, 1003.
(428) Han, J.; Burgess, K. Fluorescent Indicators for Intracellular Ph. *Chem. Rev.* **2010**, *110*, 2709−2728.
(429) Wan, Q.; Chen, S.; Shi, W.; Li, L.; Ma, H. Lysosomal Ph Rise During Heat Shock Monitored by a Lysosome-Targeting near-Infrared Ratiometric Fluorescent Probe. *Angew. Chem., Int. Ed.* **2014**, *53*, 10916−10920.
(430) Bao, Y.; De Keersmaecker, H.; Corneillie, S.; Yu, F.; Mizuno, H.; Zhang, G.; Hofkens, J.; Mendrek, B.; Kowalczuk, A.; Smet, M. Tunable Ratiometric Fluorescence Sensing of Intracellular Ph by Aggregation-Induced Emission-Active Hyperbranched Polymer Nanoparticles. *Chem. Mater.* **2015**, *27*, 3450−3455.
(431) Wang, X. D.; Stolwijk, J. A.; Lang, T.; Sperber, M.; Meier, R. J.; Wegener, J.; Wolfbeis, O. S. Ultra-Small, Highly Stable, and Sensitive Dual Nanosensors for Imaging Intracellular Oxygen and Ph in Cytosol. *J. Am. Chem. Soc.* **2012**, *134*, 17011−17014.
(432) Pan, W.; Wang, H.; Yang, L.; Yu, Z.; Li, N.; Tang, B. Ratiometric Fluorescence Nanoprobes for Subcellular Ph Imaging with a Single-Wavelength Excitation in Living Cells. *Anal. Chem.* **2016**, *88*, 6743−6748.
(433) Huang, J.; Ying, L.; Yang, X.; Yang, Y.; Quan, K.; Wang, H.; Xie, N.; Ou, M.; Zhou, Q.; Wang, K. Ratiometric Fluorescent Sensing of Ph Values in Living Cells by Dual-Fluorophore-Labeled I-Motif Nanoprobes. *Anal. Chem.* **2015**, *87*, 8724−8731.
(434) Näreoja, T.; Deguchi, T.; Christ, S.; Peltomaa, R.; Prabhakar, N.; Fazeli, E.; Perälä, N.; Rosenholm, J. M.; Arppe, R.; Soukka, T.; et al. Ratiometric Sensing and Imaging of Intracellular Ph Using Poly-

DOI: 10.1021/acs.chemrev.8b00226
Chem. Rev. 2019, 119, 231−292

ethylenimine-Coated Photon Upconversion Nanoprobes. *Anal. Chem.* **2017**, *89*, 1501−1508.
(435) Kruss, S.; Salem, D. P.; Vukovic, L.; Lima, B.; Vander Ende, E.; Boyden, E. S.; Strano, M. S. High-Resolution Imaging of Cellular Dopamine Efflux Using a Fluorescent Nanosensor Array. *Proc. Natl. Acad. Sci. U. S. A.* **2017**, *114*, 1789−1794.
(436) Mahmoudi, M.; Shokrgozar, M. A.; Behzadi, S. Slight Temperature Changes Affect Protein Affinity and Cellular Uptake/Toxicity of Nanoparticles. *Nanoscale* **2013**, *5*, 3240−3244.
(437) Zhang, A.; Guan, Y.; Xu, L. X. Theoretical Study on Temperature Dependence of Cellular Uptake of Qds Nanoparticles. *J. Biomech. Eng.* **2011**, *133*, 124502.
(438) Conti, B.; Hansen, M. A Cool Way to Live Long. *Cell* **2013**, *152*, 671−672.
(439) Homma, M.; Takei, Y.; Murata, A.; Inoue, T.; Takeoka, S. A Ratiometric Fluorescent Molecular Probe for Visualization of Mitochondrial Temperature in Living Cells. *Chem. Commun.* **2015**, *51*, 6194−6197.
(440) Han, X.; Song, X.; Yu, F.; Chen, L. A Ratiometric Fluorescent Probe for Imaging and Quantifying Anti-Apoptotic Effects of Gsh under Temperature Stress. *Chem. Sci.* **2017**, *8*, 6991−7002.
(441) Cui, L.; Zhong, Y.; Zhu, W.; Xu, Y.; Du, Q.; Wang, X.; Qian, X.; Xiao, Y. A New Prodrug-Derived Ratiometric Fluorescent Probe for Hypoxia: High Selectivity of Nitroreductase and Imaging in Tumor Cell. *Org. Lett.* **2011**, *13*, 928−931.
(442) Luo, S.; Zou, R.; Wu, J.; Landry, M. P. A Probe for the Detection of Hypoxic Cancer Cells. *ACS Sens.* **2017**, *2*, 1139−1145.
(443) Zhang, J.; Liu, H.-W.; Hu, X.-X.; Li, J.; Liang, L.-H.; Zhang, X.-B.; Tan, W. Efficient Two-Photon Fluorescent Probe for Nitroreductase Detection and Hypoxia Imaging in Tumor Cells and Tissues. *Anal. Chem.* **2015**, *87*, 11832−11839.
(444) Li, Y.; Sun, Y.; Li, J.; Su, Q.; Yuan, W.; Dai, Y.; Han, C.; Wang, Q.; Feng, W.; Li, F. Ultrasensitive near-Infrared Fluorescence-Enhanced Probe for in Vivo Nitroreductase Imaging. *J. Am. Chem. Soc.* **2015**, *137*, 6407−6416.
(445) Woodford, N.; Livermore, D. M. Infections Caused by Gram-Positive Bacteria: A Review of the Global Challenge. *J. Infect.* **2009**, *59*, S4−S16.
(446) Peleg, A. Y.; Hooper, D. C. Hospital-Acquired Infections Due to Gram-Negative Bacteria. *N. Engl. J. Med.* **2010**, *362*, 1804−1813.
(447) Riedel, S.; Carroll, K. C. Blood Cultures: Key Elements for Best Practices and Future Directions. *J. Infect. Chemother.* **2010**, *16*, 301−316.
(448) Capita, R.; Alonso-Calleja, C. Antibiotic-Resistant Bacteria: A Challenge for the Food Industry. *Crit. Rev. Food Sci. Nutr.* **2013**, *53*, 11−48.
(449) Varadi, L.; Luo, J. L.; Hibbs, D. E.; Perry, J. D.; Anderson, R. J.; Orenga, S.; Groundwater, P. W. Methods for the Detection and Identification of Pathogenic Bacteria: Past, Present, and Future. *Chem. Soc. Rev.* **2017**, *46*, 4818−4832.
(450) Sauer, S.; Kliem, M. Mass Spectrometry Tools for the Classification and Identification of Bacteria. *Nat. Rev. Microbiol.* **2010**, *8*, 74.
(451) Pechorsky, A.; Nitzan, Y.; Lazarovitch, T. Identification of Pathogenic Bacteria in Blood Cultures: Comparison between Conventional and Pcr Methods. *J. Microbiol. Methods* **2009**, *78*, 325−330.
(452) Karasinski, J.; Andreescu, S.; Sadik, O. A.; Lavine, B.; Vora, M. N. Multiarray Sensors with Pattern Recognition for the Detection, Classification, and Differentiation of Bacteria at Subspecies and Strain Levels. *Anal. Chem.* **2005**, *77*, 7941−7949.
(453) Hotel, O.; Poli, J.-P.; Mer-Calfati, C.; Scorsone, E.; Saada, S. A Review of Algorithms for Saw Sensors E-Nose Based Volatile Compound Identification. *Sens. Actuators, B* **2018**, *255*, 2472−2482.
(454) Heo, J.; Hua, S. Z. An Overview of Recent Strategies in Pathogen Sensing. *Sensors* **2009**, *9*, 4483−4502.
(455) Mortari, A.; Lorenzelli, L. Recent Sensing Technologies for Pathogen Detection in Milk: A Review. *Biosens. Bioelectron.* **2014**, *60*, 8−21.
(456) Zulkifli, S. N.; Rahim, H. A.; Lau, W.-J. Detection of Contaminants in Water Supply: A Review on State-of-the-Art Monitoring Technologies and Their Applications. *Sens. Actuators, B* **2018**, *255*, 2657−2689.
(457) Carey, J. R.; Suslick, K. S.; Hulkower, K. I.; Imlay, J. A.; Imlay, K. R. C.; Ingison, C. K.; Ponder, J. B.; Sen, A.; Wittrig, A. E. Rapid Identification of Bacteria with a Disposable Colorimetric Sensing Array. *J. Am. Chem. Soc.* **2011**, *133*, 7571−7576.
(458) Lonsdale, C. L.; Taba, B.; Queralto, N.; Lukaszewski, R. A.; Martino, R. A.; Rhodes, P. A.; Lim, S. H. The Use of Colorimetric Sensor Arrays to Discriminate between Pathogenic Bacteria. *PLoS One* **2013**, *8*, e62726.
(459) Lim, S. H.; Mix, S.; Xu, Z.; Taba, B.; Budvytiene, I.; Berliner, A. N.; Queralto, N.; Churi, Y. S.; Huang, R. S.; Eiden, M.; et al. Colorimetric Sensor Array Allows Fast Detection and Simultaneous Identification of Sepsis-Causing Bacteria in Spiked Blood Culture. *J. Clin. Microbiol.* **2014**, *52*, 592−598.
(460) Lim, S. H.; Mix, S.; Anikst, V.; Budvytiene, I.; Eiden, M.; Churi, Y.; Queralto, N.; Berliner, A.; Martino, R. A.; Rhodes, P. A.; et al. Bacterial Culture Detection and Identification in Blood Agar Plates with an Optoelectronic Nose. *Analyst* **2016**, *141*, 918−925.
(461) Lim, S. H.; Mix, S.; Xu, Z. Y.; Taba, B.; Budvytiene, I.; Berliner, A. N.; Queralto, N.; Churi, Y. S.; Huang, R. S.; Eiden, M.; et al. Colorimetric Sensor Array Allows Fast Detection and Simultaneous Identification of Sepsis-Causing Bacteria in Spiked Blood Culture. *J. Clin. Microbiol.* **2014**, *52*, 592−598.
(462) Lim, S. H.; Martino, R.; Anikst, V.; Xu, Z. Y.; Mix, S.; Benjamin, R.; Schub, H.; Eiden, M.; Rhodes, P. A.; Banaei, N. Rapid Diagnosis of Tuberculosis from Analysis of Urine Volatile Organic Compounds. *ACS Sens.* **2016**, *1*, 852−856.
(463) Phillips, R. L.; Miranda, O. R.; You, C.-C.; Rotello, V. M.; Bunz, U. H. F. Rapid and Efficient Identification of Bacteria Using Gold-Nanoparticle−Poly(Para-Phenyleneethynylene) Constructs. *Angew. Chem., Int. Ed.* **2008**, *47*, 2590−2594.
(464) Han, J.; Cheng, H.; Wang, B.; Braun, M. S.; Fan, X.; Bender, M.; Huang, W.; Domhan, C.; Mier, W.; Lindner, T.; et al. A Polymer/Peptide Complex-Based Sensor Array That Discriminates Bacteria in Urine. *Angew. Chem., Int. Ed.* **2017**, *56*, 15246−15251.
(465) Li, X.; Kong, H.; Mout, R.; Saha, K.; Moyano, D. F.; Robinson, S. M.; Rana, S.; Zhang, X.; Riley, M. A.; Rotello, V. M. Rapid Identification of Bacterial Biofilms and Biofilm Wound Models Using a Multichannel Nanosensor. *ACS Nano* **2014**, *8*, 12014−12019.
(466) Manesse, M.; Phillips, A. F.; LaFratta, C. N.; Palacios, M. A.; Hayman, R. B.; Walt, D. R. Dynamic Microbead Arrays for Biosensing Applications. *Lab Chip* **2013**, *13*, 2153−2160.
(467) Zhang, Y.; Askim, J. R.; Zhong, W.; Orlean, P.; Suslick, K. S. Identification of Pathogenic Fungi with an Optoelectronic Nose. *Analyst* **2014**, *139*, 1922−1928.
(468) Shrestha, N. K.; Lim, S. H.; Wilson, D. A.; SalasVargas, A. V.; Churi, Y. S.; Rhodes, P. A.; Mazzone, P. J.; Procop, G. W. The Combined Rapid Detection and Species-Level Identification of Yeasts in Simulated Blood Culture Using a Colorimetric Sensor Array. *PLoS One* **2017**, *12*, e0173130.
(469) Wu, L.; Qu, X. Cancer Biomarker Detection: Recent Achievements and Challenges. *Chem. Soc. Rev.* **2015**, *44*, 2963−2997.
(470) Shan, J.; Ma, Z. A Review on Amperometric Immunoassays for Tumor Markers Based on the Use of Hybrid Materials Consisting of Conducting Polymers and Noble Metal Nanomaterials. *Microchim. Acta* **2017**, *184*, 969−979.
(471) Queralto, N.; Berliner, A. N.; Goldsmith, B.; Martino, R.; Rhodes, P.; Lim, S. H. Detecting Cancer by Breath Volatile Organic Compound Analysis: A Review of Array-Based Sensors. *J. Breath Res.* **2014**, *8*, 027112.
(472) Montuschi, P.; Mores, N.; Trové, A.; Mondino, C.; Barnes, P. J. The Electronic Nose in Respiratory Medicine. *Respiration* **2013**, *85*, 72−84.
(473) Fitzgerald, J. E.; Bui, E. T. H.; Simon, N. M.; Fenniri, H. Artificial Nose Technology: Status and Prospects in Diagnostics. *Trends Biotechnol.* **2017**, *35*, 33−42.

DOI: 10.1021/acs.chemrev.8b00226
Chem. Rev. 2019, 119, 231−292

(474) Lim, S. H.; Martino, R.; Anikst, V.; Xu, Z.; Mix, S.; Benjamin, R.; Schub, H.; Eiden, M.; Rhodes, P. A.; Banaei, N. Rapid Diagnosis of Tuberculosis from Analysis of Urine Volatile Organic Compounds. *ACS Sens.* **2016**, *1*, 852−856.
(475) Queralto, N.; Berliner, A. N.; Goldsmith, B.; Martino, R.; Rhodes, P.; Lim, S. H. Detecting Cancer by Breath Volatile Organic Compound Analysis: A Review of Array-Based Sensors. *J. Breath Res.* **2014**, *8*, 027112.
(476) Mazzone, P. J. Analysis of Volatile Organic Compounds in the Exhaled Breath for the Diagnosis of Lung Cancer. *J. Thorac. Oncol.* **2008**, *3*, 774−780.
(477) Mazzone, P. J.; Wang, X.-F.; Xu, Y.; Mekhail, T.; Beukemann, M. C.; Na, J.; Kemling, J. W.; Suslick, K. S.; Sasidhar, M. Exhaled Breath Analysis with a Colorimetric Sensor Array for the Identification and Characterization of Lung Cancer. *J. Thorac. Oncol.* **2012**, *7*, 137−142.
(478) Wu, X.; Liu, H.; Liu, J.; Haley, K. N.; Treadway, J. A.; Larson, J. P.; Ge, N.; Peale, F.; Bruchez, M. P. Immunofluorescent Labeling of Cancer Marker Her2 and Other Cellular Targets with Semiconductor Quantum Dots. *Nat. Biotechnol.* **2003**, *21*, 41−46.
(479) Buchman, J. T.; Gallagher, M. J.; Yang, C.-T.; Zhang, X.; Krause, M. O. P.; Hernandez, R.; Orr, G. Research Highlights: Examining the Effect of Shape on Nanoparticle Interactions with Organisms. *Environ. Sci.: Nano* **2016**, *3*, 696−700.
(480) Salvati, A.; Pitek, A. S.; Monopoli, M. P.; Prapainop, K.; Bombelli, F. B.; Hristov, D. R.; Kelly, P. M.; Åberg, C.; Mahon, E.; Dawson, K. A. Transferrin-Functionalized Nanoparticles Lose Their Targeting Capabilities When a Biomolecule Corona Adsorbs on the Surface. *Nat. Nanotechnol.* **2013**, *8*, 137.
(481) Mirshafiee, V.; Mahmoudi, M.; Lou, K.; Cheng, J.; Kraft, M. L. Protein Corona Significantly Reduces Active Targeting Yield. *Chem. Commun.* **2013**, *49*, 2557−2559.
(482) Carril, M.; Padro, D.; del Pino, P.; Carrillo-Carrion, C.; Gallego, M.; Parak, W. J. In Situ Detection of the Protein Corona in Complex Environments. *Nat. Commun.* **2017**, *8*, 1542.
(483) Caputo, D.; Papi, M.; Coppola, R.; Palchetti, S.; Digiacomo, L.; Caracciolo, G.; Pozzi, D. A Protein Corona-Enabled Blood Test for Early Cancer Detection. *Nanoscale* **2017**, *9*, 349−354.
(484) Bajaj, A.; Rana, S.; Miranda, O. R.; Yawe, J. C.; Jerry, D. J.; Bunz, U. H. F.; Rotello, V. M. Cell Surface-Based Differentiation of Cell Types and Cancer States Using a Gold Nanoparticle-Gfp Based Sensing Array. *Chem. Sci.* **2010**, *1*, 134−138.
(485) Jiang, Z.; Le, N. D. B.; Gupta, A.; Rotello, V. M. Cell Surface-Based Sensing with Metallic Nanoparticles. *Chem. Soc. Rev.* **2015**, *44*, 4264−4274.
(486) Rana, S.; Elci, S. G.; Mout, R.; Singla, A. K.; Yazdani, M.; Bender, M.; Bajaj, A.; Saha, K.; Bunz, U. H. F.; Jirik, F. R.; et al. Ratiometric Array of Conjugated Polymers−Fluorescent Protein Provides a Robust Mammalian Cell Sensor. *J. Am. Chem. Soc.* **2016**, *138*, 4522−4529.
(487) Le, N. D. B.; Yesilbag Tonga, G.; Mout, R.; Kim, S.-T.; Wille, M. E.; Rana, S.; Dunphy, K. A.; Jerry, D. J.; Yazdani, M.; Ramanathan, R.; et al. Cancer Cell Discrimination Using Host−Guest "Doubled" Arrays. *J. Am. Chem. Soc.* **2017**, *139*, 8008−8012.
(488) *Coffee: Recent Developments*; Clarke, R. J., Vitzthum, O. G., Eds.; Blackwell Science: Oxford, 2001.

DOI: 10.1021/acs.chemrev.8b00226
Chem. Rev. 2019, 119, 231−292